The rheology of jamming

Dinkgreve, M.

Publication date
2018
Document Version
Final published version
License
Other

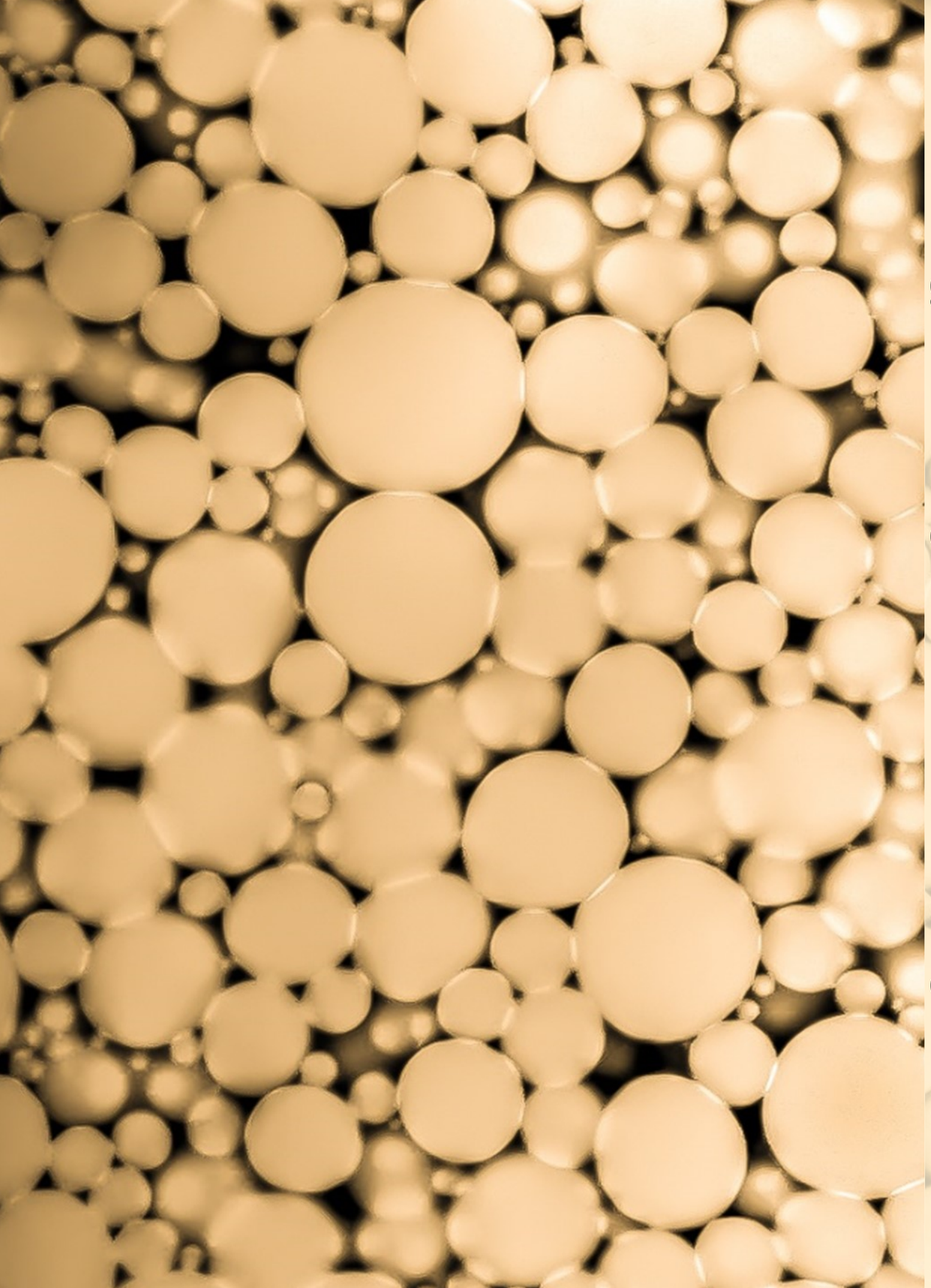

The Rheology of Jamming

Maureen Dinkgreve 2018

The Rheology of Jamming

Maureen Dinkgreve

The Rheology of Jamming

ACADEMISCH PROEFSCHRIFT

ter verkrijging van de graad van doctor
aan de Universiteit van Amsterdam
op gezag van de Rector Magnificus
prof. dr. ir. K.I.J Maex
ten overstaan van een door het college voor promoties
ingestelde commissie,
in het openbaar te verdedigen in de Agnietenkapel
op vrijdag 9 februari 2018, te 10:00 uur

door

Maureen Dinkgreve

geboren te Amsterdam

Promotiecommissie

Promotor:	prof. dr. D. Bonn	Universiteit van Amsterdam
Co-promotor:	dr. N. F. Sahidzadeh	Universiteit van Amsterdam
Overige leden:	prof. dr. M. M. Denn	City College of New York
	prof. dr. L. Berthier	Université de Montpellier
	prof. dr. S. Woutersen	Universiteit van Amsterdam
	prof. dr. K. P. Velikov	Universiteit van Amsterdam
	dr. E. Lerner	Universiteit van Amsterdam

Faculteit der Natuurwetenschappen, Wiskunde en Informatica.

The research reported in this thesis was carried out at the Van der Waals-Zeeman Institute/ Institute of Physics, University of Amsterdam.

"I have no special talent. I am only passionately curious."

Albert Einstein

ISBN: 978-94-028-0910-7

The author can be reached at:
maureen.dinkgreve@gmail.com

Contents

Chapter 1

Introduction

1.1 Soft condensed matter

Soft condensed matter is a subfield of condensed matter physics encompassing a variety of materials that are very common in everyday life (e.g. soap, toothpaste, glue or gel) and in industry (e.g. cement, paints or rubber) [1–6]. These materials are neither simple liquids nor crystalline solids; specific examples of soft matter systems are colloidal suspensions, polymer melts, solutions or gels, liquid crystals and colloidal or polymer glasses [7]. Because of their wide range of technical applications it is important to understand their mechanical properties and flow behavior.

1.2 Jamming phase diagram

Interesting mechanical behavior arises in soft matter systems, and this behavior can be difficult to predict. Understanding the transition between solid-like and liquid-like behavior that is observed in some of these materials is one of the outstanding challenges [8]. Consider for instance an emulsion that is a liquid with dispersed droplets. When the concentration of droplets is low the emulsion behaves like a Newtonian liquid (for example milk, which is an aqueous phase containing dispersed fat droplets). However, when the drop concentration increases there is a point at which the emulsion no longer flows and becomes jammed (for example mayonnaise, which also has a continuous phase that is aqueous with dispersed oil droplets). This concentrated emulsion does not flow at rest but starts to flow when a threshold stress (the yield stress) is exceeded. This transition between solid-like and liquid-like behavior is sometimes called the *jamming transition*. Figure 1.1 shows the "Jamming Phase Diagram" as was first proposed by Liu and Nagel in 1998 [9]; later Trappe et al. published a similar experimental phase diagram for colloidal systems [10]. In the phase diagram, jamming relates to temperature T, load or stress σ and inverse density or volume fraction ϕ. Materials inside the yellow portion of the sphere are jammed but can undergo a transition from the jammed solid-like behavior, to liquid-like behavior by applying a sufficient stress (load) or decreasing the density. Similarly, for thermal systems increasing the temperature (meaning increasing the thermal motion) will induce jammed materials to unjam; in this case we speak of the glass transition.

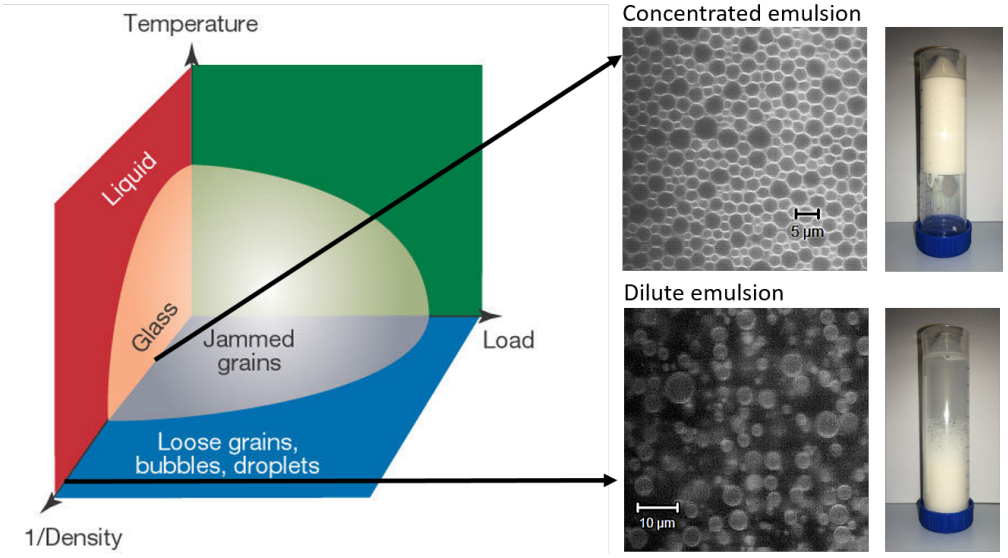

FIGURE 1.1: Schematic jamming phase diagram as proposed by Liu and Nagel in 1998 [9]. Pictures on the right are confocal images of emulsion droplets (silicone oil-in-water) at high (top) and low (bottom) droplet concentration.

1.2.1 Thermal motion and the glass transition

The emulsions in figure 1.1 have relatively large droplets (a diameter of $d \sim 5\mu m$), in the limit of large particles one can neglect thermal motion and consider the zero temperature plane of Fig. 1.1. In this case we have an athermal jamming transition at a critical volume fraction $\phi_J \approx 0.64$ [11]. The system becomes jammed when the concentration of droplets is at random close packing (RCP), and when $\phi > \phi_J$ the emulsion will not flow unless a high enough stress is applied. If we would decrease the droplet size and look at colloidal suspensions (typically at $d \sim 1\mu m$ or smaller) temperature becomes more important. These small particles exhibit thermal motion or *Brownian motion* (named after Robert Brown, 1827 [12]); the particles move randomly due to collisions with fast-moving atoms or molecules in the suspended liquid. At high concentrations these thermal systems also become jammed, however, the critical concentration is lower, namely $\phi_G \approx 0.58$, this is the *colloidal glass transition* [13]. In experiments, the equilibrium relaxation time, usually called "alpha-relaxation" time τ_α, becomes so large that the particles do not significantly diffuse over the experimental time scale [14]. At packing fractions above ϕ_G the colloidal particles are mainly moving inside effective cages formed by their neighbors.

1.2.2 Microscopic dynamics

The jamming and colloidal glass transition for soft repulsive particles share important similarities at the rheological level. In both cases, there is a 'critical' volume fraction at which solidity emerges and the amorphous solid at large volume fraction responds elastically for small deformation but flows when a large enough stress is applied (although most 'real' glasses break at high stresses). Yet the jamming and glass transition show different microscopic dynamics. Thermal systems are dominated by thermal fluctuations, while in purely athermal ones elasticity is more important.

If we consider a system of soft repulsive spheres, the system has two characteristic energy scales: 1) the thermal energy, k_BT, where k_B is the Boltzmann's constant and T the temperature, and 2) the interaction energy of the particles, ϵ. The ratio between the two energies (k_BT/ϵ) is an important control parameter and both jamming and glass effects can be distinguished in the low-softness limit $k_BT/\epsilon \to 0$. To study the jamming transition of athermal systems one can take the limit of vanishing kinetic energy ($T \to 0$), at a fixed repulsion energy scale ϵ. In that case, the stress scale, σ_0, controlling the yield stress has an energetic nature:

$$\sigma_0 = \frac{\epsilon}{R^3}, \tag{1.1}$$

where R is the particle radius and ϵ governs the mechanical properties of the particles (essentially the softness). As a result the yield stress can be written as $\sigma_y = \sigma_0 f(\phi)$ where $f(\phi < \phi_J) = 0$. This will be further discussed in chapter 7 and 8.

Alternatively, when the temperature is constant and $\epsilon \to \infty$, this will result in studying the physics of a thermal hard sphere system having a glass transition. In glassy materials the yield stress is a function of temperature and density, because a purely hard sphere potential contains no energy scale. The thermal stress scale, σ_T, is given by thermal fluctuations:

$$\sigma_T = \frac{k_BT}{R^3}, \tag{1.2}$$

and the yield stress can be written by $\sigma_y = \sigma_T g(\phi)$ where $g(\phi < \phi_G) = 0$.

The above stress scales become comparable when the particle softness is large enough, $k_BT/\epsilon \approx 1$, while they diverge in the athermal limit, $\epsilon \gg k_BT$ [15].

1.3 Rheology

Understanding the flow properties of complex fluids or elastic behavior of soft materials is very important for fundamental and industrial purposes. The study of flow and deformation of matter is called rheology [16]. A simple example to understand basic rheology is to consider two parallel plates, of area A and separation h, with a material in between (Fig. 1.2). When a force, F is applied on the top plate it moves a distance d. The *shear stress* is then defined as the force per unit area:

$$\sigma = \frac{F}{A} \tag{1.3}$$

and *shear strain* is given by the ratio of deformation:

$$\gamma = \frac{d}{h}. \tag{1.4}$$

For a perfectly elastic solid (Hooke's law), the strain is simply proportional to the applied stress with a constant proportionality that is the *shear modulus*:

$$G = \sigma/\gamma. \tag{1.5}$$

For a liquid an applied stress will result in a time dependent strain. The resistance to continuous deformation by shear stress is the *viscosity*:

$$\eta = \sigma/\dot{\gamma} \tag{1.6}$$

where $\dot{\gamma}$ is the *shear rate* which is the time derivative of the shear strain.

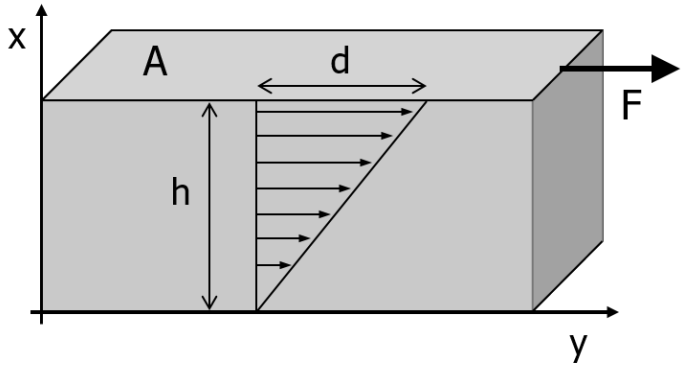

FIGURE 1.2: Parallel plate representation of rheology.

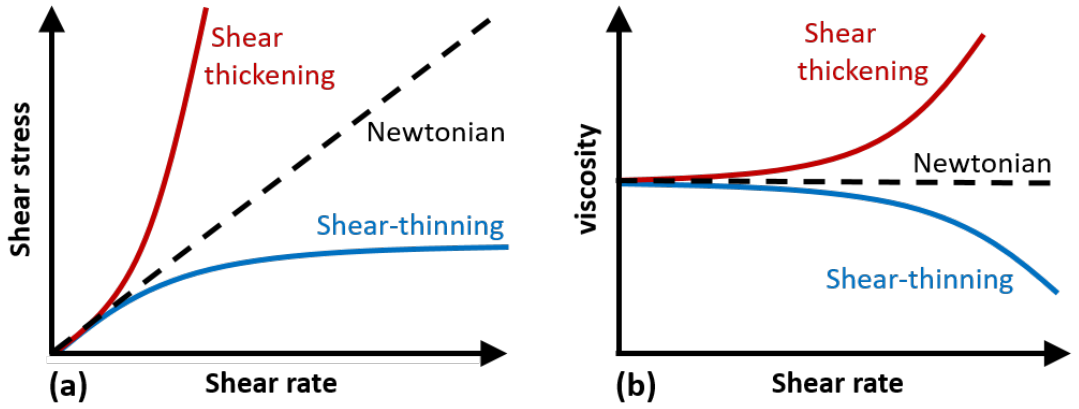

FIGURE 1.3: Representation of flow curves of different types of fluids: Newtonian, shear-thinning and shear-thickening.

1.3.1 Flow curves

By plotting the shear stress as a function of the shear rate one can quantify the flow behavior of a material, such plots are called flow curves. Depending on the type of material we can distinguish different types of typical flow curves; Newtonian, shear-thinning or shear-thickening (Figure 1.3). For the latter two, the viscosity depends on the applied shear rate; with increasing rate the viscosity decrease for shear-thinning materials (like mayonnaise or hairgel) [17–20] and increase for shear-thickening materials (cornstarch for example) [17, 21–23].

1.4 Yield-stress materials

One interesting and widely applied class of soft condensed materials are yield-stress fluids. For small applied stresses these fluids behave elastically, but once a threshold stress is exceeded the they start to flow. Bingham was the first to introduced the yield stress, using the following notation [24]:

$$\sigma = \sigma_y + \eta\dot{\gamma} \qquad \text{if } \sigma > \sigma_y \tag{1.7}$$

$$\dot{\gamma} = 0 \qquad \text{if } \sigma \leq \sigma_y \tag{1.8}$$

where σ_y is the yield stress. Thus if $\sigma \leq \sigma_y$ there is no flow and for $\sigma > \sigma_y$ the stress increases linearly with $\dot{\gamma}$ with a constant post-yield viscosity.

A commonly used model to describe yield-stress materials is the Herschel-Bulkley model [25]:

$$\sigma = \sigma_y + K\dot{\gamma}^{\beta} \tag{1.9}$$

where K and β are adjustable parameters. After the yield stress is overcome, if $\beta = 1$ the material has a constant viscosity, whereas if $\beta < 1$ the viscosity decreases with increasing $\dot{\gamma}$ (shear-thinning) or if $\beta > 1$ the viscosity increases with increasing $\dot{\gamma}$ (shear-thickening).

1.4.1 Emulsions

An emulsion is a mixture of two (or more) liquids that are usually immiscible (typically oil and water), but by adding an emulsifier a dispersion of one component into the other can be obtained. Usually a surfactant is used as emulsifier [26], this is a surface active agent that lowers the surface tension between the two liquids, but also solid particles can be used as emulsifiers [27].

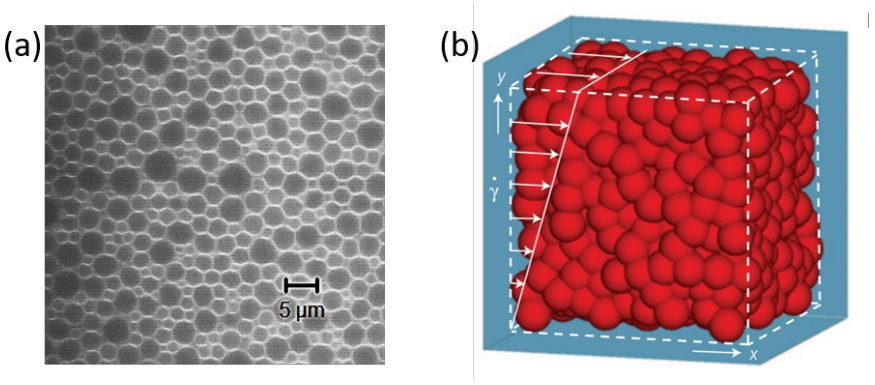

FIGURE 1.4: (a) Confocal image of a concentrated emulsion $\phi = 0.8$. (b) Schematic representation of jammed elastic spheres at $\phi = 0.8$ [28].

Droplet deformation and Laplace pressure

By increasing the droplet concentration in an emulsion one can obtain a yield-stress fluid[1]. Normally the droplet concentration is described by the *volume fraction* (ϕ), which is the ratio of the volume of the dispersed phase to the total volume of the emulsion. If the dispersed droplets are athermal ($R \gg 1\mu m$) they can be considered as soft non-Brownian elastic spheres (see figure 1.4) and when $\phi >$

[1]It is quite amazing that when you mix two liquids together you get a solid-like material, without any chemical reaction occurring.

$\phi_J \approx 0.64$ the droplets start to deform increasingly with increasing volume fraction, while the surfactant prevents the droplets from coalescing. The elastic response of the droplets is determined by the Laplace pressure, the pressure difference between the inside and outside of a curved surface is given by [29]

$$\Delta P = \Sigma \left(\frac{1}{R_1} + \frac{1}{R_2} \right) \tag{1.10}$$

where Σ is the surface tension and R_1 and R_2 are the principal radii of curvature. If we assume perfect spheres $R_1 = R_2 = R$ the formula reduces to

$$\Delta P = \frac{2\Sigma}{R}. \tag{1.11}$$

1.5 Scope of this thesis

The main research question in this thesis is: can we describe, understand and predict the rheology of jamming? Most of the studied systems are made by the author and rheology is the main tool the measure the flow properties. This thesis is organized as follows:

Chapter 2: The experimental techniques and the different materials that were used for this thesis are discussed.

Chapter 3: We review the definition of the yield stress and demonstrate the significance of the pre-yielding behavior through a number of elementary measurements on a model yield-stress fluids, a Carbopol gel.

Chapter 4: We compare different methods of measuring the yield stress with conventional rheometers that have been used in the literature on a variety of materials. Subsequently, we give an overview of the different values that are found for the yield stress and yield strain.

Chapter 5: We investigate the role of Laponite clay particles on high internal phase emulsion stability. By using confocal microscopy we visualize the clay particles and study the contribution of particles absorbing at the fluid interface and a particle network in the continuous phase to the overall emulsion stability.

Chapter 6: We investigate why Carbopol, normally viewed as a simple yield-stress fluid, can undergo a transition to thermally induced shear banding. A set of

rheological tests are done to study this phenomenon in differently prepared Carbopol gels. Flow visualization experiments, with fluorescently labelled Carbopol, elucidate the difference between simple and shear banding behavior.

Chapter 7: Here we attempt to describe, understand and predict the flow behavior (stress vs. shear rate) of athermal yield-stress fluids in general. The experimental flow curves of four different "simple" athermal yield-stress fluids are studied near the jamming point.

Chapter 8: In this last chapter we investigate the cross-over between thermal and athermal yield-stress regimes, by looking at the effect of volume fraction, particles size and the inter-particle interactions on the flow behavior.

References

[1] P. de Gennes. Soft matter (nobel lecture). *Angewandte Chemie International Edition*, 31(7):842–845, 1992.

[2] R. G. Larson. *The structure and rheology of complex fluids*, volume 150. Oxford university press New York, 1999.

[3] P. Coussot. *Rheometry of pastes, suspensions, and granular materials: applications in industry and environment*. John Wiley & Sons, 2005.

[4] G. A. van Aken. Aeration of emulsions by whipping. *Colloids and Surfaces A: Physicochemical and Engineering Aspects*, 190(3):333 – 354, 2001.

[5] M. Kogan, L. Ducloué, J. Goyon, X. Chateau, O. Pitois, and G. Ovarlez. Mixtures of foam and paste: suspensions of bubbles in yield stress fluids. *Rheologica Acta*, 52(3):237–253, 2013.

[6] C. Chang, Q. D. Nguyen, and H. P. Rønningsen. Isothermal start-up of pipeline transporting waxy crude oil. *Journal of Non-Newtonian Fluid Mechanics*, 87(2):127 – 154, 1999.

[7] R. A. L. Jones. *Soft condensed matter*, volume 6. Oxford University Press, 2002.

[8] D. Bonn, M. M. Denn, L. Berthier, T. Divoux, and S. Manneville. Yield stress materials in soft condensed matter. *Rev. Mod. Phys.*, 89:035005, Aug 2017.

[9] A. J. Liu and S. R. Nagel. Nonlinear dynamics: Jamming is not just cool any more. *Nature*, 396(6706):21–22, 1998.

[10] V. Trappe, V. Prasad, L. Cipelletti, P. N. Segre, and D. A. Weltz. Jamming phase diagram for attractive particles. *Nature*, 411(6839):772, 2001.

[11] J. D. Bernal and Mason J. Packing of spheres: Co-ordination of randomly packed spheres. *Nature*, 188:910–911, 1960.

[12] R. Brown and Linnean Society (London). *Character and description of Kingia: a new genus of plants found on the south-west coast of New Holland, with observations on the structure of its unimpregnated ovulum, and on the female flower of Cycadeae and Coniferae*. 1827.

[13] P. N. Pusey and W. van Megen. Observation of a glass transition in suspensions of spherical colloidal particles. *Phys. Rev. Lett.*, 59:2083–2086, Nov 1987.

[14] G. Brambilla, D. El Masri, M. Pierno, L. Berthier, L. Cipelletti, G. Petekidis, and A. B. Schofield. Probing the equilibrium dynamics of colloidal hard spheres above the mode-coupling glass transition. *Phys. Rev. Lett.*, 102:085703, 2009.

[15] A. Ikeda, L. Berthier, and P. Sollich. Disentangling glass and jamming physics in the rheology of soft materials. *Soft Matter*, 9(32):7669–7683, 2013.

[16] H. A. Barnes, J. F. Hutton, and K. Walters. *An introduction to rheology*, volume 3. Elsevier, 1989.

[17] M. C. Newstein, H. Wang, N. P. Balsara, A. A. Lefebvre, Y. Shnidman, H. Watanabe, K. Osaki, T. Shikata, H. Niwa, and Y. Morishima. Microstructural changes in a colloidal liquid in the shear thinning and shear thickening regimes. *The Journal of chemical physics*, 111(10):4827–4838, 1999.

[18] M. M. Cross. Relation between viscoelasticity and shear-thinning behaviour in liquids. *Rheologica Acta*, 18(5):609–614, 1979.

[19] S. T. Milner. Relating the shear-thinning curve to the molecular weight distribution in linear polymer melts. *Journal of Rheology*, 40(2):303–315, 1996.

[20] G. P. Roberts, H. A. Barnes, and P. Carew. Modelling the flow behaviour of very shear-thinning liquids. *Chemical Engineering Science*, 56(19):5617–5623, 2001.

[21] A. Fall, N. Huang, F. Bertrand, G. Ovarlez, and D. Bonn. Shear thickening of cornstarch suspensions as a reentrant jamming transition. *Physical Review Letters*, 100(1):018301, 2008.

[22] W. J. Frith, P. d'Haene, R. Buscall, and J. Mewis. Shear thickening in model suspensions of sterically stabilized particles. *Journal of rheology*, 40(4):531–548, 1996.

[23] R. L. Hoffman. Explanations for the cause of shear thickening in concentrated colloidal suspensions. *Journal of Rheology*, 42(1):111–123, 1998.

[24] E. C. Bingham. *Fluidity and plasticity*, volume 2. McGraw-Hill, 1922.

[25] W. H. Herschel and R. Bulkley. Measurement of consistency as applied to rubber-benzene solutions. In *Am. Soc. Test Proc*, volume 26, pages 621–633, 1926.

[26] J. Sjoblom. *Emulsions and Emulsion Stability: Surfactant Science Series/61*, volume 132. CRC Press, 2005.

[27] S. U. Pickering. Cxcvi. *J. Chem. Soc., Trans*, 91(0):2001–2021, 1907.

[28] J. R. Seth, L. Mohan, C. Locatelli-Champagne, M. Cloitre, and R. T. Bonnecaze. A micromechanical model to predict the flow of soft particle glasses. *Nature materials*, 10(11):838, 2011.

[29] P. de Gennes, F. Brochard-Wyart, and D. Quéré. Capillarity and gravity. In *Capillarity and Wetting Phenomena*, pages 33–67. Springer, 2004.

Chapter 2

Experimental Techniques and Materials

2.1 Experimental techniques

The experimental techniques that were used in this research are described in this section. Rheology was the main method used to understand the flow properties of the different systems that are studied here. In addition, confocal microscopy was used to study the microscopic structures of the systems and pendant drop measurements were done to determine surface and interfacial tensions.

2.1.1 Rheology

In chapter 1 an example of two parallel plates is presented to explain the basic idea of a rheological test. In reality, measurements are done on a rheometer with slightly different (and more complex) geometries than our basic example, nevertheless the principle remains the same [1, 2]. Here we discuss the different geometries we used, define the corresponding parameters and describe a series of typical rheological measurements that were done.

2.1.1.1 Rheometer and geometries

Most of the measurements were done on an Anton Paar MCR 302 rheometer (figure 2.1). This rheometer has both a direct stress and strain controller, which allows for controlled shear stress (CSS) and controlled shear rate (CSR) tests. In a CSS test, a torque is imposed and the angular displacement is measured. Whereas in case of a CSR test, a rotational speed is imposed and the torque is

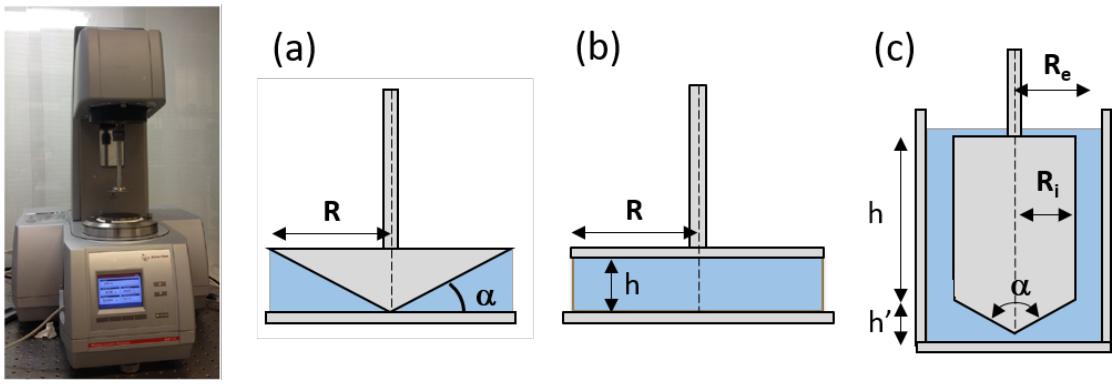

FIGURE 2.1: Anton Paar MCR 302 rheometer with schematic representations of different geometries: (a) cone-plate, (b) plate-plate and (c) cylindrical geometry.

measured. In general, three different geometries were used: cone-plate, plate-plate and a cylindrical couette geometry. The cone-plate geometry was the most used in this thesis, a 50mm-diameter cone-and-plate geometry with a 1° cone and roughened surfaces to avoid wall slip [3, 4]. But for completeness we describe all three geometries here.

(a) The *cone-plate geometry* is rheologically ideal because the angled cone gives a homogeneous shear field; the shear stress and rate do not depend on the radial distance from the center. The cone rotates and the plate is static, accordingly the shear rate $\dot{\gamma}$ and shear stress σ are defined as follows [5]:

$$\dot{\gamma} = \frac{\omega}{tan(\alpha)} \approx \frac{\omega}{\alpha} \tag{2.1}$$

$$\sigma = \frac{3M}{2\pi R^3} \tag{2.2}$$

where ω is the angular frequency, α the angle of the cone, M the torque and R the radius of the cone. For small angles α we can make the approximation $tan(\alpha) \approx \alpha$.

(b) The *plate-plate geometry* has a rotating and a static plate with a gap h between the plates. In this geometry the shear rate and shear stress are defined as follows [5]:

$$\dot{\gamma} = \frac{R\omega}{h} \tag{2.3}$$

$$\sigma = \frac{2M}{\pi R^3} \tag{2.4}$$

where ω is the angular frequency, M the torque and R is the radius of the plate. An advantage of this geometry is that the gap can be altered, however the shear rate varies with the radial distance from the center therefore this is not as rheologically ideal as the cone-plate geometry.

(c) The *cylindrical Couette geometry* is often used for low viscous fluids, whereas these can flow out of the other two geometries. In this geometry, when using a large gap cylinder, the shear rate and shear stress are related to the surface of the inner cylinder (i.e. to R_i)[5]:

$$\dot{\gamma} = \frac{2\omega R_e^2}{(R_e^2 - R_i^2)} \tag{2.5}$$

$$\sigma = \frac{M}{(2\pi h R_i^2)} \tag{2.6}$$

where ω is the angular frequency, M the torque and R_i is the radius of the inner cylinder ("internal radius") and R_e is the cup radius ("external radius").

2.1.1.2 Rheological measurements

Material properties can be measured by means of different rheological tests. Some materials are very sensitive to the way these tests are conducted. For example, the measuring time can have a significant effect on the material parameters that are measured; this is the difference between a transient or steady state. Here we describe a series of standard measurements that are used in this study.

Steady shear measurements
In (steady) shear experiments a shear rate or shear stress sweep is imposed on the sample and the response stress or rate is measured, respectively. If the measurement time is sufficiently long (depending on the material properties) a steady state is reached. Usually, the outcome of steady state tests are presented as flow curves by plotting the stress versus shear rate. In this thesis often up-and-down shear rate sweeps were performed, imposing first an increasing, and then decreasing shear rate sweep. This experiment is a way to check if the material exhibits rheological hysteresis. If the up-and-down sweeps give the same value we have a simple flow curve, whereas a difference between the up-and-down going flow curves indicates hysteresis, that is often due to thixotropy.

Stress growth and start-up measurements
In stress growth and start-up measurements a constant shear rate is imposed and the stress evaluation in time is studied. In start-up measurements the focus is on the first response at the start of a measurement. For example a visco-elastic material first behaves elastically for small deformations, but starts to flow after a critical strain is reached. Start-up measurements are also useful to check when a steady stated is reached.

Oscillation measurements
This measurement consists of imposing an oscillatory shear, that allows to determine the storage and loss moduli, which give insight in the visco-elasticity of a material. The storage modulus (G') is a measure for the storage of elastic energy, and the loss modulus (G'') is associated with the dissipation of viscous energy per cycle of deformation [2, 6]. Consider a sinusoidal shear strain γ with an amplitude

γ_0 and angular frequency ω, given by $\gamma = \gamma_0 sin(\omega t)$. Accordingly, the shear stress $\sigma(t)$ at low-amplitude deformation is proportional to γ with a phase difference:

$$\sigma(t) = \sigma_0 sin(\omega t + \delta) = \gamma_0[G'(\omega)sin(\omega t) + G''(\omega)cos(\omega t)] \tag{2.7}$$

where δ represents the phase difference between the stress and strain response. In case of a perfectly elastic material, $G'' = 0$ and $\delta = 0$, whereas for viscous materials $G' = 0$ and $\delta = 90°$. For yield-stress materials both G' and G'' are nonzero and $0° < \delta < 90°$.

Viscosity bifurcation measurements

In viscosity bifurcation measurements a constant shear stress is imposed while measuring the evolution of the shear rate and hence the viscosity in time. For yield-stress fluids, when a stress is applied above the yield stress the material flows, the viscosity will go towards a steady state value. For stresses below the yield stress, the viscosity will be infinitely high, because there is no flow. These experiments are very useful for testing if yield-stress materials are thixotropic or show hysteresis, because in these cases the yield stress is not easy to define, as aging and rejuvenation play an important role in the evolution of the viscosity.

Creep

A creep test is very similar to viscosity bifurcation measurements; a constant stress is imposed but now the strain response in time is studied. For stresses higher than the yield stress the strain increases indefinitely in time; a constant shear rate then indicates that the material is flowing. Whereas for stresses lower than the yield stress, the material behaves like an elastic solid, the strain will increase in time toward a constant strain value.

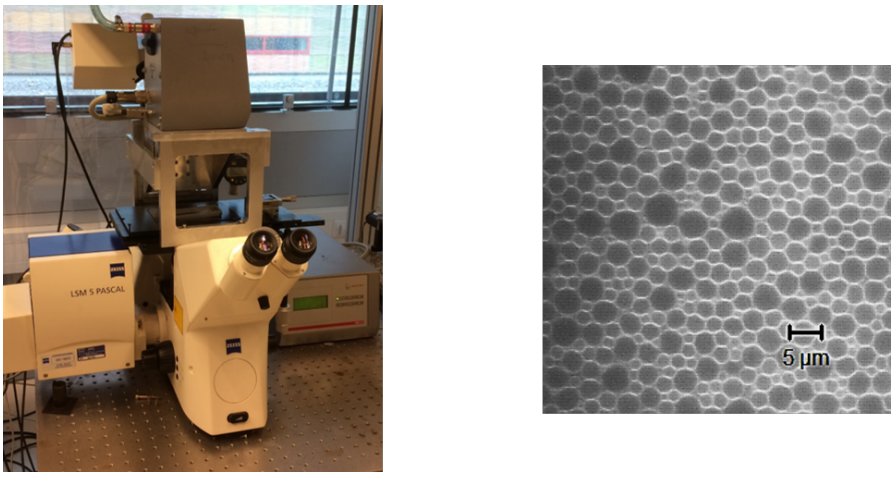

FIGURE 2.2: Confocal Laser Scanning Microscope (CLSM) with an Anton Paar DSR 301 rheometer head on top (left). Confocal impage of an oil in water emulsion (right).

2.1.2 Confocal scanning microscopy

The flow behavior of the emulsions and Carbopol are studied using a Confocal Laser Scanning Microscope (CLSM), Zeiss Pascal Live (figure 2.2). This imaging technique has an increased optical resolution compared to traditional optical microscopes. A pinhole placed at the confocal plane of the lens eliminates out-of-focus light and enables the three-dimensional reconstruction of structures at different depths [7, 8]. For this technique the samples have to be transparent (to prevent laser light diffusion by the sample) and fluorescently labeled.

To simultaniously measure the rheology and visualize flow profiles a rheometer head (Anton Paar DSR 301) is put on top of the confocal microscope (figure 2.2). While imposing a constant shear rate we can measure the velocity profile by recording the motion at different heights between a cone and plate [9].

2.1.3 Pendant drop

The surface tension of a liquid or the interfacial tension between two liquids can be determined with the pendant drop method. In this simple experiment a liquid drop is hanging on the tip of a needle (the end of a fine capillary tube), and by analyzing the contour of the droplet from an optical image the surface tension can be calculated [10, 11]. Similarly, the interfacial tension can be calculated, but then the liquid drop is hanging in another liquid face instead of air.

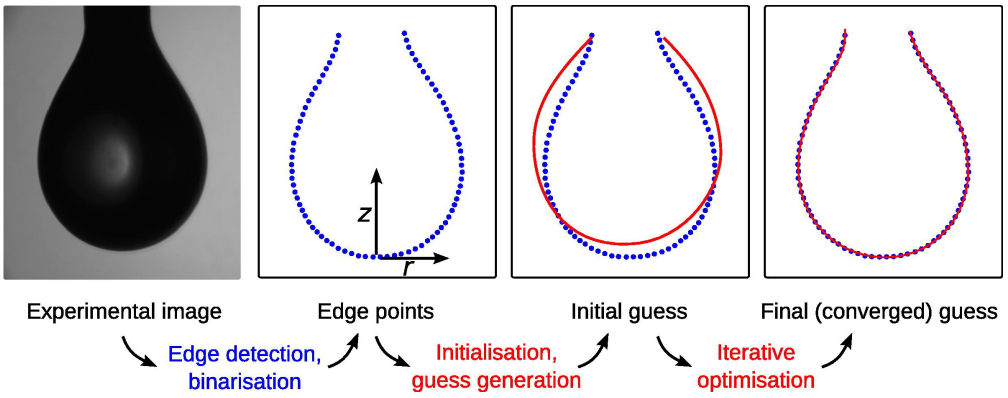

FIGURE 2.3: Schematic of the pendant drop process, going from a raw experimental image to a fitted solution from which Σ can be obtained[11].

The shape of the droplet is determined by the surface tension and gravitation. The surface tension tends to minimize the surface area by making the drop spherical. Gravity stretches the drop from this spherical shape in a typical pear-like form (figure 2.3). In equilibrium, the surface tension Σ can be calculated from the balance between the Laplace pressure (ΣC) and the hydrostatic term ($\rho g z$)[12]:

$$\Sigma C = \rho g z \tag{2.8}$$

where C is the curvature of the droplet-surface, ρ the density of the liquid and g the gravitational acceleration. The curvature can be expressed in a cylindrical coordinate system, because the drop is symmetric around the z-axis (z is the direction of gravity). By defining $r_z = \frac{dr}{dz}$ and $r_{zz} = \frac{d^2r}{dz^2}$, the curvature is obtained as [12]:

$$C = -\frac{r_{zz}}{(1+r_z^2)^{3/2}} + \frac{1}{r(1+r_z^2)^{1/2}} \tag{2.9}$$

Equation 2.8 can then be solved numerically. Accordingly, the surface tension is taken as an adjustable parameter until the best possible fit for the curvature of the droplet is found (figure 2.3).

2.2 Materials

Two main systems are used in this thesis, Carbopol gels and emulsions, to study the rheology of jammed systems. We use these systems because, first of all, Carbopol is a widely used material that behaves as a model yield-stress fluid [13–16], it is therefore used as a reference system. And secondly, emulsions at high volume fractions of the dispersed phase are yield-stress fluids, with the benefit that the volume fraction can be tuned to study the jamming point.

In this section we will discuss the preparation protocol for the different systems and small nuances to these.

2.2.1 Carbopol gel

Carbopol is a widely used gel within many industries because of its efficient rheology modifications; a simple yield-stress fluid with enhanced self-wetting for ease of use [17]. Carbopol is a cross-linked polyacrylic acid polymer, that is usually provided as a dry white powder. In a water solution at neutral pH, polymers absorb and retain water and swell to many times their original volume. It is this tremendous swelling that creates jamming of the polymer 'sponges' and therefore the fluid has a yield stress. The procedure to create a Carbopol gel with a simple yield stress behavior is the following:

1. Disperse 1wt% Carbopol (Ultrez U10 grade) in demineralized water (milli-Q ®) by stirring with a magnetic stir bar for 1 hour at room temperature.
2. Homogenize the Carbopol by adding a diluted NaOH solution (1M). Add the base drop by drop while the sample is stirred constantly at 50 rpm.
3. Stir the sample for one more hour when the pH is approximately 7.
4. Leave to rest for one day.

It turns out that the preparation method can change the flow behavior of the Carbopol. In chapter 6 we study the influence of heavy stirring during the homogenization process on the sample composition and the rheology. These samples are stirred with a simple propeller as presented in figure 2.4.

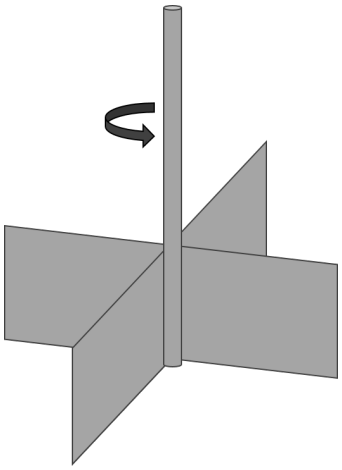

FIGURE 2.4: Schematic presentation of stirring wheel for homogenizing of the Carbopol gel.

2.2.2 Emulsions

The emulsions used in this thesis are castor oil-in-water emulsions and silicone oil-in-water emulsions. Different emulsifiers were used to stabilize the emulsions. Most of the emulsions were stabilized using surfactants, but also emulsions stabilized with clay particles (and no surfactant) were studied here.

2.2.2.1 Emulsion with surfactants

Castor oil-in-water emulsions are prepared using various surfactant compositions creating, as we call them, *mobile*, *rigid* and *soft interaction* emulsions. In general most type of surfactant-stabilized emulsions are considered as having mobile droplet surfaces and it is usually assumed that this leads to harmonic interactions between the droplets [18]. Our *mobile* emulsions were stabilized using Sodium Dodecyl Sulfate (SDS, from Sigma-Aldrich), which is an ionic surfactant with molar formula $CH_3(CH_2)_{11}SO_4^-Na^+$, the negative charge at the droplet surface creates a repulsive interaction between the drops. The *rigid* emulsions were stabilized using a protein solution composed of bovine serum albumin (BSA, from Sigma-Aldrich) and a co-surfactant propylene glycerol alginate (PGA, from Dextra); this combination creates rigid surfaces on the droplets and will thereby increase the drops' resistance to deformation [19]. Mobile and rigid interfaces have been studied in the drainage of foams, where insoluble surfactant molecules are expected to form rigid interfacial layers, enforcing zero-velocity boundary conditions for the

flow through the liquid channels between the bubbles. Whereas small soluble surfactant molecules yield significant interfacial mobility and faster drainage [20–22]. As a consequence, the mechanical properties of the system change and one would expect to see a difference in the stress-strain flow curves (e.g. the value of the yield stress at a certain volume fraction).

Mobile Castor oil-in-water emulsions were prepared in the following way:

1. The continuous phase was prepared by dissolving SDS in demineralized water (Milli-Q ®), obtaining a solution with 1wt% SDS concentration.
2. The dispersed phase consisted of Castor oil (Sigma-Aldrich).
3. Emulsification: the oil was gradually added to the aqueous phase while stirring with a Silverson l5m-a emulsifier at 10,000 rpm for 2 minutes. During emulsification the sample was cooled in an ice bath to prevent heating of the sample. The internal volume fraction was $\phi_{oil} = 0.8$.
4. Emulsions with lower ϕ were prepared by diluting the original emulsion ($\phi_{oil} = 0.80$) with the 1% SDS solution.

Rigid systems were prepared in a similar way, but with 0.4wt% PGA and 0.4wt% BSA instead of 1wt% SDS in the continuous phase. Finally, *soft interaction* emulsions are prepared by adding salt to the mobile emulsion to screen the electrostatic repulsion due to the SDS, these emulsions therefore have less electrostatic interaction than the *mobile* emulsions.

For optical miscoscopy observations, we prepare transparent emulsions in which the continuous phase is refractive index matched to the oil phase (Silicone oil Rhodorsil® 47 V500) by adding glycerol (99% GC, from Sigma-Aldrich) to the aqueous phase. The rest of the preparation protocol is the same as mentioned above.

2.2.2.2 Emulsions with clay

In addition to surfactant stabilized emulsions we prepare particle stabilized emulsions. In these so called Pickering emulsions particles are adsorbed at the oil-water

interface where they form a continuous layer around the dispersed drops impending coalescence and hence stabilizing the emulsion. We prepared emulsions with Laponite® clay particles as stabilizer particles [23].

The continuous aqueous phase is first prepared by suspending 2wt% Laponite® RD in a 0.1M Sodium Chloride (NaCl, Ultrapure, from Sigma-Aldrich) solution in deminiralized water (Milli-Q ®)[24]. To disperse the particles, we use a high intensity ultrasonic disperser (Branson solifier 250, tip diameter 5mm), operating at 20kHz and 100W for 30 minutes. Finally castor oil-in-water emulsions are prepared following the procedure of the mobile emulsions (from step 3).

References

[1] C. W. Macosko and R. G. Larson. Rheology: principles, measurements, and applications. 1994.

[2] R. G. Larson. *The structure and rheology of complex fluids*, volume 150. Oxford university press New York, 1999.

[3] V. Bertola, F. Bertrand, H. Tabuteau, D. Bonn, and P. Coussot. Wall slip and yielding in pasty materials. *Journal of Rheology*, 47(5):1211–1226, 2003.

[4] P. C. F. Møller, A. Fall, and D. Bonn. Origin of apparent viscosity in yield stress fluids below yielding. *EPL (Europhysics Letters)*, 87(3):38004, 2009.

[5] T. G. Mezger. *The rheology handbook: for users of rotational and oscillatory rheometers*. Vincentz Network GmbH & Co KG, 2006.

[6] Q. D. Nguyen and D. V. Boger. Measuring the flow properties of yield stress fluids. *Annual Review of Fluid Mechanics*, 24(1):47–88, 1992.

[7] C. J. R. Sheppard and D. M. Shotton. *Confocal laser scanning microscopy*. BIOS Scientific Publishers, 1997.

[8] S. J. Wright, V. E. Centonze, S. A. Stricker, P. J. DeVries, S. W. Paddock, and G. Schatten. Introduction to confocal microscopy and three-dimensional reconstruction. *Methods in cell biology*, 38:1–45, 1993.

[9] J. Paredes, N. Shahidzadeh-Bonn, and D. Bonn. Shear banding in thixotropic and normal emulsions. *Journal of Physics: Condensed Matter*, 23(28):284116, 2011.

[10] F. Bashforth and J. C. Adams. *An attempt to test the theories of capillary action: by comparing the theoretical and measured forms of drops of fluid. With an explanation of the method of integration employed in constucting the tables which give the theoretical forms of such drops.* University Press, 1883.

[11] J. D. Berry, M. J. Neeson, R. R. Dagastine, D. Y. C. Chan, and R. F. Tabor. Measurement of surface and interfacial tension using pendant drop tensiometry. *Journal of colloid and interface science*, 454:226–237, 2015.

[12] P. De Gennes, F. Brochard-Wyart, and D. Quéré. *Capillarity and wetting phenomena: drops, bubbles, pearls, waves.* Springer Science & Business Media, 2004.

[13] P. Møller, A. Fall, V. Chikkadi, D. Derks, and D. Bonn. An attempt to categorize yield stress fluid behaviour. *Philosophical Transactions of the Royal Society of London A: Mathematical, Physical and Engineering Sciences*, 367(1909):5139–5155, 2009.

[14] D. Bonn and M. M. Denn. Yield stress fluids slowly yield to analysis. *Science*, 324(5933):1401–1402, 2009.

[15] G. Ovarlez, S. Cohen-Addad, K. Krishan, J. Goyon, and P. Coussot. On the existence of a simple yield stress fluid behavior. *Journal of Non-Newtonian Fluid Mechanics*, 193:68–79, 2013.

[16] N. J. Balmforth, I. A. Frigaard, and G. Ovarlez. Yielding to stress: recent developments in viscoplastic fluid mechanics. *Annual Review of Fluid Mechanics*, 46:121–146, 2014.

[17] Carbopol ultrez 10 polymer description lubrizol. `https://www.lubrizol.com/Personal-Care/Products/Product-Finder/Products-Data/112`. Accessed: 2017-10-17.

[18] B. P. Tighe. Relaxations and rheology near jamming. *Physical review letters*, 107(15):158303, 2011.

[19] S. A. Koehler, S. Hilgenfeldt, E. R. Weeks, and H. A. Stone. Drainage of single plateau borders: Direct observation of rigid and mobile interfaces. *Phys. Rev. E*, 66:040601 (R), 2002.

[20] M. Durand, G. Martinoty, and D. Langevin. Liquid flow through aqueous foams: From the plateau border-dominated regime to the node-dominated regime. *Phys. Rev. E*, 60:R6307–R6308, Dec 1999.

[21] S. A. Koehler, S. Hilgenfeldt, and H. A. Stone. Liquid flow through aqueous foams: the node-dominated foam drainage equation. *Physical review letters*, 82(21):4232, 1999.

[22] S. A. Koehler, S. Hilgenfeldt, and H. A. Stone. A generalized view of foam drainage: experiment and theory. *Langmuir*, 16(15):6327–6341, 2000.

[23] Laponte® RD. manufactured by BYK Additives & Instruments.

[24] N. P. Ashby and B. P. Binks. Pickering emulsions stabilised by laponite clay particles. *Physical Chemistry Chemical Physics*, 2(24):5640–5646, 2000.

Chapter 3

"Everything flows?": elastic effects on startup flows

3.1 Various definitions of the yield stress

Many materials found in daily life exhibit properties characteristic of either solids or liquids, depending on the imposed stress. At small stresses these materials deform essentially in an elastic manner, but flow once a critical stress is exceeded; this critical value is called the yield stress (σ_y), and materials exhibiting a yield stress are called yield-stress materials. Examples of yield-stress materials include concentrated emulsions like cosmetic creams or margarine, toothpaste, foams, polymer gels like Carbopol, slurries, and some composites [1–3].

As already mentioned, the notion of a yield-stress fluid was introduced by Bingham, who included such fluids in the context of yielding in many classes of materials in his 1922 book Fluidity and Plasticity [4]. In 1985, Barnes and Walters published a provocative paper entitled "The yield stress myth?" [5], in which they asserted that the yield stress is an experimental artifact, and notably that all fluids will show viscous (indeed, Newtonian) behavior at sufficiently small stresses. They stated that "the yield stress hypothesis, which has hitherto been a useful empiricism, is no longer necessary, and... fluids which flow at high stresses will flow at all lower stresses; i.e., the viscosity, although large, is always finite and there is no yield stress."[1] This assertion by two very prominent rheologists caused a flurry of discussions and publications, with substantial parsing of the meaning of the words "yield stress;" i.e., is the yield stress a material property or a useful approximation for materials that exhibit a large reduction in viscosity over a narrow shear stress range? Barnes and Walters supported their assertion with data obtained using a constant-stress rheometer that showed a Newtonian regime at stresses lower than the apparent yield stress, and Barnes subsequently showed similar data on a number of different materials [6, 7], including Carbopol.

Modern interest in yield-stress fluids largely dates from work by Oldroyd [8] and Prager [9, 10], that put the description of such materials into an invariant continuum formulation that can be applied to flows in complex geometries. Both Oldroyd and Prager assumed that there is a transition between a solid and a fluid at a critical value of a stress invariant, typically taken to be a yield surface defined by the von Mises criterion [10]. Prager assumed that no deformation was possible on the "solid" side of the yield surface. Oldroyd assumed that the material is an

[1] Barnes has described the paper as having been presented at the Fourth International Congress on Rheology in 1984 in a number of publications, but the paper does not appear in the Congress proceedings.

incompressible elastic (Hookean) solid before yielding, with a stress proportional to the strain, and a viscous material thereafter, with a stress that is linear in the rate of deformation. Most subsequent investigators have assumed that the solid has an infinite modulus, in which case no deformation is possible prior to yielding, and the assumption of linearity after yielding has been generalized to include power-law behavior and even viscoelasticity. The Oldroyd-Prager formulation, with a discontinuous transition between solid and liquid, is at the heart of the yield stress controversy initiated by Barnes and Walters.

In this chapter we discuss "the myth" of the yield stress and address the pre-yielding behavior. We focus on the most basic of yield-stress fluids, an aqueous Carbopol that is a simple (i.e., non-thixotropic) yield-stress fluid for which the yield stress is the same whether increasing or decreasing the shear rate in a cyclic manner [11–15]. A modern rheometer is used to examine the response of the Carbopol to a variety of deformations in order to elucidate how the mechanics of the unyielded material manifest themselves in some standard rheological tests.

The main issues that have been discussed over the past decades and that we address here are:

- Is the yield stress a flow-no flow transition? i.e., per Barnes and Walters (1985)[5], is there viscous flow below the yield stress?
- Can the yield stress be inferred by extrapolation of the flow curve to zero shear rate?
- Can the yield stress be inferred from start-up experiments?
- Are nonlinear oscillatory shear measurements a better way to infer the yield stress?

3.2 Rheological measurements

Our model yield-stress fluid is a 0.6 wt% solution of Carbopol Ultrez U10 in demineralized water (mili-Q) that has been stirred for one hour and adjusted to a pH of approximately 7 by adding drops of a 20 wt% Sodium Hydroxide (Sigma-Aldrich) solution. The Carbopol gel is homogenized by shaking and stirring manually. All rheological measurements were carried out using an Anton Paar MCR302 rheometer equipped with a 50mm-diameter cone-and-plate geometry with a 1° cone and roughened surfaces to avoid wall slip. To characterize the system, we first consider the response of the Carbopol gel to small-amplitude oscillatory shear. The storage (G') and loss (G'') moduli at a strain of 0.05 are shown in Fig. 3.1. G' is much larger than G'', more than an order of magnitude so at frequencies below 1 Hz. The unyielded material is thus clearly a viscoelastic solid, with a nearly constant storage modulus ($G' \sim \omega^{0.05}$), but the frequency dependence of the loss modulus ($G'' \sim \omega^{0.32}$ for $\omega \geq 0.8$ Hz) is weaker than that of a single Kelvin-Voigt element. We return to oscillatory forcing subsequently.

3.2.1 Extrapolation to zero shear rate: flow curves

We now turn to the measurement of flow curves. As noted by Barnes (1999), the yield stress obtained by extrapolation of the steady-state flow curve to zero shear rate depends on the shear rate range chosen. We therefore performed experiments over different shear rate ranges, both increasing and decreasing the shear rate in a shear rate ramp. Figure 3.2 shows the result of twelve independent runs with a maximum shear rate of $100s^{-1}$, six with increasing shear rate and six with

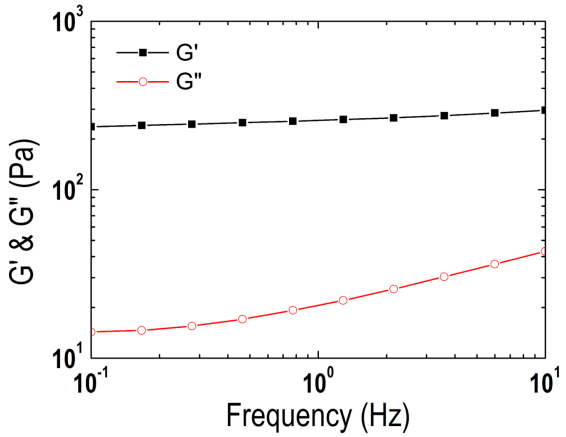

FIGURE 3.1: Linear viscoelastic response at a strain of 0.05.

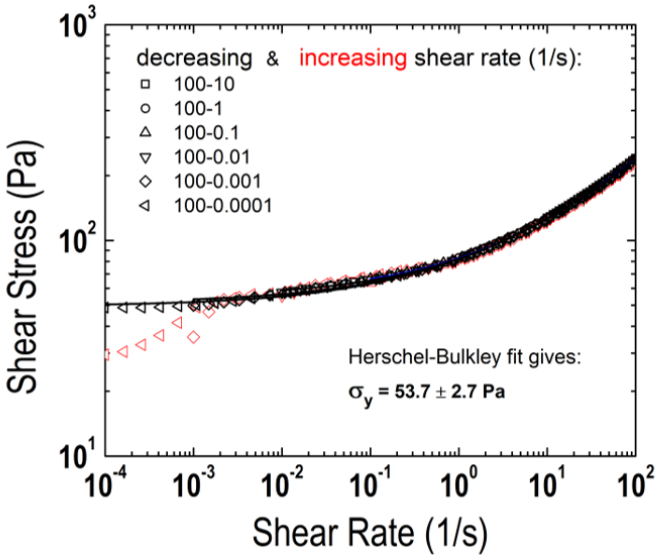

FIGURE 3.2: Flow curves for increasing (red symbols) and decreasing (black symbols) imposed shear rates. Measuring time per point is 10 seconds. The yield stresses are extrapolated from the flow curves of the decreasing imposed rates by fitting with the Herschel-Bulkley model, giving a mean yield stress of $\sigma_y = 53.7 \pm 2.7$.

decreasing shear rate, all with different minimum shear rates ranging from 10 to $10^{-4}s^{-1}$. All of the data overlap for shear rates slightly above $10^{-3}s^{-1}$ and are well fit by a Herschel-Bulkley model with a yield stress of 53.7 ± 2.7 Pa and a power-law exponent $\beta = 0.4$. Extrapolation of the flow curves obtained starting from high rates appears to give a reliable value of the yield stress. Initial data from the two lowest increasing runs, with starting shear rates of $10^{-4}s^{-1}$ and $10^{-3}s^{-1}$, respectively, lie below the curve and apparently reflect insufficient accumulated strain to reach steady flow. This is consequently a residual effect of the elasticity of the unyielded material seen in Fig. 3.2 and should not be taken into account: it is not steady state behavior.

3.2.2 Flow to no flow transition

As already mentioned, Barnes and Walters (1985) showed data obtained using a constant-stress rheometer that exhibited a Newtonian regime at stresses lower than the apparent yield stress, and they inferred from this that the yield-stress material flows with a very high viscosity below the yield stress. Møller et al. [16] subsequently showed that these high viscosities do not correspond to a steady state, and thus should be discarded. For the system studied here, the apparent

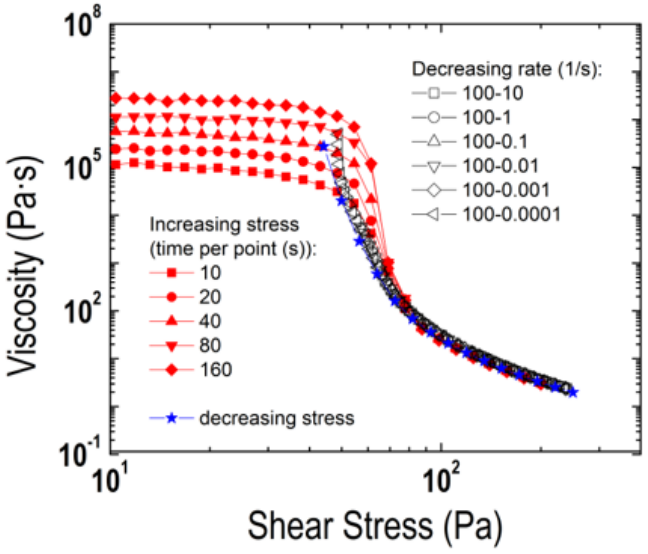

FIGURE 3.3: Apparent viscosity versus stress for increasing imposed stresses (filled red symbols), together with data at decreasing stress (blue stars) and decreasing imposed shear rates (open black symbols).

viscosity is shown in Fig. 3.3 as a function of shear stress for measurements taken at imposed constant stresses with different waiting times, plotted together with stress-controlled data at decreasing stresses and the decreasing rate data. The decreasing stress data lie on the same Herschel-Bulkley curve as the decreasing rate data. The increasing stress data show the phenomenon observed by Barnes, namely an apparent viscosity at low stresses that is nearly constant and five or more orders of magnitude larger than the high-rate viscosity of the fully yielded material. The data also show the phenomenon observed by Møller et al. [16] wherein the apparent viscosity plateau increases with increasing measuring time, in this case diverging with a power-law exponent of 0.4.

3.2.3 Startup: experiments at a constant shear rate

Figures 3.2 and 3.3 raise the question how to understand startup flows. The buildup of the apparent viscosity as a function of time at constant imposed shear rate is shown for our Carbopol sample in Fig. 3.4a. The steady-state values are the same as those shown in Fig. 3.2 at the same shear rates. It is more instructive to consider the same data replotted in Fig. 3.4b as stress versus strain. Here there is overlap up to a strain of about 0.1, then a small rate-dependent separation until all curves exhibit a sharp break to a constant stress at a strain between 0.2 and 0.3. The yield stress that is inferred from the break in slope at the lowest shear

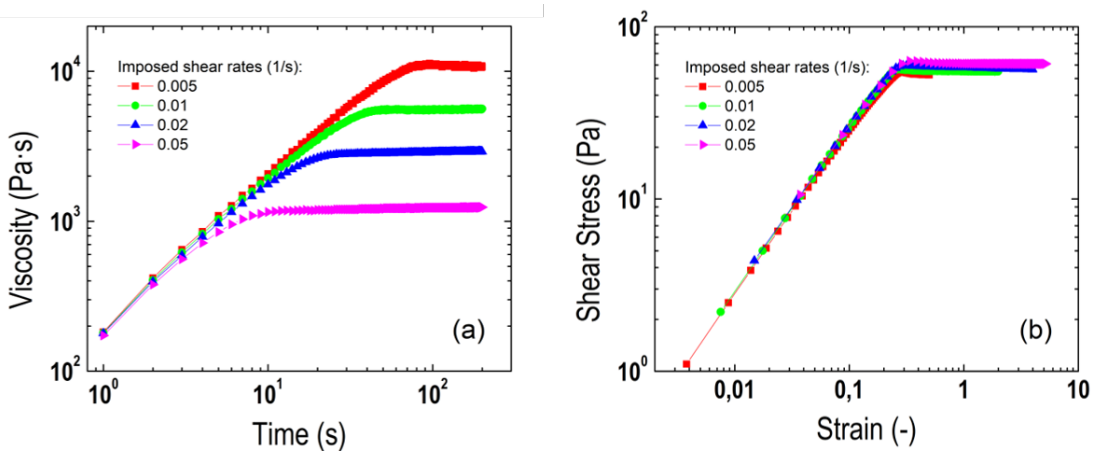

FIGURE 3.4: (a) Buildup of apparent viscosity as a function of time for four imposed shear rates. (b) The same measurements, but with the data plotted as shear stress as a function of strain.

rate is about 54Pa, which is in agreement with the value found from the flow curves in Fig. 3.2. The flow curve obtained at decreasing rates contains the same information as the start-up measurement, but the extrapolation of the flow curve minimizes the effect of finite rate on the determination of the yield stress. A stress overshoot, which is not observed in our material, could be a complicating factor in the use of a startup measurement, since the sharp transition observed in Fig. 3.4a would be absent. Observations and discussions of stress overshoot may be found, for example, in [17, 18].

3.2.4 Oscillatory measurements

We now return to oscillatory measurements, this time carried out to large strains to see the yielding strains. G' and G'' are shown in Fig. 3.5a as functions of strain for different frequencies. The material is linear up to a strain of about 0.1, after which a strain dependence is observed. The strain dependence of G' and G'' becomes significant at strains of about 0.3, with increasing dissipation and ultimately with G' becoming smaller than G'' at strains of order unity. (G' and G'' are the fundamental terms in a harmonic representation of the oscillatory stress response. Higher harmonics are negligible for this material in the strain range studied.)

The same data are plotted as total stress versus strain for different frequencies in Fig. 3.5b. This is a revealing way to visualize the data, as shown by Christopoulou et al. [19] for a colloidal glass and by us [20] for non-thixotropic yield-stress fluids

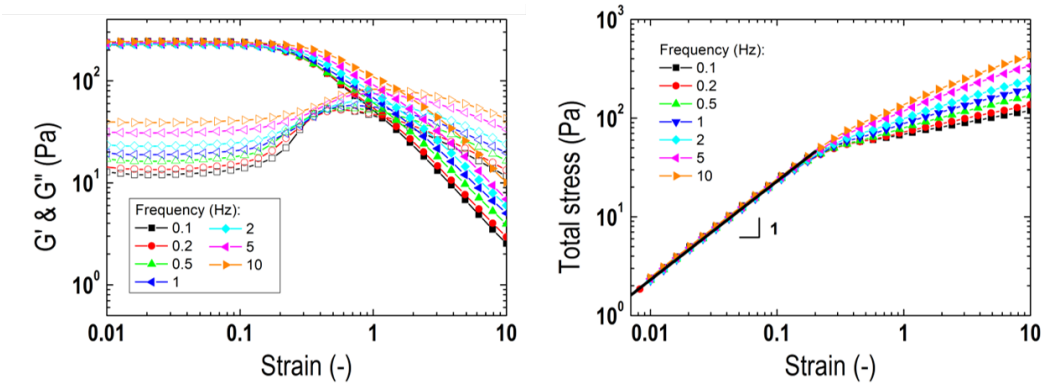

FIGURE 3.5: (a) G' and G" as functions of strain at different frequencies. (b) Total stress in oscillatory shear as a function of strain at different frequencies.

including emulsions, foam, and Carbopol. There is a linear stress-strain relation with a modulus of 235 Pa at all frequencies up to a strain of about 0.1, after which there is a small frequency dependence that accompanies the transition to a softer material. The transition strain is equal to 0.22 for all frequencies up to 1 Hz, with a small increase thereafter. The transition stress increases with increasing frequency above 1 Hz, from about 50 Pa to 72 Pa. This behavior is reminiscent of the start-up at constant shear rate data shown in Fig. 5. The increase in the transition stress with frequency mirrors the increase in G'', and it is likely that the transition is determined by the strain, with the small increase in stress as a consequence of the fact that an increasing portion of the stress is from dissipative non-recoverable strain. An ideal Oldroyd-Prager yield-stress fluid would exhibit no frequency dependence.

3.3 The effect of viscoelasticity: pre-yielding mechanism

Perhaps the main question from the above observations is how to understand the effect(s) of elasticity that become important at small deformations. We can gain some insight by considering the simplest viscoelastic models for small strains, the Kelvin-Voigt solid and the Maxwell fluid:

$$\text{Kelvin-Voigt solid:} \qquad \tau = G\gamma + \eta\dot{\gamma} \tag{3.1a}$$

$$\text{Maxwell fluid:} \qquad \tau + \lambda\dot{\tau} = \eta\dot{\gamma} \tag{3.1b}$$

The Maxwell fluid asymptotically approaches a stress equal to $\eta\dot{\gamma}$ in a constant shear rate deformation, while the response for $t \ll \lambda$ is $\tau = \gamma t$; this is qualitatively the behavior seen in Fig. 3.4, except that experimental viscosity is a (strongly) decreasing function of the shear rate. The stress for the Kelvin-Voigt model for this deformation is proportional to strain, but with an offset equal to $\eta\dot{\gamma}$, so there is no superposition in the elastic regime as seen in Fig. 3.4b.

The Maxwell fluid simply exhibits Newtonian behavior in a constant stress deformation, with no time dependence. The strain in the Kelvin-Voigt solid evolves exponentially as

$$\gamma = \frac{\tau}{G}\left(1 - e^{-Gt/\eta}\right), \tag{3.2}$$

which can be manipulated into the form

$$\frac{\tau}{\dot{\gamma}} = \eta_{app} = \eta e^{Gt/\eta}. \tag{3.3}$$

That is, the Kelvin-Voigt solid appears to have a shear viscosity in a constant stress deformation that is independent of stress and deformation rate but increases with waiting time. This is qualitatively the behavior seen for the increasing controlled stress data in Fig. 3.2 and is a qualitative explanation of the observation of a Newtonian regime below the yield stress by Barnes and Walters. The single Kelvin-Voigt element model is instructive, but it is too elementary to be of quantitative use, however.

Of course, a material cannot be roughly a Maxwell fluid in one class of deformations and roughly a Kelvin-Voigt solid in another unless there is a hidden variable in a more general formulation that interpolates between the behaviors. This is the

case in the Kinematic Hardening model used by Dimitriou and coworkers [21], for example, in which the "back stress" evolves dynamically and affects the mechanics. The back stress can be viewed as a "lambda parameter" [11] in simple shear flow and causes the location of the yield surface to adjust, depending on the deformation state, as in the general framework of the evolution of the yield stress surface for elastoviscoplastic solids that was developed by Naghdi and Srinivasa [22]. The Kinetic Hardening model can be shown to be roughly Maxwellian for small deformations at constant shear rate, and to be Maxwellian for the difference $\tau = \tau_y$ close to yielding, so it reflects the behavior seen in Fig. 3.4. Dimitrou et al. [21] have shown via a numerical simulation at constant stress that the model predicts behavior qualitatively like that shown in Fig. 3.3.

3.4 Conclusion

The significance of the description of the pre-yielded material in considering the mechanics of yield-stress fluids is highlighted. For the simple yield-stress fluid considered here the transition appears to be based on a critical strain, with the possibility of dissipative deformations in a viscoelastic solid that make the critical stress under transient conditions deformation dependent. It is clear experimentally that the appearance of a Newtonian fluid regime at stresses below the yield stress is an artifact that would be observed with the simplest viscoelastic solid representation, namely a Kelvin-Voigt solid. We have not addressed the likely failure of the Oldroyd-Prager formalism following yielding, but there is convincing evidence that a viscoelastic fluid description is necessary for materials like the Carbopol studied here. Indeed, Fraggedakis et al. [23] have employed both kinematic hardening and a viscoelastic model by Saramito [24] to describe the kinematics and settling dynamics of a spherical particle through a Carbopol gel.

Finally, we note that for the ideal (non-thixotropic) yield-stress fluid studied here, the transition in a plot of total stress versus strain in finite-amplitude oscillatory shear gives a value of the yield stress that is consistent with the yield stress obtained by extrapolation of the flow curve and the value obtained in a startup experiment, with the added information of the yield strain. This method has the advantage of eliminating artifacts associated with startup flows or extrapolation of the flow curve. Any of these methods properly used, however, can give a reliable value of the yield stress.

References

[1] R. B. Bird, G. C. Dai, and B. J. Yarusso. The rheology and flow of viscoplastic materials. *Reviews in Chemical Engineering*, 1(1):1–70, 1983.

[2] A. Yoshimura and R. K. Prud'homme. Wall slip corrections for couette and parallel disk viscometers. *Journal of Rheology*, 32(1):53–67, 1988.

[3] S. Clayton, T. G. Grice, and D. V. Boger. Analysis of the slump test for on-site yield stress measurement of mineral suspensions. *International journal of mineral processing*, 70(1):3–21, 2003.

[4] E. C. Bingham. *Fluidity and plasticity*, volume 2. McGraw-Hill Book Company, Incorporated, 1922.

[5] H. A. Barnes and K. Walters. The yield stress myth? *Rheologica acta*, 24(4):323–326, 1985.

[6] H. A. Barnes. The yield stress—a review or '$\pi\alpha\nu\tau\alpha\ \rho\varepsilon\iota$'—everything flows? *Journal of Non-Newtonian Fluid Mechanics*, 81(1):133–178, 1999.

[7] G. P. Roberts and H. A. Barnes. New measurements of the flow-curves for carbopol dispersions without slip artefacts. *Rheologica Acta*, 40(5):499–503, 2001.

[8] J. G. Oldroyd. A rational formulation of the equations of plastic flow for a bingham solid. In *Mathematical Proceedings of the Cambridge Philosophical Society*, volume 43, pages 100–105. Cambridge University Press, 1947.

[9] K. von Hohenemser and W. Prager. Über die ansätze der mechanik isotroper kontinua. *ZAMM-Journal of Applied Mathematics and Mechanics/Zeitschrift für Angewandte Mathematik und Mechanik*, 12(4):216–226, 1932.

[10] W. Prager. Introduction to the mechanics of continua. ginn and company, 1961.

[11] D. Bonn and M. M. Denn. Yield stress fluids slowly yield to analysis. *Science*, 324(5933):1401–1402, 2009.

[12] P. Møller, A. Fall, V. Chikkadi, D. Derks, and D. Bonn. An attempt to categorize yield stress fluid behaviour. *Philosophical Transactions of the Royal Society of London A: Mathematical, Physical and Engineering Sciences*, 367(1909):5139–5155, 2009.

[13] G. Ovarlez, S. Cohen-Addad, K. Krishan, J. Goyon, and P. Coussot. On the existence of a simple yield stress fluid behavior. *Journal of Non-Newtonian Fluid Mechanics*, 193:68–79, 2013.

[14] N. J. Balmforth, I. A. Frigaard, and G. Ovarlez. Yielding to stress: recent developments in viscoplastic fluid mechanics. *Annual Review of Fluid Mechanics*, 46:121–146, 2014.

[15] P. Coussot. Yield stress fluid flows: A review of experimental data. *Journal of Non-Newtonian Fluid Mechanics*, 211:31–49, 2014.

[16] P. C. F. Møller, A. Fall, and D. Bonn. Origin of apparent viscosity in yield stress fluids below yielding. *EPL (Europhysics Letters)*, 87(3):38004, 2009.

[17] R. T. Bonnecaze and J. F. Brady. Yield stresses in electrorheological fluids. *Journal of Rheology*, 36(1):73–115, 1992.

[18] P. V. Liddel and D. V. Boger. Yield stress measurements with the vane. *Journal of non-newtonian fluid mechanics*, 63(2):235–261, 1996.

[19] C Christopoulou, G. Petekidis, B. Erwin, M. Cloitre, and D. Vlassopoulos. Ageing and yield behaviour in model soft colloidal glasses. *Philosophical Transactions of the Royal Society of London A: Mathematical, Physical and Engineering Sciences*, 367(1909):5051–5071, 2009.

[20] M. Dinkgreve, J. Paredes, M. M. Denn, and D. Bonn. On different ways of measuring "the" yield stress. *Journal of Non-Newtonian Fluid Mechanics*, 238:233–241, 2016.

[21] C. J. Dimitriou, R. H. Ewoldt, and G. H. McKinley. Describing and prescribing the constitutive response of yield stress fluids using large amplitude oscillatory shear stress (laostress). *Journal of Rheology*, 57(1):27–70, 2013.

[22] P. M. Naghdi and A. R. Srinivasa. On the dynamical theory of rigid-viscoplastic materials. *The Quarterly Journal of Mechanics and Applied Mathematics*, 45(4):747–773, 1992.

[23] D. Fraggedakis, Y. Dimakopoulos, and J. Tsamopoulos. Yielding the yield-stress analysis: a study focused on the effects of elasticity on the settling of a single spherical particle in simple yield-stress fluids. *Soft matter*, 12(24):5378–5401, 2016.

[24] P. Saramito. A new constitutive equation for elastoviscoplastic fluid flows. *Journal of Non-Newtonian Fluid Mechanics*, 145(1):1–14, 2007.

Chapter 4

Different ways of measuring the yield stress

4.1 Introduction

Determining the yield stress is critical in industrial processes; the yield stress is required to know the minimum pressure needed to start a slurry in a pipeline, for example, or to know the stiffness of dairy products [1]. In some applications the yield stress determines whether air bubbles will remain trapped [2]. Yet the best way to obtain the value of the yield stress for any given material has been the subject of considerable debate (figure 4.1).

Over the years many methods have been proposed for determining the yield stress; it has been demonstrated that variations of more than one order of magnitude can arise, however, depending on the method used and the handling of the sample [4–6]. This has led, amongst other things, to the suggestion that there may be two yield stresses, dynamic and static; the former would be given by the minimum stress needed to start a flow and the latter would be the smallest stress applied before a sample stops flowing. In addition, several works, including [7–11], have proposed that yield-stress materials can be classified into two categories: 'simple' and thixotropic. For 'simple' yield-stress materials the viscosity depends only on the shear rate, and the yield stress is well defined; the yield stress can therefore be considered a material property. For thixotropic yield-stress materials the viscosity depends not only on the shear rate but also on the (deformation) history of the sample, implying that for this type of material the rheological behavior is given by a competition between aging – spontaneous build-up of some microstructure – and shear rejuvenation – breakdown of the microstructure by flow. (Ovarlez et

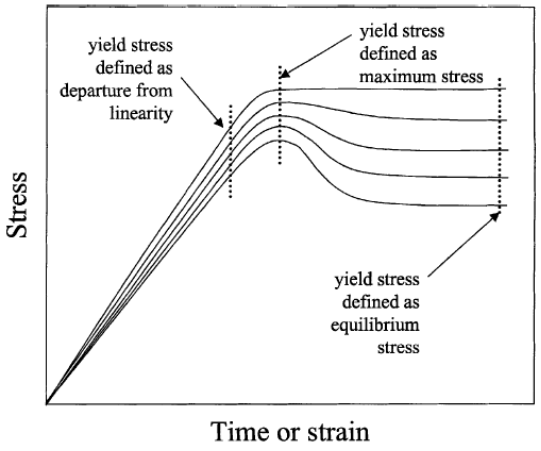

FIGURE 4.1: Sketch of the stress response in a start-up experiment at constant shear rate, with various definitions that have been used to define the yield stress [3].

al. [12] have recently suggested that a third class of yield-stress material exists in which the yield stress can be tuned by an appropriate flow history.) Very recently, Balmforth et al. [13] and Coussot [14] showed that for a 'simple' yield-stress material the static and the dynamic yield stresses are indeed the same, while for thixotropic yield-stress materials these stresses are different.

4.2 Rheological measurements

In chapter 2 a number of different types of rheological measurements are discussed. Here we compare the yield stresses and yield strains obtained from steady shear, oscillatory shear, stress growth, and creep experiments. The pros and cons of different tests are discussed and an overview is given of the range of values that are found from the different measurements.

Our measurements were carried out using a controlled-shear-stress rheometer (CSS, Physica MCR302) and a controlled-shear-rate rheometer (CSR, ARES), both with a 50mm-diameter cone-and-plate geometry with a 1° cone and roughened surfaces to avoid wall slip [7, 15]. Before performing any experiments, samples were pre-sheared at a shear rate of 100 s^{-1} for 30 s, followed by a rest period of 30 s in order to create a controlled initial state in the samples [14, 16]. The static normal stresses in all samples were zero after the rest period.

The materials that were used are Castor oil-in-water emulsions stabilized with 1wt% SDS (mobile emulsion), Carbopol gels, a commercial hair gel, and a shaving foam. The emulsions and carbopol are prepared as described in chapter 2. The hair gel was a commercial product (Albert Heijn). This is basically a Carbopol gel in which the pH is adjusted by using triethanolamine rather than NaOH. The foam was a commercial shaving foam, Gillette Foamy Regular. The liquid volume fraction of the shaving foam was $9.2 \pm 0.5\%$, with a mean bubble radius of about 18 micrometers, in fair agreement with previously reported data on the same brand [17].

4.2.1 Steady shear measurements

The steady shear experiments were performed with the CSR rheometer by carrying out shear rate sweeps from $100 s^{-1}$ to $1 \times 10^{-3} s^{-1}$ (to 10^{-4} for the oil-in-water

emulsions), obtaining flow curves that were fit to the Herschel-Bulkley model. (High-to-low rate sweeps are preferable for systems that exhibit no thixotropy, because short-term transients caused by the transition from viscoelastic solid to mobile liquid at fluidization are avoided.) Flow curves obtained for all our simple yield-stress materials are shown in Figure 4.2. The flow curves are clearly approaching plateaus at low shear rates within the range at which data were obtained, and all can be fit to the Herschel-Bulkley model. (The model fits are based on the range of accessible shear rates, and it is possible that the power-law index might change if higher rates could be explored, but our interest is in the fit to the yield stress, which should be insensitive to rates above $100s^{-1}$.)

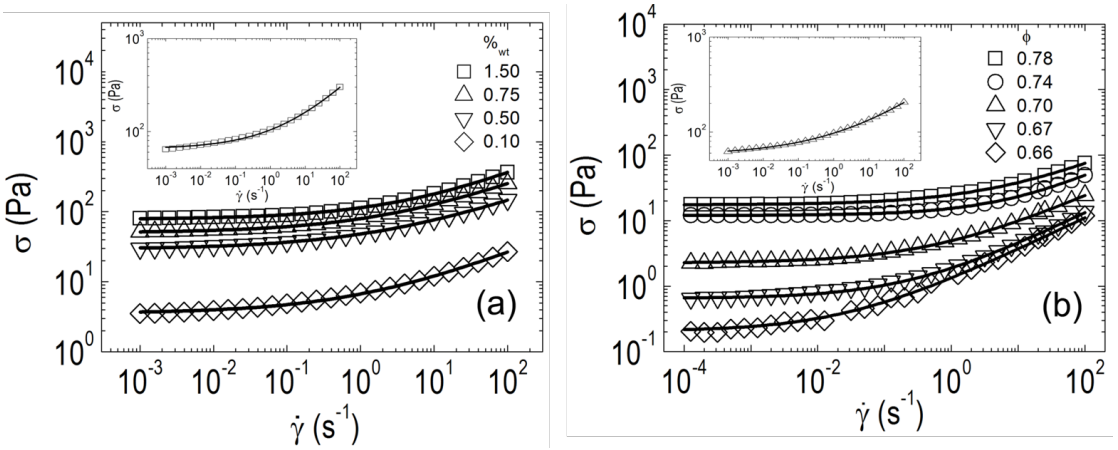

FIGURE 4.2: Flow curves obtained by means of steady shear measurements. (a) Carbopol at different mass concentrations. Inset: Hair gel. (b) Emulsions with different internal volume fractions. Inset: foam. Lines are the fits of the flow curves to the Herschel-Bulkley model.

4.2.2 Oscillatory measurements

The oscillatory measurements were performed with the CSS rheometer by carrying out shear stress sweeps from 1×10^{-2} Pa to 5×10^{2} Pa at a constant frequency of 1Hz, generating curves of G' and G'' as functions of σ or γ. The linear viscoelastic storage modulus G' is insensitive to frequency in this range for all materials studied; the linear loss modulus G'' is always much smaller than G' and is insensitive to frequency for all but the emulsion, where there is a transition from a frequency dependence of about $\omega^{1/4}$ to $\omega^{1/2}$ in the neighborhood of 1 Hz. (See Supplementary Material.) Curves of G' and G'' as functions of σ and γ at a frequency of 1 Hz are shown in Figures 4.3 and 4.4, respectively. At low amplitudes, G' and G'' are independent of stress magnitude and represent the entire elastic or dissipative

contributions, respectively. Higher harmonics appear in the LAOS measurements at larger amplitudes, and the coefficients of the harmonics become strain dependent. The coefficients of the fundamental (the frequency of the stress or strain input) are still conventionally called G' and G'', and we follow that convention here, but these functions no longer represent the complete elastic or dissipative portions of the stress in the nonlinear regime. Treatments of the nonlinear data are discussed in, for example, [18–22].

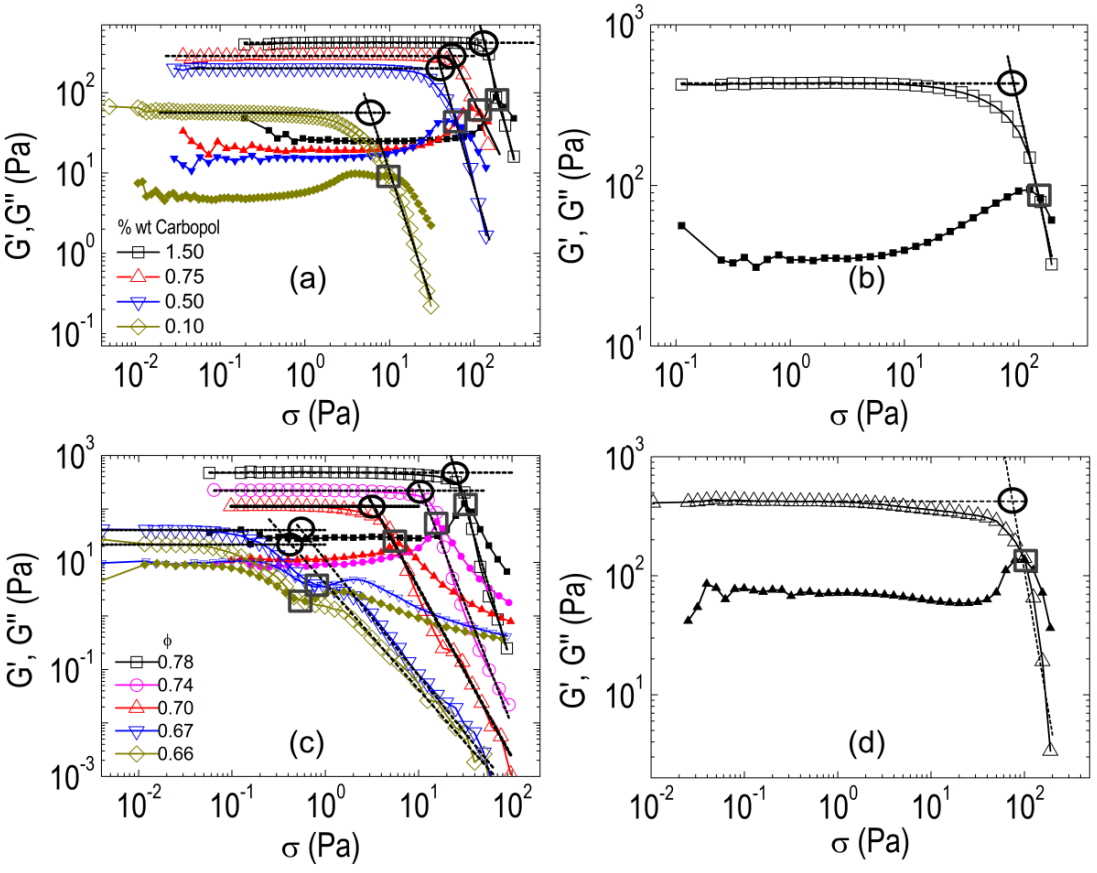

FIGURE 4.3: Storage (G') and loss (G'') moduli as functions of σ for (a) Carbopol samples, (b) hair gel, (c) emulsions, and (d) foam. Open symbols correspond to G', filled symbols to G''. Black lines are power-law fits of the behavior well above yield point, whose intersection with the horizontal line through the linear G' data is shown by the black circles. Gray squares show σ at the characteristic modulus, $G' = G''$.

Now, the question is how to extract the yield stress from these data? As noted by [23], *"There is no unique and rigorously motivated criterion allowing a yield stress to be determined from oscillatory data."* For example, [24–26] define the yield stress as the stress for which $G' = G''$ (the characteristic modulus), where the viscous and the elastic contributions to the fundamental are equal; at higher

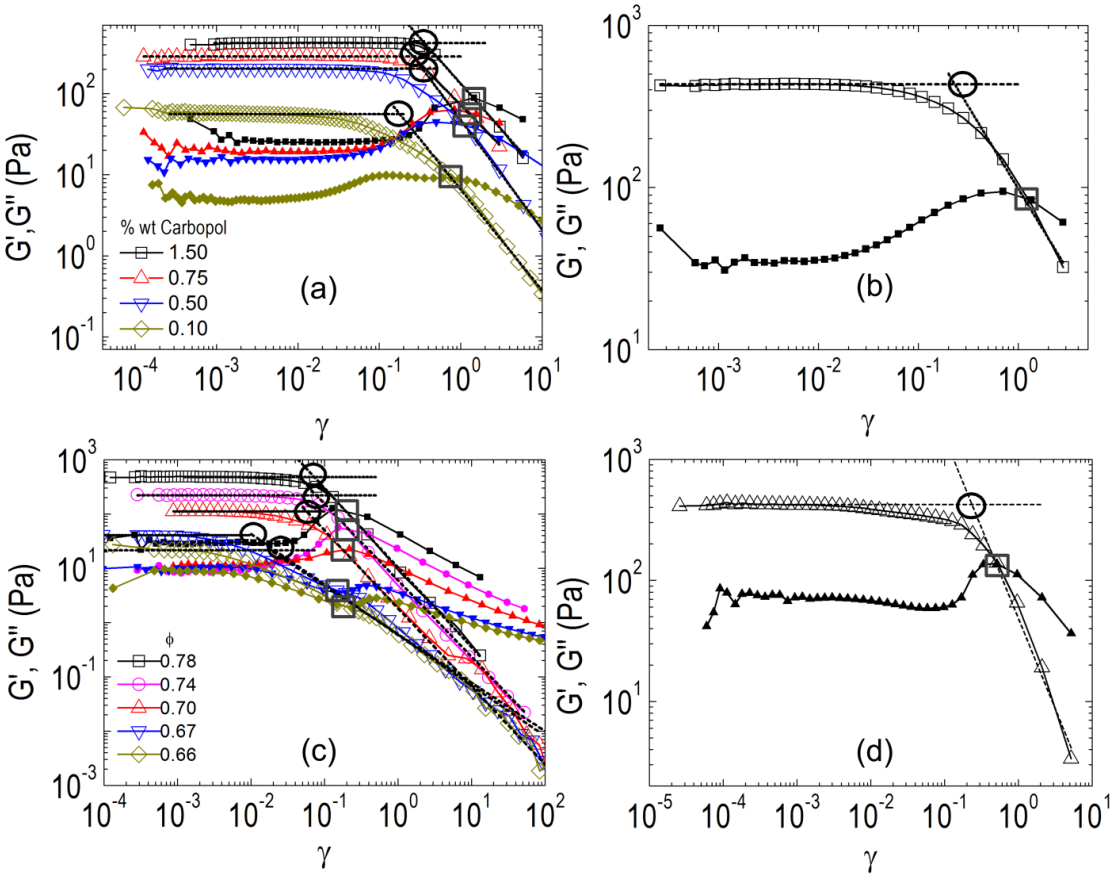

FIGURE 4.4: Storage (G') and loss (G'') moduli as functions of γ for (a) Carbopol samples, (b) hair gel, (c) emulsions, and (d) foam. Open symbols correspond to G', and filled symbols correspond to G''. Black lines are power-law fits of the behavior well above the yield point, whose intersection with the horizontal line through the linear G' data is shown by the black circles. Gray squares show γ at the characteristic modulus, $G' = G''$.

stresses the viscous contribution will dominate the elastic, indicating that the material is indeed flowing. The location of the characteristic modulus is indicated by gray squares in Figures 4.3 and 4.4. The yield stress and the yield strain can also be defined from this approach by the intersection of the horizontal line representing the behavior of G' well below the yielding point with the power-law equation representing the behavior of G' well above the yielding point; this method was used by [23] for determining the yield stress of foams. These intersections are shown as dark circles in Figures 4.3 and 4.4. We also re-plot the oscillatory data shown in Figures 4.3 and 4.4 as σ vs. γ (Figure 4.5). The data are linear at small strains with a unit slope on log-log coordinates; the magnitude of the line corresponds to G' in the linear regime. ($G' \gg G''$ in this regime, so the total stress is comprised mostly of the elastic component.) Following [Mason et al.

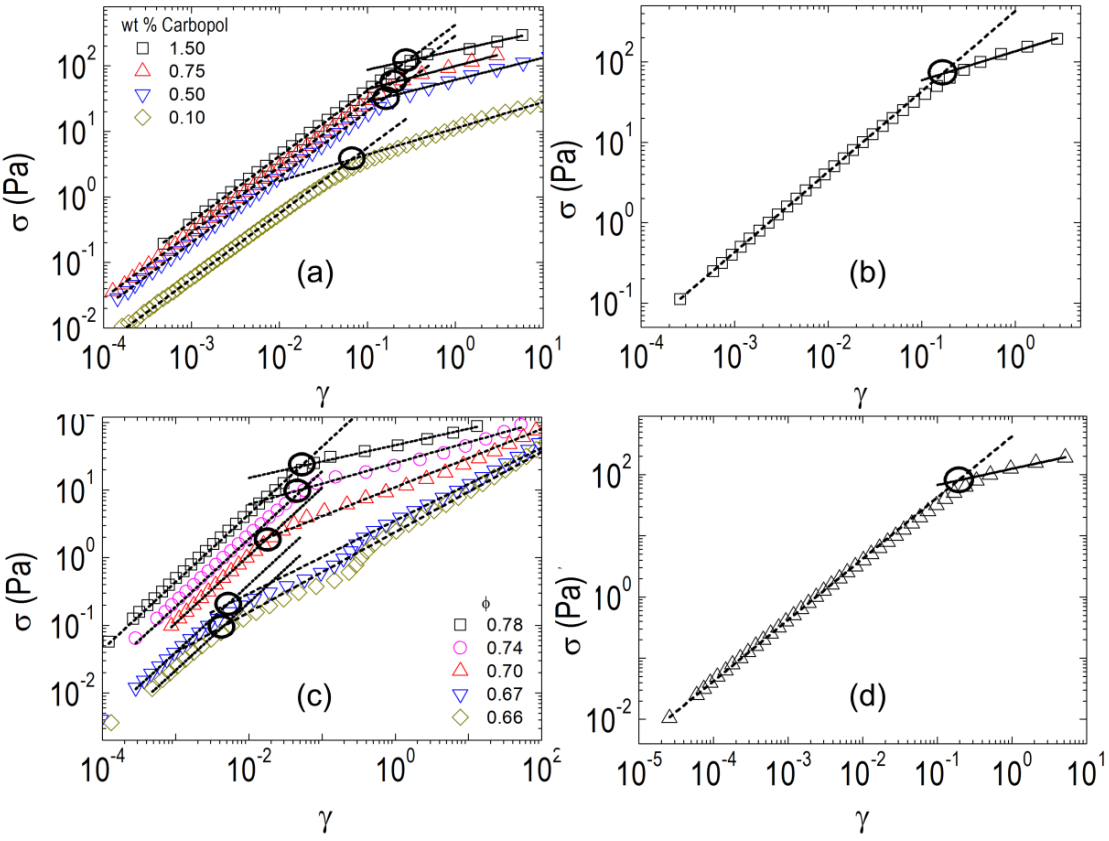

FIGURE 4.5: σ vs γ obtained from the oscillatory measurements (same data shown in Fig. 2 and 3) for (a) Carbopol samples, (b) hair gel, (c) emulsions, and (d) foam. Lines are power-law fits of the behavior well above and well below the yielding point, whose intersection is shown by the black circles.

(1996)], [27], and [28] for similar systems, σ_y and γ_y can then be obtained from the intersection of the line at low strains and a power law drawn through the data at high strains.

These methods employing oscillatory data are empirical and are all based on departures from the linear viscoelastic regime. Only the use of the characteristic modulus is unambiguous; the other methods require extrapolations that will depend on the quality of data and the range selected for fitting a power law. The transitions in the plots of σ vs. γ in Fig. 4.5 appear sharper to the eye than those of G' versus σ or γ in Figs. 4.3 and 4.4, respectively. One interesting feature of these data for most systems is that the intersection of G' and G'' as functions of σ occurs at or near the maximum in G''; i.e., the maximum value of G'' is very close to the characteristic modulus.

4.2.3 Stress growth experiments

The stress growth experiments were performed with the CSR rheometer by imposing a constant shear rate $\dot{\gamma} = 10^{-2}s^{-1}$ and recording σ for 300s, equivalent to a total deformation $\gamma = 3$. Finally, the creep experiments were carried out with the CSS rheometer with increasing imposed stresses starting near to but below the expected yield stress, as determined by the other measurements. The creep experiments were carried out at a later date, using new samples prepared according to the same protocols. The evolution of σ as a function of γ at an imposed strain rate $\dot{\gamma} = 10^{-2}s^{-1}$ is shown in Figure 4.6. The stress initially grows with increasing strain in what is an elastic or viscoelastic solid response, followed by a transition to a steady stress that characterizes a fluid response; in some cases there is a stress overshoot. Here, too, there are a number of ways in which the yield stress and yield strain can be defined [3]: (i) the highest σ(or corresponding γ) at which the response is still elastic, (ii) the maximum σ (or corresponding γ), or (iii) the stress at which a steady state is achieved.

Defining the yield point as the highest stress at which the response is still elastic is ambiguous. One approach is to choose the point at which the stress-strain response deviates from linearity, but this depends on the time resolution and the imposed rate. Furthermore, the deviation from linearity might simply be a transition to a non-linear elastic response, or it might reflect viscoelasticity; see, for example, [29]. We choose to define the deviation from an elastic response empirically as the intersection between the line with unit slope on logarithmic coordinates that is tangent to the data at low deformations and the horizontal steady-state stress. The former should have a magnitude corresponding to G', although it is clear from the plots that the line does not pass through the data at the lowest strains. The use of the maximum in the stress-strain curve to determine both σ_y and γ_y, to the contrary, provides a precise value, but this value is highly dependent on the imposed strain rate and waiting time, as reported by [30–33]. Additionally, a stress overshoot is not always present, as demonstrated by the experiments presented here, where a stress overshoot is only observed for samples with more than 0.5 wt% Carbopol . Finally, defining σ_y by the steady state gives a precise value of the yield stress, although the value may be dependent on the strain rate, but then the determination of the yield strain is no longer possible.

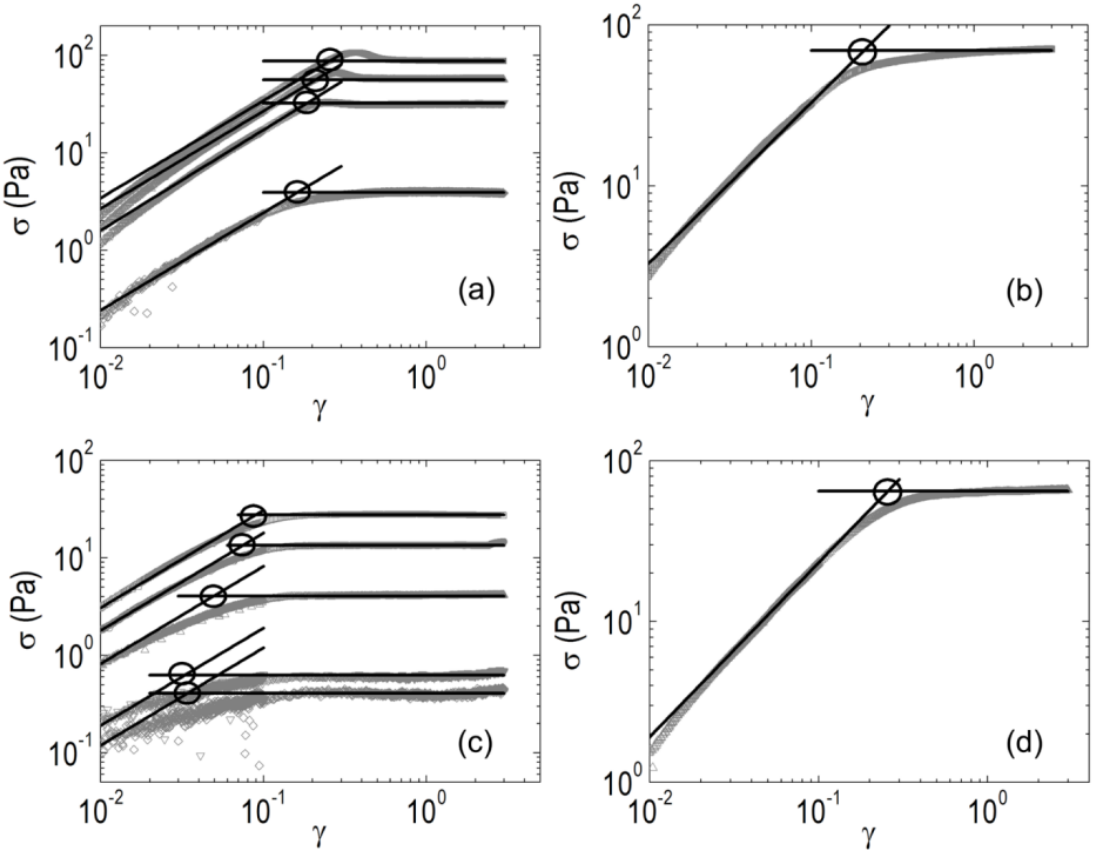

FIGURE 4.6: σ as a function of γ at an imposed $\dot{\gamma} = 1 \times 10^{-2} s^{-1}$ for (a) Carbopol samples with wt%-Carbopol: 1.5, 0.75, 0.50, and 0.10 (top to bottom), (b) hair gel, (c) emulsions with $\phi = 0.78$, 0.74, 0.70, 0.67, and 0.66 (top to bottom), and (d) foam.

4.2.4 Creep experiments

Creep data are usually shown as creep compliance $J(t) = \gamma(t)/\sigma$ versus time, where $\gamma(t)$ is the time-dependent shear strain and sigma the constant imposed stress. Creep experiments were carried out within a stress range determined from the results of the previous experiments. In principle, J will go to a constant value at imposed stresses below the yield stress, while it will continue to grow in the liquid state at stresses beyond yielding. Creep compliance data are shown in Figure 4.7 for 0.75 wt% Carbopol, the hair gel, 0.78 vol% emulsion, and the foam. The horizontal arrows on the figures indicate the yield stress from the Herschel-Bulkley fit to the steady shear data. The distinction between unyielded and flowing behavior is clear for the Carbopol and the emulsion. It is difficult to identify the location of the change of curvature for the hair gel, although the curvature is clearly different at the lowest and highest stresses. [34] noted in creep

measurements on a different Carbopol that there appears to be an intermediate regime in which there is no stable steady flow over the course of the experiment, and it is possible that this behavior is reflected in the hair gel.) The foam data are difficult to interpret because of the upturn at even the small stresses at long times, perhaps because of a change in structure in the unyielded foam; the yield stress is likely given by the apparent loss of an inflection point in the curve. Overall, conducting creep measurements to find a good estimate of the yield stress appears to be rather inefficient; not only is a priori knowledge of the approximate yield stress required, but the method appears to be more sensitive to structural changes during the long time required at a constant stress relative to, for example, a Herschel-Bulkley fit.

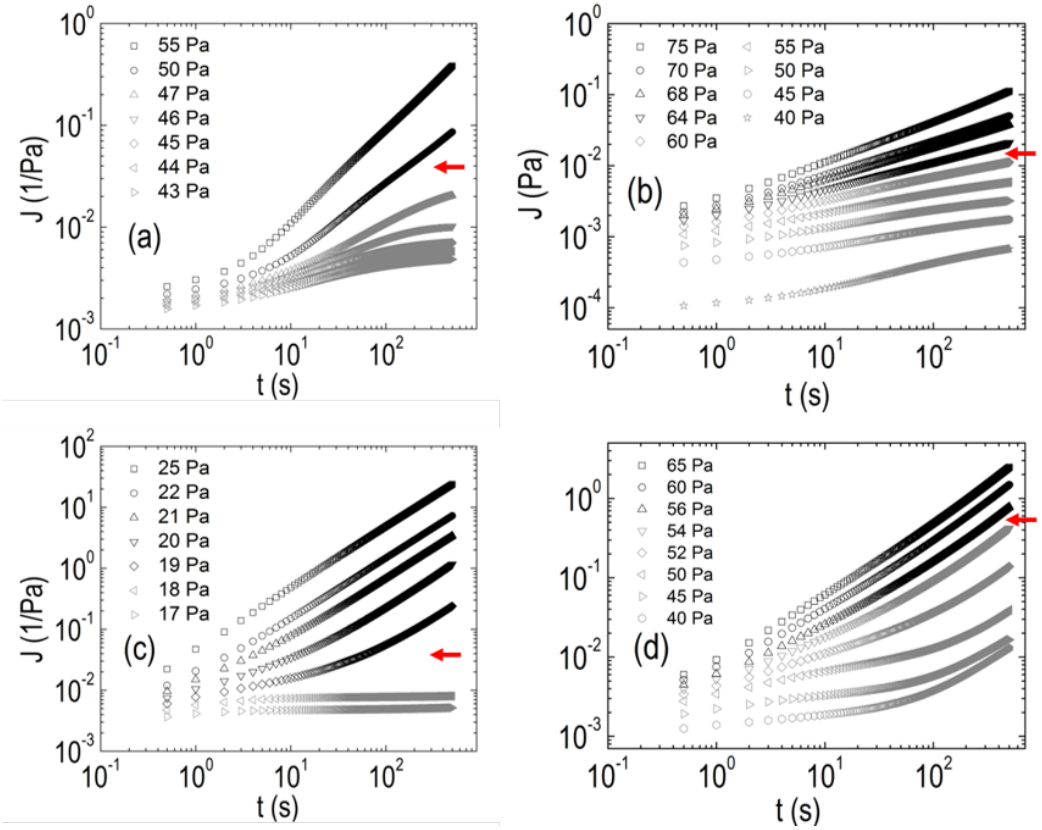

FIGURE 4.7: J vs t obtained from creep measurements for (a) carbopol sample of 0.75wt%, (b) hair gel, (c) emulsion of 78% vol of oil, and (d) foam. The horizontal arrows indicate the yield stress from the Herschel-Bulkley fit to the steady shear data.

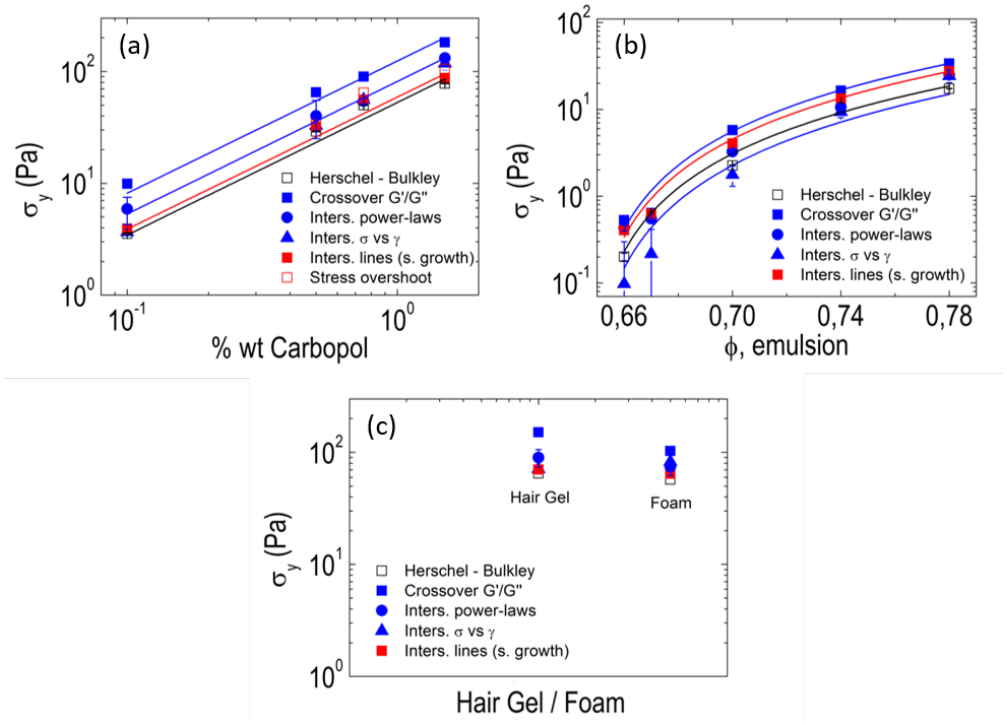

FIGURE 4.8: Yield stress values from different methods for (a) Carbopol, (b) emulsions, and (c) hair gel and foam. Black symbols are the values obtained from steady shear experiments, in which flow curves were fit to the Herschel-Bulkley model. Blue symbols are values obtained from the oscillatory measurements. Red symbols are values obtained from the stress growth experiments. Lines are $\sigma_y \sim$(wt% Carbopol)$^{1.18}$ and $\sigma_y \sim (\Delta\phi)^2$, with $\phi_c = 0.645$, for the Carbopol and emulsion, respectively.

4.3 Comparing values obtained from different methods

4.3.1 Yield stress

Figure 4.8 shows that different methods do indeed give different yield stress values (error bars correspond to statistical error limits from the fitting parameters). Values obtained from the crossover of G' and G'' (characteristic modulus) are the highest for all cases; this is not surprising, as there is already significant viscous dissipation by the time that $G' = G''$. Yield stresses obtained from the crossover of G' and G'' are about twice the values obtained from the Herschel-Bulkley model, which are generally the lowest and are close to the transitions seen in the creep experiments for the Carbopol and emulsion. Values obtained from the stress-strain plot derived from the oscillatory data are typically close to the Herschel-Bulkley

values, and, as discussed subsequently, these two methods appear to give the most reliable values of the yield stress among those considered here. (This conclusion is consistent with the observation of [Christopoulou et al. (2009)], who identified the intersection of the stress-strain lines as the yield point and the intersection of G' and G'' as the onset of "complete fluidization".) The scaling with concentration is the same for all methods of measurement, however; $\sigma_y \sim (\text{wt\% Carbopol})^{1.18}$ for the Carbopol gels, while, $\sigma_y \sim (\phi - \phi_c)^2$, with $\phi_c = 0.645$, for the emulsion. Previous work [Nordstrom et al. (2010)] has shown similar scaling of σ_y with $\Delta\phi$ for similar systems. The value of $\phi_c = 0.645$ has previously been reported by [Paredes et al. (2013)] for the same system, and is close to the expected value for random close packing, $\phi_{RCP} \approx 0.64$ [35–37]; above ϕ_c emulsions jam and a yield stress appears.

4.3.2 Yield strain

Yield strain values obtained with different methods are different, in some cases by an order of magnitude, as shown in Figure 4.9 (statistical variations are within the symbols). Yield strains obtained from the characteristic modulus are the highest; as already noted for the yield stress, this is not surprising, as equality of G' and G'' indicates that there has already been a significant amount of dissipation, so the material must have yielded prior to the strain at which $G' = G''$. The values obtained from the stress growth experiments in Fig. 5 are dependent on the particular choice of fitting the low-strain data, and the lines used in all cases have magnitudes equal to only about 80% of G', possibly because of a finite rate effect. Yield strains obtained from the intersection of power-law equations describing the behaviors at low and high γ in oscillatory flow (Figure 4.5) are nearly always the lowest; these strains correspond to the yield stresses that are consistent with the fits to the Herschel-Bulkley equation and are probably closest to the true yield strain among the methods studied. Figure 8 shows that γ_y scales with the amount of polymer for the Carbopol, and with $(\phi - \phi_c) = \Delta\phi$, the distance to jamming, for the emulsion, with $\phi_c = 0.645$, as noted above. These scalings are shown in Table 4.1, and it is evident that the scalings are highly dependent on the measuring method; indeed, the results can be different if the same data are plotted in different ways, as can be seen by comparing the yield strains from oscillatory data obtained by plotting G' vs. γ and σ vs. γ.

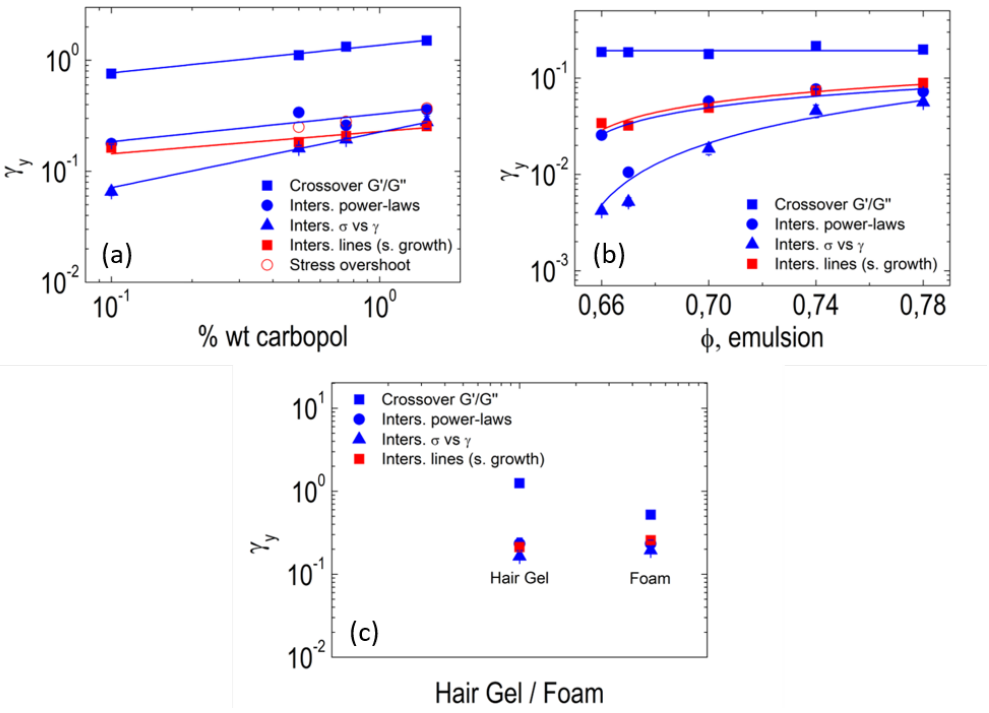

FIGURE 4.9: Yield strain values obtained from different methods for (a) Carbopol, (b) emulsions, and (c) hair gel and foam. Blue symbols are values obtained from the oscillatory measurements. Red symbols are values obtained from the stress growth experiments. Lines represent scaling of σ_y with wt% Carbopol for the Carbopol or $\Delta\phi$ for the emulsions.

TABLE 4.1: Scaling of the yield strain with wt% Carbopol for Carbopol samples and ϕ for emulsions.

Rheological measurements	**Scaling of γ_y**	
	Carbopol	**Emulsion**
Oscillatory:		
Crossover G' and G" (fig 4.4)	$\sim(\text{wt}\%)^{0.25}$	$\sim \Delta\phi^{0}$
Intersect power-law equations, G' vs. γ (fig 4.4)	$\sim(\text{wt}\%)^{0.25}$	$\sim \Delta\phi^{0.50}$
Intersect power-law equations, σ vs. γ (fig 4.5)	$\sim(\text{wt}\%)^{0.50}$	$\sim \Delta\phi^{1.0}$
Stress growth:		
Intersect lines σ vs. γ (fig 4.6)	$\sim(\text{wt}\%)^{0.20}$	$\sim \Delta\phi^{0.5}$
Stress overshoot (fig 4.6)	$\sim(\text{wt}\%)^{0.37}$	-

4.4 Synthesis and conclusion

The above results clearly show that both the apparent yield strain and the yield stress are dependent on the method and criteria used for determining their values. In many of the cases studied here the properties determined in different ways exhibit the same scaling with respect to the dispersed phase, although with different magnitudes.

For the simple yield-stress fluids, the value defined by a Herschel-Bulkley fit to a shear-rate sweep consistently gave the lowest yield stress among all methods used. In most cases the intersection between pre-yield and post-yield asymptotes of a stress vs strain curve constructed from oscillatory data gave similar results, and this method consistently gave the lowest value of the yield strain. These values are consistent with each other and, where a valid comparison may be made, with data from the creep experiment. The stress versus strain curve constructed from the oscillatory data generally showed a sharp transition from the linear viscoelastic regime to a power-law response that extended well into the nonlinear regime of substantial dissipation and flow, so it is likely that this transition is close to the point of initiation of flow and provides a good estimate of the yield stress. Hence the Herschel-Bulkley fit and the stress-strain curve from the oscillatory data appear to be the most reliable values among the various methods employed on conventional rheometers, although the former depends on reaching a low enough shear rate and sufficient waiting time to enable reliable extrapolation. The yield stress obtained from stress growth is ambiguous and depends on the time resolution and imposed rate. Generally, determining the yield stress from oscillatory measurements is ambiguous because of the fitting the slopes to find the intersection. The intersection of the G' and G'' curves as functions of strain (the *characteristic modulus*) is unambiguous but consistently gave the highest values of the yield stress and yield strain; this is to be expected, since the material must have already yielded in order to experience the observed increase in the dissipative modulus G'', and this cannot be considered to be a valid estimate of the yield stress. (In fact, the characteristic modulus was usually close to the maximum of G'' as a function of strain, which is an observation that deserves further exploration.) Table 4.2 gives an overview of the concluding remarks. The use of a stress growth curve gives yield stress and yield strain values in most cases that are intermediate, which is undoubtedly a consequence of the ambiguity of the method when there is significant curvature prior to yielding, and this does not appear to be a good method for determining either the static or dynamic yield stress. The same conclusion can be reached for the use of the intersection of high- and low-strain values of G' in the LAOS experiment.

TABLE 4.2: Overview of rheological measurements and concluding remarks in determining the yield stress.

Rheological measurements	**Ambiguity**	**Remark**
Oscillatory:		
Crossover G' and G" (fig 4.3)	No	High σ_y, past yielding?
Intersect power-law equations, G' vs. γ (fig 4.4)	Slope	Definition of crossover point?
Intersect power-law equations, σ vs. γ (fig 4.5)	Slope	Definition of crossover point?
Stress growth:		
Intersect lines σ vs. γ (fig 4.7)	Slope	Depends on $\dot{\gamma}$ and waiting time
Stress overshoot (fig 4.6)	Still elastic?	Not always present
Herschel-Bulkley (fig 3.2)	No	Apply low enough $\dot{\gamma}$
Creep (fig 4.7)	No	Inefficient

References

[1] Q. D. Nguyen and D. V. Boger. Measuring the flow properties of yield stress fluids. *Annual Review of Fluid Mechanics*, 24(1):47–88, 1992.

[2] P. C. F. Møller, J. Mewis, and D. Bonn. Yield stress and thixotropy: on the difficulty of measuring yield stresses in practice. *Soft matter*, 2(4):274–283, 2006.

[3] H. A. Barnes and Q. D. Nguyen. Rotating vane rheometry—a review. *Journal of Non-Newtonian Fluid Mechanics*, 98(1):1–14, 2001.

[4] A. E. James, D. J. A. Williams, and P. R. Williams. Direct measurement of static yield properties of cohesive suspensions. *Rheologica Acta*, 26(5):437–446, 1987.

[5] L. Zhu, N. Sun, K. Papadopoulos, and D. De Kee. A slotted plate device for measuring static yield stress. *Journal of Rheology*, 45(5):1105–1122, 2001.

[6] Q. D. Nguyen, T. Akroyd, D. C. De Kee, L. Zhu, et al. Yield stress measurements in suspensions: an inter-laboratory study. *Korea-Australia Rheology Journal*, 18(1):15–24, 2006.

[7] P. C. F. Møller, A. Fall, and D. Bonn. Origin of apparent viscosity in yield stress fluids below yielding. *EPL (Europhysics Letters)*, 87(3):38004, 2009.

[8] P. Møller, A. Fall, V. Chikkadi, D. Derks, and D. Bonn. An attempt to categorize yield stress fluid behaviour. *Philosophical Transactions of the Royal Society of London A: Mathematical, Physical and Engineering Sciences*, 367(1909):5139–5155, 2009.

[9] D. Bonn and M. M. Denn. Yield stress fluids slowly yield to analysis. *Science*, 324(5933):1401–1402, 2009.

[10] A. Fall, J. Paredes, and D. Bonn. Yielding and shear banding in soft glassy materials. *Physical review letters*, 105(22):225502, 2010.

[11] G. Ovarlez, S. Cohen-Addad, K. Krishan, J. Goyon, and P. Coussot. On the existence of a simple yield stress fluid behavior. *Journal of Non-Newtonian Fluid Mechanics*, 193:68–79, 2013.

[12] G. Ovarlez, L. Tocquer, F. Bertrand, and P. Coussot. Rheopexy and tunable yield stress of carbon black suspensions. *Soft Matter*, 9(23):5540–5549, 2013.

[13] N. J. Balmforth, I. A. Frigaard, and G. Ovarlez. Yielding to stress: recent developments in viscoplastic fluid mechanics. *Annual Review of Fluid Mechanics*, 46:121–146, 2014.

[14] P. Coussot. Yield stress fluid flows: A review of experimental data. *Journal of Non-Newtonian Fluid Mechanics*, 211:31–49, 2014.

[15] V. Bertola, F. Bertrand, H. Tabuteau, D. Bonn, and P. Coussot. Wall slip and yielding in pasty materials. *Journal of Rheology*, 47(5):1211–1226, 2003.

[16] H. A. Barnes. Thixotropy—a review. *Journal of Non-Newtonian fluid mechanics*, 70(1-2):1–33, 1997.

[17] M. U. Vera, A. Saint-Jalmes, and D. J. Durian. Scattering optics of foam. *Applied optics*, 40(24):4210–4214, 2001.

[18] R. H. Ewoldt, A. E. Hosoi, and G. H. McKinley. New measures for characterizing nonlinear viscoelasticity in large amplitude oscillatory shear. *Journal of Rheology*, 52(6):1427–1458, 2008.

[19] K. Hyun, M. Wilhelm, C. O. Klein, K. S. Cho, J. G. Nam, K. H. Ahn, S. J. Lee, R. H. Ewoldt, and G. H. McKinley. A review of nonlinear oscillatory shear tests: Analysis and application of large amplitude oscillatory shear (laos). *Progress in Polymer Science*, 36(12):1697–1753, 2011.

[20] S. A. Rogers, B. M. Erwin, D. Vlassopoulos, and M. Cloitre. A sequence of physical processes determined and quantified in laos: Application to a yield stress fluid. *Journal of Rheology*, 55(2):435–458, 2011.

[21] M. J. Armstrong, A. N. Beris, S. A. Rogers, and N. J. Wagner. Dynamic shear rheology of a thixotropic suspension: Comparison of an improved structure-based model with large amplitude oscillatory shear experiments. *Journal of Rheology*, 60(3):433–450, 2016.

[22] B. C. Blackwell and R. H. Ewoldt. A simple thixotropic–viscoelastic constitutive model produces unique signatures in large-amplitude oscillatory shear (laos). *Journal of Non-Newtonian Fluid Mechanics*, 208:27–41, 2014.

[23] F. Rouyer, S. Cohen-Addad, and R. Höhler. Is the yield stress of aqueous foam a well-defined quantity? *Colloids and Surfaces A: Physicochemical and Engineering Aspects*, 263(1):111–116, 2005.

[24] F. Renou, J. Stellbrink, and G. Petekidis. Yielding processes in a colloidal glass of soft star-like micelles under large amplitude oscillatory shear (laos). *Journal of Rheology*, 54(6):1219–1242, 2010.

[25] C. Perge, N. Taberlet, T. Gibaud, and S. Manneville. Time dependence in large amplitude oscillatory shear: A rheo-ultrasonic study of fatigue dynamics in a colloidal gel. *Journal of Rheology*, 58(5):1331–1357, 2014.

[26] C. Kugge, N. Vanderhoek, and D. W. Bousfield. Oscillatory shear response of moisture barrier coatings containing clay of different shape factor. *Journal of colloid and interface science*, 358(1):25–31, 2011.

[27] A. Saint-Jalmes and D. J. Durian. Vanishing elasticity for wet foams: Equivalence with emulsions and role of polydispersity. *Journal of Rheology*, 43(6):1411–1422, 1999.

[28] C. Christopoulou, G. Petekidis, B. Erwin, M. Cloitre, and D. Vlassopoulos. Ageing and yield behaviour in model soft colloidal glasses. *Philosophical Transactions of the Royal Society of London A: Mathematical, Physical and Engineering Sciences*, 367(1909):5051–5071, 2009.

[29] M. M. Denn and D. Bonn. Issues in the flow of yield-stress liquids. *Rheologica acta*, 50(4):307–315, 2011.

[30] J. R. Stokes and J. H. Telford. Measuring the yield behaviour of structured fluids. *Journal of Non-Newtonian Fluid Mechanics*, 124(1):137–146, 2004.

[31] S. A. Rogers, P. T. Callaghan, G. Petekidis, and D. Vlassopoulos. Time-dependent rheology of colloidal star glasses. *Journal of Rheology*, 54(1):133–158, 2010.

[32] T. Divoux, C. Barentin, and S. Manneville. Stress overshoot in a simple yield stress fluid: An extensive study combining rheology and velocimetry. *Soft Matter*, 7(19):9335–9349, 2011.

[33] C. P. Amann, M. Siebenbürger, M. Krüger, F. Weysser, M. Ballauff, and M. Fuchs. Overshoots in stress-strain curves: Colloid experiments and schematic mode coupling theory. *Journal of Rheology*, 57(1):149–175, 2013.

[34] H. Tabuteau, P. Coussot, and J. R. de Bruyn. Drag force on a sphere in steady motion through a yield-stress fluid. *Journal of rheology*, 51(1):125–137, 2007.

[35] J. D. Bernal and J. Mason. Packing of spheres: co-ordination of randomly packed spheres. *Nature*, 188(4754):910–911, 1960.

[36] E. R. Nowak, J. B. Knight, E.i Ben-Naim, H. M. Jaeger, and S. R. Nagel. Density fluctuations in vibrated granular materials. *Physical Review E*, 57(2):1971, 1998.

[37] D. A. Weitz. Packing in the spheres. *Science*, 303(5660):968–969, 2004.

Chapter 5

Stability of Laponite-stabilized Pickering emulsions under shear

5.1 Introduction

Emulsions are of great importance for the cosmetic, oil and food industry. Most frequently, emulsions are stabilized with surfactants [1], however these are not always stable under shear [2] and alternative stabilization mechanisms have therefore being intensively explored in recent years [3]. Amongst these, particle stabilized emulsions have attracted much attention, notably for their high stability and possible role in food applications, in the design of more environmentally friendly agricultural formulations and for the realization of high internal phase emulsions [4]. This type of emulsion is called Pickering emulsion; particles are adsorbed at the oil-water interface with a high stabilization energy and are believed to form a continuous layer around the dispersed drops impeding coalescence [5] and hence stabilizing the emulsion. Such Pickering emulsions are stabilized by solid particles only [6–9]. If a surfactant is also present the particle wetting preference can be changed, and possibly the particles will not adsorb; in this case, another type of emulsion can form that is mainly stabilized by the presence of a surfactant layer at the surface of the drops. For the rheology, it is known that colloidal clay particles in emulsions can induce a depletion interaction between the emulsion droplets that can cause these emulsions to be thixotropic, i.e., have a time-dependent rheology [10]. Also, in foams aging effects have been observed when Laponite® clays were added to the foam [11].

Clays are frequently-used solid particles in oil-in-water emulsion stabilization, often with rather high clay concentrations. This makes it likely that the continuous aqueous phase between the oily emulsion drops forms a gel, which should influence both the stability and the rheology of the emulsions [12–14]; such an effect does not appear to have been taken into account in prior experiments on emulsion stability and rheology in the presence of clay particles [15–18]. Reports that do take the gelation of clay particles into account are always in the presence of a surfactant. Lagaly et al. [19] discussed the two mechanisms by which clay in addition to a surfactant based emulsion can stabilize drops. The first is “stabilization by envelopes of particles around the oil droplets” and the second is ”stabilization by entrapment and immobilization of oil drops in three-dimensional network of particles”. They also remark that the stabilization by a particle network may be comparable to the role of liquid-crystalline phases in stabilizing emulsions [20]. Bon and Clover [21] used Laponite® as stabilizer in the miniemulsion polymerization of styrene to obtain L atex particles armored with Laponite® particles.

They showed that a three-dimensional network of clay particles in the continuous phase of the emulsions is required to obtain a stable Laponite® coated latex. All these observations pose the question what the difference is between clay and clay/surfactant stabilized emulsions. This question is particularly important for concentrated emulsions where shear induced instabilities have a higher impact on droplet coalescence and hence emulsion stability.

In this chapter we compare the stability to shear of three emulsion systems; the first is stabilized with surfactant only, the second with surfactant and clay particles and finally emulsions stabilized with clay particles only. The emulsions are castor oil-in-water and silicone oil-in-water emulsions.

5.2 Different type of emulsions

The three different systems have different continuous phases: surfactant only, surfactant + clay; and clay only. To study the influence of clay, different concentration of Laponite® RD are added before emulsifying (in wt% of the total weight of the emulsion). Laponite® is a synthetic clay that consists of disc-like particles, with a diameter of 30nm and thickness of 1nm obtained from BYK Additives & Instruments [22]. The Laponite® disks have a negative charge on the sides and can be slightly positively charged on the edges. The surfactant used is Sodium Dodecyl Sulfate (SDS, from Sigma Aldrich). The preparation protocol for the emulsions is described in Chapter 2. We consider rather high clay concentration and high surfactant (ionic strength) or salt concentrations, therefore an attractive gel forms [23].

5.2.1 Emulsions with surfactant and clay + surfactant

The emulsions stabilized with SDS are stable for months to coalescence and are stable to shear. Figure 5.1a shows an up-and-down shear rate sweep for castor oil-in-water emulsion ($\phi_{oil} = 0.80$) with SDS and different concentrations of Laponite®. We observe that without clay, the flow curve is perfectly reversible doing an up-and-down shear rate sweep. However, adding clay to the same emulsion, the flow curves develop a hysteresis that becomes more pronounced with increasing clay content. These emulsions can be characterized rheologically as thixotropic

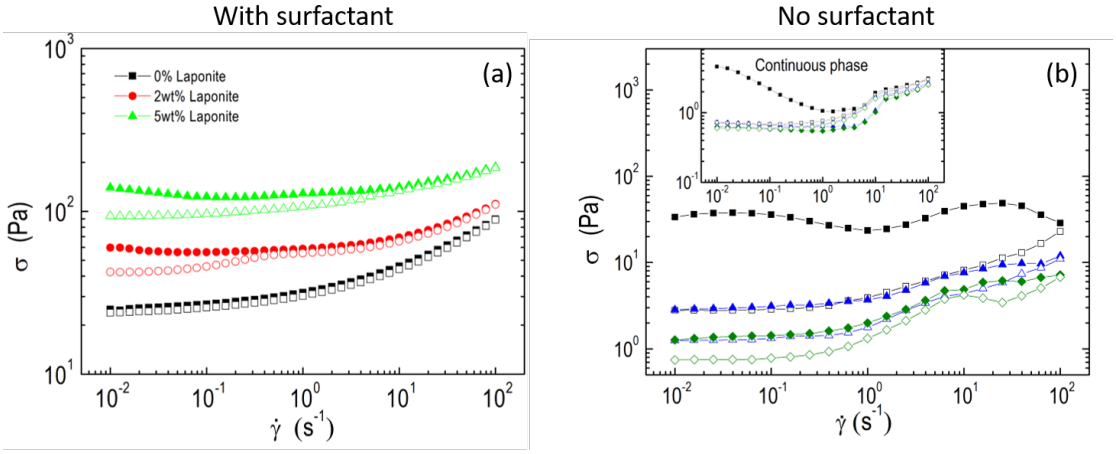

FIGURE 5.1: Flow curves for castor oil-in-water emulsions. On the left, stabilized with SDS and different clay concentrations ($\phi_{oil} = 0.8$). On the right, stabilized with Laponite® only, without surfactant ($\phi_{oil} = 0.7$); continuous phase exists of 2wt% Laponite® in 0.1M NaCl. Directly after samples are prepared the stress is measured by applying increasing (filled symbols) and decreasing (empty symbols) shear rate. Three increasing/decreasing sweeps are done, in the following order black, blue and green. (inset) Same measurement for the continuous phase, sample has left to rest for 2 hours before the first shear rate sweep starts. Symbols correspond to increasing (filled) and decreasing (empty) shear rate.

yield-stress materials [10]. Besides the thixotropy, the addition of clay does not have a significant effect on the emulsions stability in these experiments. By the definition of thixotropy, the changes in the rheological behavior are reversible; they are also reversible in these rheology experiments, showing that the shear doen not induce any macroscopic destabilization of the emulsion itself.

5.2.2 Emulsions with clay only (no surfactant)

If emulsions are only stabilized with clay, we find that the emulsions exhibit good stability to coalescence at rest: leaving the samples for several weeks does not result in any visible changes of the aspect of the emulsion. However during the rheological measurements the emulsions destabilize quite spectacularly. Figure 5.1b shows the result of up-and-down shear rate sweeps performed repeatedly (three times consecutively) on the castor oil-in-water emulsion. Similar results are obtained for the silicone oil-in-water emulsion. The emulsions show a rapid decrease in viscosity when performing multiple shear rate sweeps; this is in stark contrast to what is observed for surfactant-stabilized emulsions, for which the flow curve is perfectly reversible in up-and-down stress.

Visual inspection after shearing reveals that the Laponite®-stabilized emulsions are unstable to shear: after the rheological tests a clear phase separation between the oil and the water phases is observed. A similar decrease of the viscosity is observed if the same experiment is done on the continuous phase only. At the clay and salt concentrations that compose the continuous phase, aqueous Laponite® suspensions are known to form an attractive colloidal gel that is very sensitive to shear [24]. The rheological experiment shows that after the first up-and-down shear rate sweep, the viscosity decreases by an order of magnitude, and remains very low if the sample is sheared in subsequent sweeps (Figure 5.1b, inset).

5.3 Structure of clay particles in the continuous phase

The picture that emerges from the ensemble of these experiments is that the flow destabilizes the colloidal clay gel that forms the continuous phase separating the drops; this allows the droplets to contact each other and coalesce, which in turn destabilizes the emulsion. To check this scenario on a more microscopic level, confocal fluorescence microscopy is used to visualize both the Laponite® suspension by itself and the emulsions containing Laponite®. As a fluorescent dye we use Rhodamine G6 (from Sigma Aldrich), a hydrophilic fluorescent molecule that is completely adsorbed onto the Laponite® particles. The behavior of the transparent silicone oil-in-water emulsions, before, during and after shearing, is observed with the confocal microscope in combination with a rheometer. The Laponite® particles are clearly visible; they form aggregated flocs in the continuous phase, but are also clearly visible on the interface of the oil droplets with the continuous phase (Figure 5.2a). The continuous phase is more heterogeneous. In contrast, in the presence of surfactant the clay particles for a continuous (homogeneous) network surrounding the particles and are not specifically located at the interface (Figure 5.2b). Moreover, the droplet size is different.

Separate observation on the aqueous Laponite® phase alone (before emulsification with the oil) also reveal the formation of a colloidal gel with a very similar structure. The continuous phase is a soft elastic solid that does not flow under the influence of gravity (Figure 5.3). To asses the effect of flow, we shear for 30 seconds at $\dot{\gamma} = 100s^{-1}$ and visualize the Laponite® structure before and after shear. We

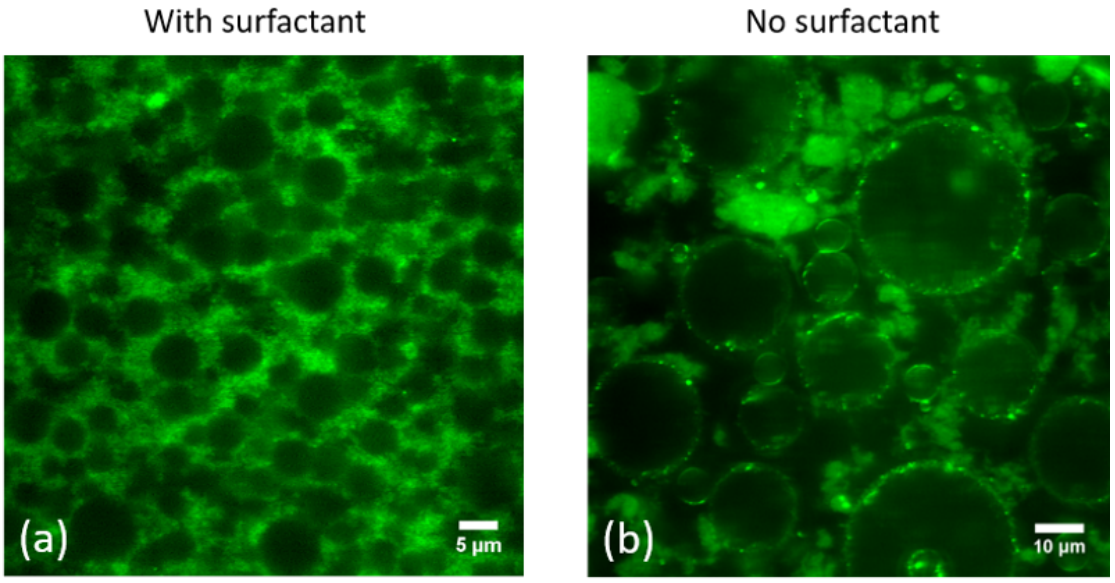

FIGURE 5.2: The emulsion visualized with confocal fluorescence microscopy image (Laponite® is dyed with Rhodamine G6). Silicone oil-in-water emulsion index matched with glycerol: in (a) stabilized by 2wt% Laponite® in 0.1M NaCl Laponite®, in (b) stabilized with 1wt% SDS in water with 2wt% Laponite®.

observe before shear a continuous network, whereas after shear the network breaks into smaller aggregates and does not appear to be percolated anymore. It is this gel that destabilizes under shear that leads to destabilization of the emulsion. This follows the observation that an emulsion with a surfactant does not destabilize.

In the usual definition of Pickering emulsions, the particles are localized at the interface to form a dense film that protects the droplets from coalescence. It is for this reason that such emulsions are believed to be very stable; for spherical particles the stabilization energy depends on the particle size [6] but is typically of the order of a few hundred k_BT [25, 26]. If the emulsions solely stabilized with Laponite® have a similar protective particle film on the drop surfaces, one would expect a similar stability for the Laponite®-stabilized emulsions. Laponite® particles are not spherical but disk-like, but still if the particles are at the interface stabilization energies should be similar. We find however that although the emulsions are stable at rest, they are extremely rapidly destabilized by shear, and hence the Laponite® layer at the surface does not provide a significant barrier against coalescence. The observation that the rheology of the emulsions and the continuous Laponite® phase are similar suggests that the stability of the emulsions at rest is due to the fact that the oil droplets are embedded in the visco-elastic Laponite® gel, that prevents the droplets from coalescencing. When the colloidal gel is destroyed by the shear

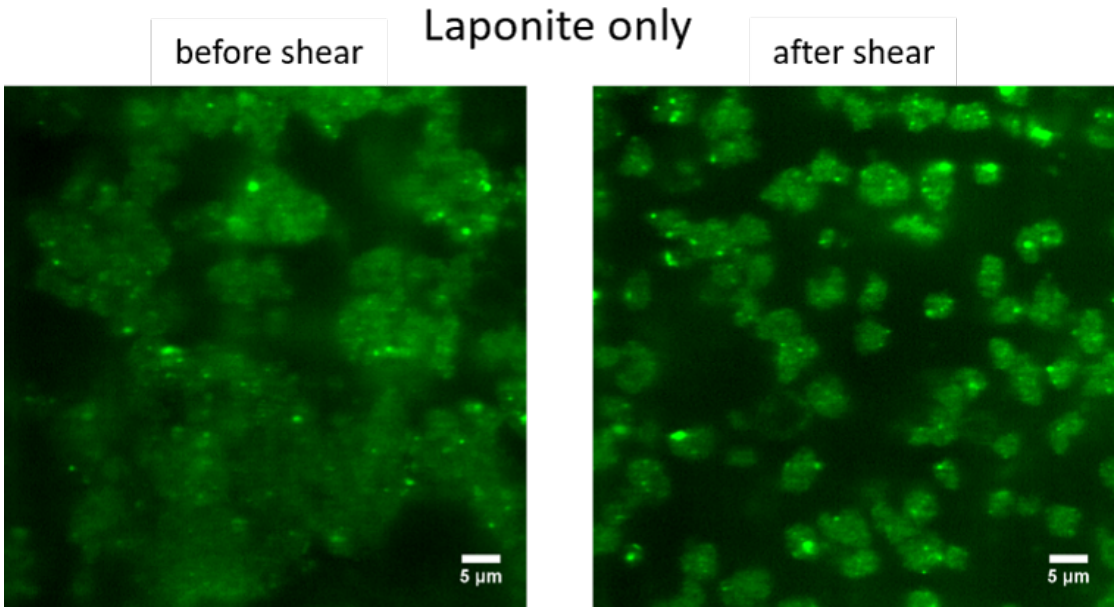

FIGURE 5.3: Confocal fluorescence images of the continuous phase; 2wt% Laponite® in 0.1M NaCl (Laponite® dyed with Rhodamine G6). Before and after shear (shear for 30 seconds at $\dot{\gamma} = 100s^{-1}$.

allowing the droplets to move and get in contact, coalescence is rapid, in agreement with all of the observations above. The aggregated Laponite® particles on the surface are not able to rearrange to provide an effective barrier against coalescence, but rather form particle aggregates that are not effective in providing effective coverage. Garcia and Whitby [27] also observed this behavior, but coalescence was not detected due to lower volume fraction of oil. Whitby and co-authors [28] however observed the shear induced coalescence in oil-in-water Pickering emulsions stabilized by silanized fumed silica particles subjected to simple shear flow.

5.4 Model system (carbopol gel)

As an independent test of the idea, that the stabilization is only due to the gel formation of the Laponite®, we can make emulsions without any particles or surfactants, but with the continuous phase being a gel with a yield stress. We therefore make emulsions with a Carbopol gel as the continuous phase. The carbopol itself is a simple yield-stress fluid [29], from which subsequently castor oil-in-gel 'emulsions' ($\phi_{oil} = 0.4$; for higher concentrations of castor oil we observe phase inversion of the emulsion) are prepared using the same procedure as for the Laponite® emulsions. We find that the Carbopol 'emulsions' show a similar rheology as we observe

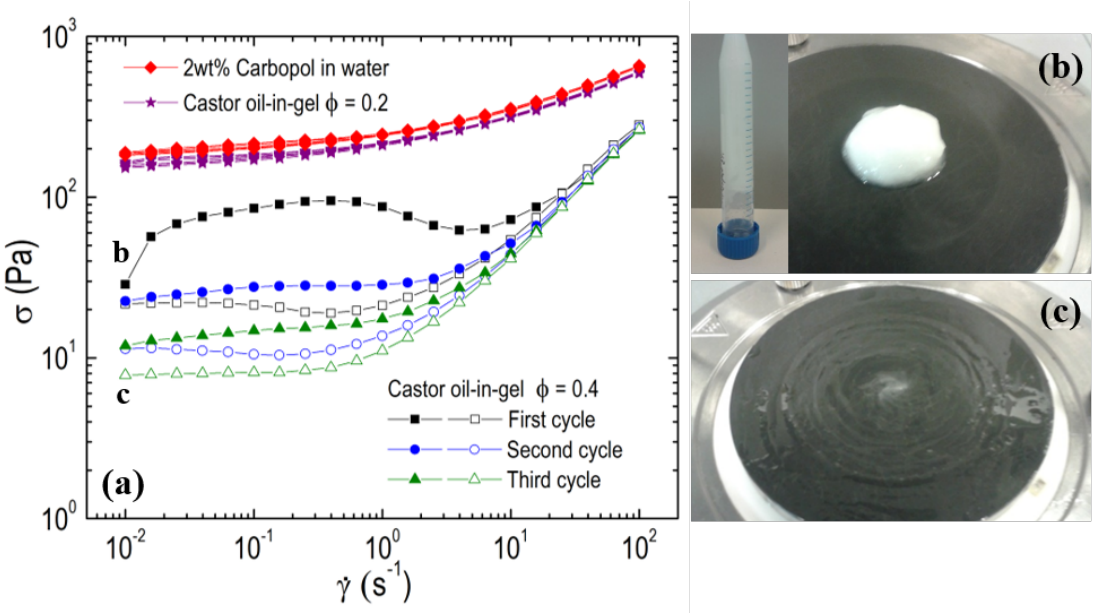

FIGURE 5.4: (a) Flow curves of Castor oil-in-water with 2wt% Carbopol in water as the continuous phase. The stress is measured applying increasing (filled symbols) and decreasing (empty symbols) shear rate. The photographs in (b) and (c) show the sample before and after shear, respectively.

for the Laponite®-stabilized emulsions (Figure 5.4); a very stable 'emulsion' at rest that is rapidly destabilized by shearing. When the continuous phase is a yield-stress fluid but nothing happens at the oil-water surface, in that case emulsions can be stable at rest but not under shear. The similarity with the results for Laponite® strongly suggest that the mechanism is the same there.

5.5 Conclusion

We have investigated the stability of Laponite®-stabilized high internal phase emulsions. A simple rheological test shows that the emulsions are not stable to shear and undergo a catastrophic coalescence. Therefore, our 'Pickering' emulsions, as evident from confocal microscopy, behave merely as a dispersion of oil droplets in a Laponite® gel. It is this gel, that destabilizes under shear, that leads to destabilization of the emulsion. This also follows from the observation that an emulsion with a good emulsifier (a surfactant) does not destabilize. This point is reinforced if we look at the conditions of formation of Laponite®-stabilized emulsions. Such emulsions were studied previously, but with lower salt concentration and lower oil volume fraction that are also in a region of the Laponite®/salt phase

diagram where the continuous phase becomes a soft visco-elastic solid. Ashby and Binks [15] have shown that in their systems, Laponite®-stabilized emulsions, are only stable if enough salt is added to effectively screen the electrostatic interactions between the Laponite® particles and hence favor the formation of the colloidal gel. If our emulsions are made with a liquid suspension of the same concentration of Laponite® but without salt, no stable emulsions are obtained. Thus we conclude that the colloidal gel formation of the clay is the essential ingredient for the emulsion preparation, however the extend of shear thinning and recovery speed of the colloidal gel play a critical role in the emulsion stabilization.

References

[1] J. Sjoblom. *Emulsions and Emulsion Stability: Surfactant Science Series/61*, volume 132. CRC Press, 2005.

[2] A. Deblais, R. Harich, D. Bonn, A. Colin, and H. Kellay. Spreading of an oil-in-water emulsion on a glass plate: Phase inversion and pattern formation. *Langmuir*, 31(22):5971–5981, 2015.

[3] C. C. Berton-Carabin and K. Schroën. Pickering emulsions for food applications: background, trends, and challenges. *Annual review of food science and technology*, 6:263–297, 2015.

[4] G. Sun, Z. Li, and T. Ngai. Inversion of particle-stabilized emulsions to form high-internal-phase emulsions. *Angewandte Chemie International Edition*, 49(12):2163–2166, 2010.

[5] S. Levine, B. D. Bowen, and S. J. Partridge. Stabilization of emulsions by fine particles i. partitioning of particles between continuous phase and oil/water interface. *Colloids and Surfaces*, 38(2):325–343, 1989.

[6] S. U. Pickering. Cxcvi. -emulsions. *J. Chem. Soc., Trans*, 91(0):2001–2021, 1907.

[7] W. Ramsden. Separation of solids in the surface-layers of solutions and 'suspensions'(observations on surface-membranes, bubbles, emulsions, and mechanical coagulation).–preliminary account. *Proceedings of the royal Society of London*, 72:156–164, 1903.

[8] B. Liu, W. Wei, X. Qu, and Z. Yang. Janus colloids formed by biphasic grafting at a pickering emulsion interface. *Angewandte Chemie*, 120(21):4037–4039, 2008.

[9] S. Sacanna, W. K. Kegel, and A. P. Philipse. Thermodynamically stable pickering emulsions. *Physical review letters*, 98(15):158301, 2007.

[10] A. Ragouilliaux, G. Ovarlez, N. Shahidzadeh-Bonn, B. Herzhaft, T. Palermo, and P. Coussot. Transition from a simple yield-stress fluid to a thixotropic material. *Physical Review E*, 76(5):051408, 2007.

[11] R. Guillermic, A. Salonen, J. Emile, and A. Saint-Jalmes. Surfactant foams doped with laponite: unusual behaviors induced by aging and confinement. *Soft Matter*, 5(24):4975–4982, 2009.

[12] S. Jabbari-Farouji, H. Tanaka, G. H. Wegdam, and D. Bonn. Multiple nonergodic disordered states in laponite suspensions: a phase diagram. *Physical Review E*, 78(6):061405, 2008.

[13] M. Dijkstra, J. P. Hansen, and P. A. Madden. Gelation of a clay colloid suspension. *Physical review letters*, 75(11):2236, 1995.

[14] B. Ruzicka, L. Zulian, and G. Ruocco. Routes to gelation in a clay suspension. *Physical review letters*, 93(25):258301, 2004.

[15] N. P. Ashby and B. P. Binks. Pickering emulsions stabilised by laponite clay particles. *Physical Chemistry Chemical Physics*, 2(24):5640–5646, 2000.

[16] Y. Jung, Y. Son, J. Lee, T. X. Phuoc, Y. Soong, and M. K. Chyu. Rheological behavior of clay–nanoparticle hybrid-added bentonite suspensions: Specific role of hybrid additives on the gelation of clay-based fluids. *ACS applied materials & interfaces*, 3(9):3515–3522, 2011.

[17] C. Li, Q. Liu, Z. Mei, J. Wang, J. Xu, and D. Sun. Pickering emulsions stabilized by paraffin wax and laponite clay particles. *Journal of colloid and interface science*, 336(1):314–321, 2009.

[18] Y. Nonomura and N. Kobayashi. Phase inversion of the pickering emulsions stabilized by plate-shaped clay particles. *Journal of colloid and interface science*, 330(2):463–466, 2009.

[19] G.s Lagaly, M. Reese, and S. Abend. Smectites as colloidal stabilizers of emulsions: I. preparation and properties of emulsions with smectites and nonionic surfactants. *Applied Clay Science*, 14(1):83–103, 1999.

[20] S. E. Friberg, L. B. Goldsmith, and M. L. Hilton. Theory of emulsions. *Theory of emulsions, Pharmaceutical dosage forms: Disperse systems*, 1:49–91, 1988.

[21] S. A. F. Bon and P. J. Colver. Pickering miniemulsion polymerization using laponite clay as a stabilizer. *Langmuir*, 23(16):8316–8322, 2007.

[22] LAPONITE® RD. is manufactured by BYK Additives & Instruments.

[23] B. Ruzicka and E. Zaccarelli. A fresh look at the laponite phase diagram. *Soft Matter*, 7(4):1268–1286, 2011.

[24] B. Abou, D. Bonn, and J. Meunier. Nonlinear rheology of laponite suspensions under an external drive. *Journal of Rheology*, 47(4):979–988, 2003.

[25] Johannes Lyklema. *Fundamentals of interface and colloid science: soft colloids*, volume 5. Academic press, 2005.

[26] S. Sacanna, W. K. Kegel, and A. P. Philipse. Thermodynamically stable pickering emulsions. *Phys. Rev. Lett.*, 98:158301, Apr 2007.

[27] P. C. Garcia and C. P. Whitby. Laponite-stabilised oil-in-water emulsions: viscoelasticity and thixotropy. *Soft Matter*, 8(5):1609–1615, 2012.

[28] C. P. Whitby, F. E. Fischer, D. Fornasiero, and J. Ralston. Shear-induced coalescence of oil-in-water pickering emulsions. *Journal of colloid and interface science*, 361(1):170–177, 2011.

[29] M. M. Denn and D. Bonn. Issues in the flow of yield-stress liquids. *Rheologica acta*, 50(4):307–315, 2011.

Chapter 6

Transition from athermal jamming to thermally induced shear banding

6.1 Introduction

Yield-stress fluids are an important class of complex fluids and their flow behavior is still a subject of considerable interest [1–3]. Yield-stress materials respond elastically to small applied stresses and start to flow once a threshold stress is exceeded; the yield stress. The flow curve of a simple yield-stress fluid can often be successfully described by the Herschel-Bulkley equation [4]: $\sigma = \sigma_y + K\dot{\gamma}^{\beta}$, where σ is the stress, σ_y the yield stress, $\dot{\gamma}$ the shear rate, and K and β are adjustable parameters. However, as often seen in nature, most materials do not behave like the ideal model system; they are significantly more complex and can exhibit for example hysteresis [5, 6], thixotropy [7] and shear banding [8]. It is therefore important to understand the mechanisms causing these distinct properties. In yield-stress fluids solidity emerges near a 'critical' volume fraction ϕ below which the material is a fluid whose viscosity rapidly increases with ϕ. Depending on the concentration and size of the dispersed phase one can have a glass or jammed material (e.g. a glassy colloidal suspension or a concentrated emulsion respectively). Glass and jamming transitions share important similarities at the rheological level. Based on these, a unified jamming phase diagram has been proposed where thermal and athermal systems appear as a single 'jammed' phase [9]. However in the crossover regime, glass and jamming transitions co-exist and give complex flow curves [10].

To investigate the flow behavior and complications of yield-stress fluids, we study a Carbopol "gel". Carbopol is a widely used material in many industries because of its efficient rheology modifications; a simple yield-stress fluid with enhanced self-wetting properties that makes it easy to use [11]. Carbopol is a cross-linked polyacrylic acid polymer, that is usually provided as a dry white powder. In a water solution at neutral pH, Carbopol is an anionic polymer, i.e. some of the side chains will lose their protons and acquire a negative charge. This makes them polyelectrolytes, with the ability to absorb and retain water and swell to many times their original volume. Therefore, the Carbopol-gel has a yield stress and is extensively used in the literature as a model yield-stress fluid [12–15]. However there is an ongoing discussion in the literature about the precise flow behavior of this "model" yield-stress fluid. Some authors report rheological hysteresis in the flow curve [16] or transient shear banding that persists for a very long time [17], which is incompatible with Carbopol being a simple yield-stress fluid.

In this chapter we study the flow behavior of simple yield-stress fluids and try to understand whether Carbopol is a simple yield-stress fluid or not. We perform rheological tests to show that the Carbopol gel is sensitive to the preparation protocol. We then try to understand what is causing hysteresis by visualizing the different Carbopol gels using confocal fluorescent microscopy. The underlying physics that for a certain preparation protocol causes the hysteresis and shear banding turns out to be an interesting competition between thermal and athermal parts dominating the system. To demonstrate the generality of these findings, the same behavior is studied in another model system: an oil-in-water emulsion with high surfactant concentration. Finally, we propose a simple theoretical approach to describe this behavior.

6.2 Experimental section

First we compare two different Carbopol gels: Carbopol Ultrez U10 (used by us [18]) and Carbopol ETD 2050 (used by Divoux et al. [17]). Both gels are traditionally prepared by mixing Carbopol powder and demineralized water leading to a liquid-like suspension of Carbopol aggregates. Subsequently a NaOH solution was added to adjust the PH of the Carbopol-water mixture to approximately 7 which induces polymer swelling and microgel formation. Our sample is homogenized by gently stirring for one hour then left to rest for one day. The other sample is stirred at a high rate for more than 20 hours, as was done in [17]. These differences make for the distinct properties for the two samples. Rheological measurements are performed with an Anton paar MCR 302 rheometer, in a sand blasted 1° cone-plate geometry (diameter 50mm). Before starting any experiment the samples are pre-sheared for 30 seconds at $\dot{\gamma} = 100s^{-1}$ and left to rest for another 30 seconds.

6.2.1 Different types of behavior

The flow curves of the two different Carbopol samples are shown in Figure 6.1a. The samples are 0,25wt% Carbopol Ultrez U10 in water (as used by us [18]) and 0,6wt% Carbopol ETD 2050 (as used by Divoux [17]). These flow curves are obtained by performing an up and down shear rate sweep twice, the waiting time for each point is 10 seconds (the rapid increase in stress response of the first increasing rate sweep is the elastic response of the material). The sample from us shows

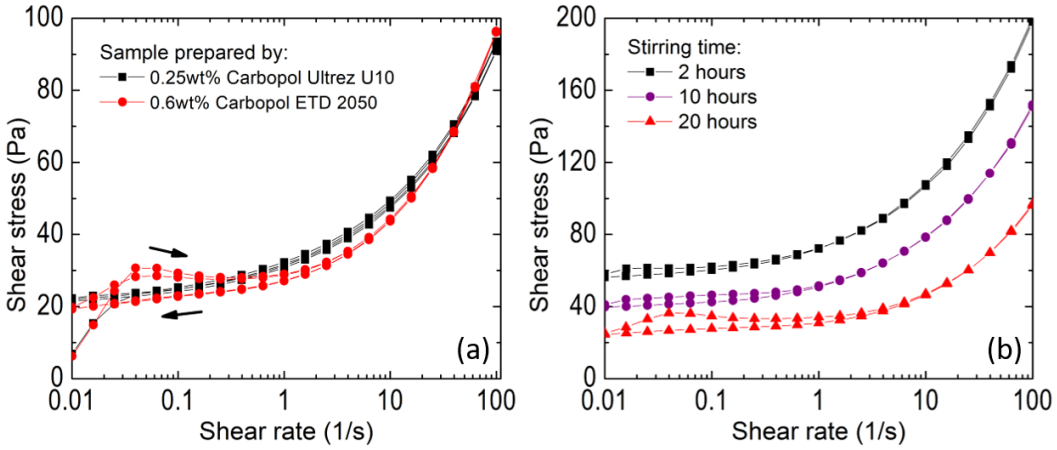

FIGURE 6.1: Flow curves of different Carbopol samples. In (a) two samples that where provided us (Carbopol Ultrez U10) and T. Divoux (Carbopol ETD 2050) [17]. And in (b) 0.6wt% Carbopol Ultrez U10 for different preparation stirring times at 2000rpm.

no significant hysteresis, while clearly the sample from Divoux shows a hysteresis between decrease and increasing shear rate sweeps for $\dot{\gamma} < 5s^{-1}$. Roughly the same yield stress is observed irrespectively of an up or down shear rate sweep. In addition, figure 6.1b shows the flow curves of Carbopol (Ultrez U10) prepared with different intensive stirring times during the preparation process. These samples come from the same Carbopol batch that shows true model yield stress behavior [18]. However, when the stirring time and intensity during the preparation of the Carbopol is increased, the flow behavior starts to differ from the simple yield stress behavior. We observe that a hysteresis loop appears and becomes more pronounced for longer stirring times and the yield stress is decreasing simultaneously, exactly as for the other type of carbopol prepared by Divoux [17], which were also stirred vigorously. The microgel macroscopic properties therefore depend on the details of the preparation protocol. The question therefore is what the relation is between the preparation protocol and the hysteresis in the flow behavior of this system? Divoux et al. [17] in addition show that they observe transient shear banding in the hysteretic region of the flow curve.

When we look at start-up measurements, a stress-overshoot is observed for the hysteretic Carbopol, figure 6.2 shows the start-up measurements for the two Carbopol samples at constant imposed shear rates. There is an overlap up to a strain of 20% showing the linear response of the yielded material after which a constant

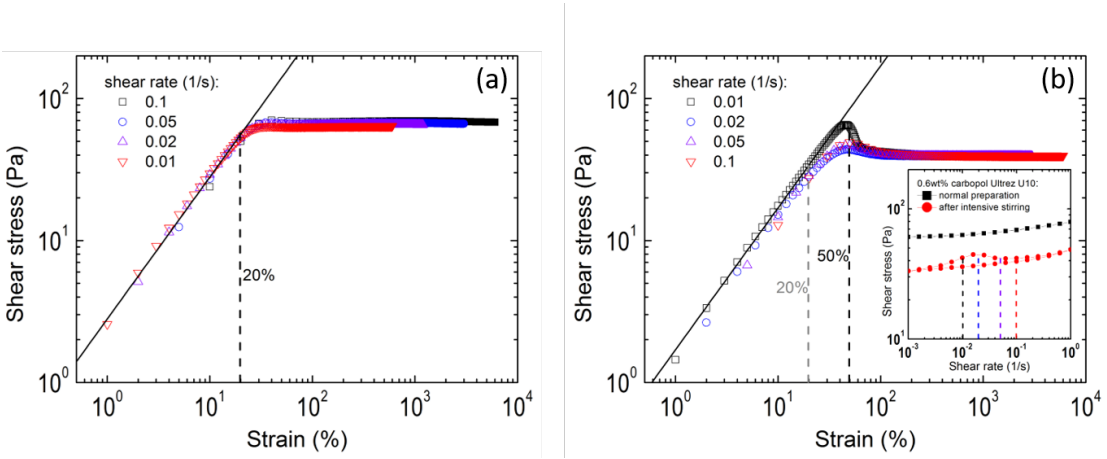

FIGURE 6.2: Startup of stress as a function of strain for constant imposed shear rates for (a) a simple yield stress Carbopol sample and (b) Carbopol after intensive stirring, corresponding flow curves are given in the inset.

stress plateau is reached. In case of the vigorously stirred Carbopol a stress overshoot appears that has a maximum at a strain of 50%. The emerging yield peak directly relates to the observed hysteresis in the flow curve, and shows that the system ages at a typical timescale $\tau_{ag} = \gamma/\dot{\gamma} \approx 50s$. Appendix A shows some more additional rheological tests. To further investigate this change in the macroscopic flow behavior we focus on the microstructure of the systems.

6.2.2 Micro structure

Figure 6.3 shows the confocal images that reveal the structures for the two Carbopol gels, dyed with rhodamine 6g (from Sigma-Aldrich). Clearly there is a size and structure difference between the two samples, that were prepared from the same material and hence should be identical: the only difference is the time of stirring. For the simple yield stress sample (figure 6.3a) there are large cross-linked structures visible. On the other hand, for the "hysteretic" sample, the structures are permanently broken into smaller parts. At rest, even after several months these structures remain unchanged. Performing a fast scanning confocal microscopy, we observe significant thermal motion (Brownian motion of the smallest particles) in the hysteretic Carbopol. Also in the normal Carbopol, some very small particles are visible that are thermal, but the thermal behavior is significantly more pronounced in the hysteretic Carbopol; Brownian motion is observed for many small polymers ($< 1\mu m$, present and visible in the sample). As a consequence of intensive stirring during the sample preparation the large cross-linked sponges

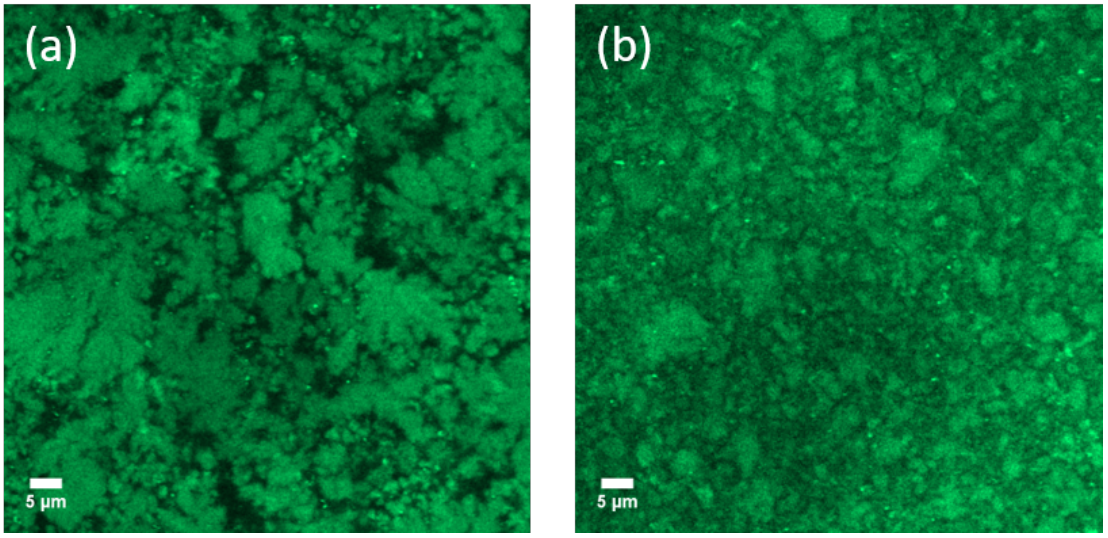

FIGURE 6.3: Confocal fluorescent microscope image of two initially identical samples of 0.5wt% Carbopol in water (Carbopol is dyed with Rhodamine 6g). In (a) simple yield stress sample and in (b) after heavy stirring the cross-linked structures are broken.

are therefore broken permanently into smaller structures thereby creating a more polydisperse system, that shows pronounced thermal effects. This then explains the hysteresis: it is well-known that thermal systems can exhibit aging and shear rejuvenation, which leads to thixotropy. One consequence of such thixotropy is hysteresis, another one is that there is and unstable part in the flow curve that is responsible for the shear banding that is generally observed for the thixotropic systems at low shear rates.

6.2.3 Velocity profiles

To look into the shear banding, velocity profiles are measured using a rheometer head on top of the confocal microscope (similar to Paredes et al. [19]). The velocity of the sample at different heights between cone and plate is measured while imposing a constant shear rate (Fig. 6.4a). The profiles are rescaled by plotting the normalized velocity v/v_c where v_c is the velocity of the cone (Fig. 6.4b). We find, as expected that the normal Carbopol sample shows an almost linear velocity profile. However the hysteretic Carbopol shows a rapid drop in velocity from the cone. This indicates that the material close to the cone has a large velocity gradient, whereas close to the plate there is almost no velocity gradient: this is shear banding. Thus, the thixotropy in the heavily stirred sample also accounts for the shear banding. Similar velocity profiles are observed by

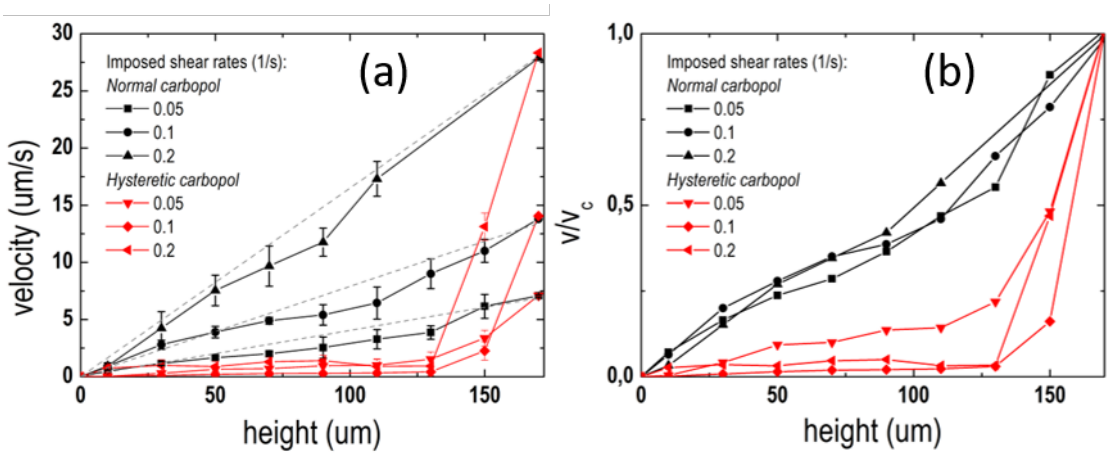

FIGURE 6.4: (a) Velocity profiles at different imposed shear rates for normal (black symbols) and hysteretic Carbopol (red symbols). The straight gray dotted lines indicate a linear Newtonian velocity profile. (b) Fluid velocity normalized by the cone velocity at different imposed shear rates for normal and hysteretic Carbopol.

Divoux et al. [17] for Carbopol ETD 2050, they also conclude that the shear band accounts for the small hysteresis observed in the flow curve.

6.2.4 Model system

A similar effect is also seen in e.g. emulsions with high surfactant concentrations [20] where the formation of SDS micelles induces attractive depletion forces between the droplets [21, 22]. This leads to flocculation of the droplets, that is in a way similar to a colloidal gel formation; building up of a structure that breaks down under shear, resulting in flow instabilities [23, 24]. We have prepared castor oil-in-water emulsions with two different SDS concentrations 1wt% and 8wt% SDS in water. The flow curves are shown in figure 6.5. The emulsion with 1wt% SDS shows a perfectly reversible flow curve for increasing/decreasing shear rate. However, the emulsion with 8wt% SDS shows a hysteresis that is similar to the observations for the hysteretic Carbopol; a negative slope at the first increasing shear rate sweep. This physical picture of attractive depletion forces can explain the flow instability at low rates that occurs in the Carbopol; the many small thermal particles (polymers) create an attractive force between the larger polymers.

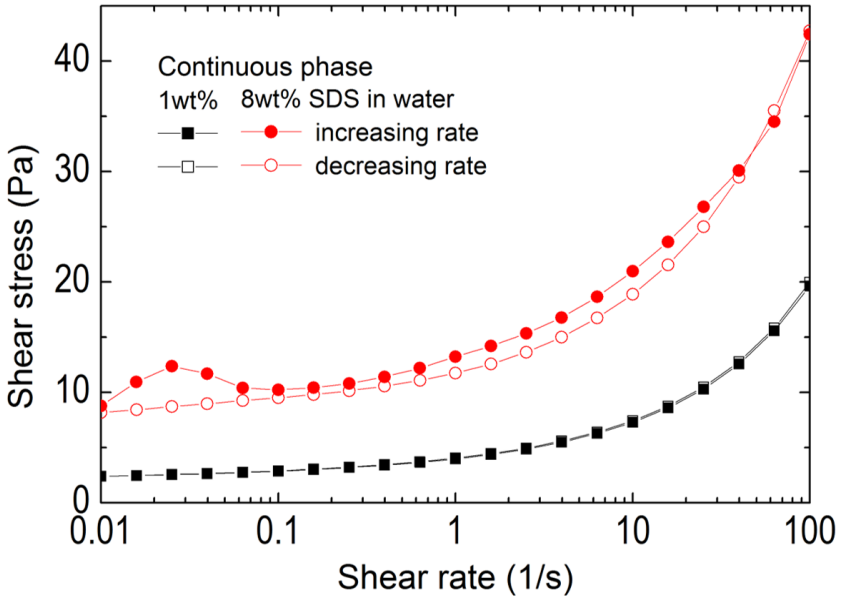

FIGURE 6.5: Flow curves for 70% Castor oil-in-water emulsion for different SDS concentration in the continuous phase. Filled/empty symbols are increasing/decreasing imposed shear rate.

6.3 Discussion and theoretical model

The above observations provide a consistent picture. We find that the flow properties of Carbopol depend on the preparation protocol; after intensive stirring during the preparation process the flow behavior starts to deviate from the initial simple yield stress behavior and shows a hysteresis loop and decreasing yield stress. The emerging yield peak in figure 6.2 shows that the vigorously pre-stirred sample ages on a typical timescale $\tau_{ag} = \gamma_{yield}/\dot{\gamma} \approx 50s$. The mechanism behind it is revealed in figure 6.3 the stirring changes the originally simple yield-stress fluid by breaking the microgels up in smaller structures, including many submicron Brownian fragments. The latter will introduce depletion forces between the repulsive larger fragments which then in absence of stress or at very low imposed rates form a continuous network. The same is observed for the emulsion were micelles act as depletants. In line with this, the yield stress decreases with increasing pre-stirring time and the upward and downward flow curves meet again at imposed rates well below the observed aging rate τ_{ag}^{-1} (figure 6.1b and figure 6.2b inset). The instability in turn allows shear banding in the downward flow curve, as in figure 6.4 (cf. Møller et al. [25]). The model system of figure 6.5 supports the picture of depletion-induced instability.

To cast this in a quantitative model we assume that the vigorously pre-stirred yield-stress fluid still obeys Herschel-Bulkley, with the underlying microscopic model as in Paredes et al. [26] and chapter 7 of this thesis: $\sigma = \sigma_y[1 + (\tau\dot{\gamma}^{\beta})]$. The relaxation time τ then reflects the 'cage escape' of the stagnant particle and will decrease with increasing fragmentation, i.e., increasing $\dot{\gamma}$. The competition between aging and rejuvenation implies an additional shear-thinning mechanism at rates just above τ_{ag}^{-1}, so $\tau = \tau(\dot{\gamma})$. Differentiating the resulting HB equation with respect to $\dot{\gamma}$ we see that mechanical instability will occur when $d\sigma/d\dot{\gamma} \leq 0$ or $dlog\tau/dlog\dot{\gamma} \leq -1$. If the times $\tau(0)$, τ_{ag} and $\tau(\infty)$ are well-separated and if no other additional timescale plays a role, the effective relaxation time τ will in a range of rates above τ_{ag}^{-1} decrease power-law with increasing $\dot{\gamma}$. This may be effectively modeled as

$$\tau = \tau(\infty) + \frac{\tau(0) - \tau(\infty)}{1 + (\tau_{ag}\dot{\gamma})^n} \tag{6.1}$$

with some positive exponent n. The condition $d\sigma/d\dot{\gamma} = 0$ for incipient mechanical instability of the homogeneous flow then becomes, after short algebra, a quadratic equation in $x \equiv (\tau_{ag}\dot{\gamma})^n$; with the shear-thinning ratio $R \equiv \tau(0)/\tau(\infty)$ it reads: $x^2 - [n(R-1) - (R+1)]x + R = 0$. Depending on the discriminant this equation may have zero, one or two solutions, so precisely the possibility of either stable flow or a single Van der Waals loop, with a critical point $R_c(n) = [(n+1)/(n-1)]^2$ above which the instability occurs; so this may happen already for n just above unity. The mathematics is given in Appendix A. For $R \gg 4/(n-1)^2$ the points of maximum and minimum stress are then given by $\tau_{ag}\dot{\gamma}_{max} \approx 1/(n-1)^{1/n}$, $\tau_{ag}\dot{\gamma}_{min} \approx (n-1)^{1/n}R^{1/n}$. For the system of Figure 6.2 we find from the start-up experiment $\tau_{ag} \approx 0.5 \cdot 10^2 s$ and from the flow curve $\dot{\gamma}_{max} = 2 \cdot 10^{-2} s^{-1}$, $\dot{\gamma}_{min} = 10^{-1} s^{-1}$, consistent with the proposed picture, with an exponent $n \approx 2$, with $R_c \approx 9$ and with $R = \tau(0)/\tau(\infty) \approx 25$. As shown in the inset of Figure 6.2. the Herschel-Bulkley shear-thinning curve is indeed shifted to higher rates by more than one decade, due to the unstable branch.

6.4 Conclusion

In conclusion, we have shown that a simple yield-stress fluid can undergo a transition to thermally induced shear banding. Our experiments show that a simple

yield-stress fluid, a Carbopol gel that has an athermal jamming transition, can be transformed to a shear banding yield-stress fluid by different preparations protocols. When intensive stirring is applied during the neutralization process the properties of the microgel change; a hysteresis loop appears in the flow curve. The Carbopol structures are visualized by confocal fluorescent microscopy and it appears that the heavy stirring causes the polymers to breakup permanently into smaller parts. This increases the amount of thermal particles (polymers) in the system that create depletion forces between the larger polymers, resulting in shear banding. Similar behavior is observed in emulsions with high surfactant concentrations where micelles induce a depletion interaction between droplets. The underlying physics that causes shear banding is an interesting competition between thermal and athermal parts dominating the system. We propose a simple theoretical approach where a shear band is formed in a repulsive yield-stress fluid if the flow curve for homogeneous flow has a Van der Waals loop. The system is composed of aggregated particles (aggregating by depletion forces) and has a typical time scale τ_c for the competition between aggregating and breaking up of a composite particle. This particle may itself break down with increasing rate, thereby leading to an acceleration of the shear thinning; creating a shear band.

References

[1] R. G. Larson. *The Structure and Rheology of Complex Fluids*. Oxford University Press, 1999.

[2] M. M. Denn and D. Bonn. Issues in the flow of yield-stress liquids. *Rheol. Acta*, 50:307, 2011.

[3] D. Bonn, J. Paredes, M. M. Denn, L. Berthier, T. Divoux, and S. Manneville. Yield stress materials in soft condensed matter. *ArXiv*, 59:1502.05281, 2015.

[4] W. H. Herschel and R. Bulkley. Measurement of consistency as applied to rubber-benzene solutions. In *Am. Soc. Test Proc*, volume 26, pages 621–633, 1926.

[5] T. Divoux, V. Grenard, and S. Manneville. Rheological hysteresis in soft glassy materials. *Physical review letters*, 110(1):018304, 2013.

[6] P. Coussot, Q. D. Nguyen, H. T. Huynh, and D. Bonn. Avalanche behavior in yield stress fluids. *Physical review letters*, 88(17):175501, 2002.

[7] P. C. F. Møller, J. Mewis, and D. Bonn. Yield stress and thixotropy: on the difficulty of measuring yield stresses in practice. *Soft matter*, 2(4):274–283, 2006.

[8] A. Fall, J. Paredes, and D. Bonn. Yielding and shear banding in soft glassy materials. *Phys. Rev. Lett.*, 105:225502, Nov 2010.

[9] A. Liu and S. R. Nagel. Nonlinear dynamics: Jamming is not just cool any more. *Nature*, 396:21, 1998.

[10] A. Ikeda, L. Berthier, and P. Sollich. *Phys. Rev. Lett.*, 109:018301, 2012.

[11] Carbopol ultrez 10 polymer description lubrizol. `https://www.lubrizol.com/Personal-Care/Products/Product-Finder/Products-Data/112`. Accessed: 2017-10-17.

[12] P. Coussot, L. Tocquer, C. Lanos, and G. Ovarlez. Macroscopic vs. local rheology of yield stress fluids. *Journal of Non-Newtonian Fluid Mechanics*, 158(1):85–90, 2009.

[13] S. P. Meeker, R. T Bonnecaze, and M. Cloitre. Slip and flow in soft particle pastes. *Physical review letters*, 92(19):198302, 2004.

[14] J. Goyon, A. Colin, G. Ovarlez, A. Ajdari, and L. Bocquet. Spatial cooperativity in soft glassy flows. *Nature*, 454(7200):84–87, 2008.

[15] J. Kim, J. Song, E. Lee, and S. Park. Rheological properties and microstructures of carbopol gel network system. *Colloid and Polymer Science*, 281(7):614–623, 2003.

[16] A. M. V. Putz, T. I. Burghelea, I. A. Frigaard, and D. M. Martinez. Settling of an isolated spherical particle in a yield stress shear thinning fluid. *Physics of Fluids*, 20(3):033102, 2008.

[17] T. Divoux, D. Tamarii, C. Barentin, and S. Manneville. Transient shear banding in a simple yield stress fluid. *Physical review letters*, 104(20):208301, 2010.

[18] M. Dinkgreve, J. Paredes, M. A. J. Michels, and D. Bonn. Universal rescaling of flow curves for yield-stress fluids close to jamming. *Physical Review E*, 92(1):012305, 2015.

[19] J. Paredes, N. Shahidzadeh-Bonn, and D. Bonn. Shear banding in thixotropic and normal emulsions. *Journal of Physics: Condensed Matter*, 23(28):284116, 2011.

[20] L. Bécu, S. Manneville, and A. Colin. Yielding and flow in adhesive and nonadhesive concentrated emulsions. *Physical review letters*, 96(13):138302, 2006.

[21] J. Bibette, D. Roux, and F. Nallet. Depletion interactions and fluid-solid equilibrium in emulsions. *Physical review letters*, 65(19):2470, 1990.

[22] H. N. W. Lekkerkerker and R. Tuinier. *Colloids and the depletion interaction*, volume 833. Springer, 2011.

[23] D. Bonn and M. M. Denn. Yield stress fluids slowly yield to analysis. *Science*, 324(5933):1401–1402, 2009.

[24] T. Divoux, M. A. Fardin, S. Manneville, and S. Lerouge. Shear banding of complex fluids. *Annual Review of Fluid Mechanics*, 48(1):81–103, 2016.

[25] P. C. F. Møller, S. Rodts, M. A. J. Michels, and D. Bonn. Shear banding and yield stress in soft glassy materials. *Physical Review E*, 77(4):041507, 2008.

[26] J. Paredes, M. A. J. Michels, and D. Bonn. Rheology across the zero-temperature jamming transition. *Physical review letters*, 111(1):015701, 2013.

Chapter 7

Universal rescaling of flow curves for yield-stress fluids close to jamming

7.1 Introduction

Understanding and predicting the flow behavior of complex fluids is a subject of considerable industrial and fundamental interest [1]. Yield-stress fluids are an important class of complex fluids, and their flow behavior remains incompletely understood [2, 3]. Most often, yield-stress fluids are a dispersion of one material in a continuous phase, e.g. suspensions of (soft) particles or polymers, foams or emulsions. When sufficiently concentrated, these systems show a transition from mechanically solid-like to fluid-like states when the stress is increased above some critical value, the yield stress. The yield stress emerges in general when the volume fraction ϕ of the dispersed phase is higher than some critical value ϕ_c. This so-called jamming transition is currently a very popular subject in the fluid dynamics/statistical-mechanics community and has received a lot of attention [4–12]. However it is not completely clear how generic the jamming description is, and whether for instance the mechanical behavior of jammed systems as a function of the volume fraction can be fully described or even predicted by considering the jamming transition to be analogous to an equilibrium critical phase transition [9, 10, 13–15]. The idea of jamming as a critical phenomenon, which is inspired by an observed power-law divergence of mechanical quantities with respect to the distance from the jamming transition, is what we will investigate here. We first consider the relevant mechanical properties. For concentrated systems above the jamming transition, the flow behavior is often successfully described by the Herschel-Bulkley equation [16]

$$\sigma = \sigma_y + K\dot{\gamma}^{\beta} = \sigma_y[1 + (\tau_{HB}\dot{\gamma})^{\beta}], \tag{7.1}$$

where σ is the shear stress, σ_y is the yield stress, $\dot{\gamma}$ the shear rate and where K and β are adjustable parameters. One can then attempt to describe the vanishing of the yield stress with decreasing volume fraction as a power law in the distance to jamming:

$$\sigma_y = \sigma_0|\Delta\phi|^{\Delta} \tag{7.2}$$

with $|\Delta\phi| = |\phi - \phi_c|$ and ϕ_c the 'critical' (jamming) point. Below ϕ_c, the generically observed Newtonian-to-shear-thinning behavior with increasing shear rate can be well described by the Cross equation [17]

$$\sigma = \eta_N\dot{\gamma}/(1 + C\dot{\gamma}^{1-\delta}) = \eta_N\dot{\gamma}/[1 + (\tau_C\dot{\gamma})^{1-\delta}] \tag{7.3}$$

where C or τ_C and δ are again adjustable parameters; note that the shear-thinning regions of 7.1 and 7.3 are of the same form, with δ and C corresponding to β and η_N/K, respectively. The Newtonian viscosity η_N often satisfies a power law in $|\Delta\phi|$, expressed by the Krieger-Dougherty equation [18]

$$\eta_N = \eta_0|\Delta\phi|^{-M}, \eta_0 = \eta_{sol}\phi_c^M; \tag{7.4}$$

η_{sol} is the viscosity of the continuous solvent phase.

The above equations, in particular some of the power laws in $\dot{\gamma}$ and $|\Delta\phi|$, have been verified for many dissimilar systems, with often but not always similar values for each of the exponents β,Δ,δ and M. For instance, the Herschel-Bulkley and Cross exponents β and δ are generally around 0.5 while for the yield stress exponent Δ and the Krieger-Dougherty exponent M typically values between 1 and 3, and regularly close to 2, are reported (see Appendix B for a compilation of literature data with references). Experimental and simulation studies report a power law similar to 7.2 also for the static shear modulus of the solid-like phase: $G = G_0|\Delta\phi|^B$. With $\sigma_Y = G\gamma_y$ this corresponds to a vanishing of the yield strain γ_y if $B < \Delta$, as sometimes reported (see e.g. [19]), but B has also been found to have a similar value as Δ [20].

All the above equations apply to a steady state; however power-law scaling in time has also been reported for the transient creeping flow of a broad variety of dense complex systems close to their yield point but far from steady state. Independent of the stress the instantaneous effective viscosity $\eta = \sigma/\dot{\gamma}$ and the cumulative strain $\gamma(t)$ often follow the so-called Andrade law [21]

$$\eta(t) \sim t^\alpha, \gamma(t) \sim t^{1-\alpha} \tag{7.5}$$

over sometimes remarkably long times t. Such behavior was already observed by Andrade for metals in 1910 and has since been reported, in the macroscopic rheology or in corresponding microscopic timescales, for e.g. crystals [13, 22–24] glasses [25], polymers [26], emulsions [27, 28], gels [27, 28], foams [27, 28], sand [29], paper [30] and even complex biomaterials [31]. The value of the creep exponent α equally remarkably then often falls in a narrow interval 0.5-0.7.

Previously, Paredes et al. [20] have investigated the scaling in all the above equations on a single well-defined yield stress system: a dense soft-sphere emulsion

with supercritical and subcritical volume fractions ϕ, and established exponent values within the mentioned numerical ranges. Paredes et al. showed that by an appropriate scaling of the stress and rate with only two independent exponents all supercritical and subcritical flow curves could be mapped onto two master curves that merge at high shear rates. This was interpreted as evidence for a critical transition in the dynamics, from fluid to solid-like behavior. Collapse of supercritical Herschel-Bulkley data, with exponents very close to those of [20], had previously been reported by Nordstrom et al. for a different soft-colloid system [32]. Earlier, in two-dimensional (2D) simulations of overdamped soft disks, Olsson and Teitel reported a similar data collapse and a critical transition, but with different power-law exponents [33]. Simulations by Otsuki and Hayakawa [34, 35] for 2D, 3D and 4D soft spheres with inertial dynamics gave qualitatively similar scaling, data collapse and transition with density, and could be rationalized with a similar Scaling-Ansatz approach; however, in this case the exponents and exponent relations proved independent of dimension and were clearly different from those in the experiments of [20] and [32] or those in the simulations of [33]. In equilibrium phase transitions, the exponents and exponent relations depend on dimensionality and symmetry, but not on details of the interactions. For jamming systems, some evidence of dimension-independent scaling, but with particle-interaction-dependent exponents different from those in [20], has been given e.g. in static simulations by O'Hern et al. [9, 10] and/or in flow studies [36, 37]. However, very recently Vågberg et al. [38] revisited this point and, based on two different simulation models, claim for their 2D case universal exponents in the flow of overdamped shear-driven frictionless systems.

The question is then whether the exponents that characterize the mechanical behavior depend on the (details of the) interparticle interactions. Paredes et al. propose that the critical transition happens because the mechanical behavior of systems near jamming is governed by a growing lengthscale associated with the heterogeneous dynamics, well above the lengthscale of the individual particles. In the loose analogy with equilibrium phase transitions one would then suppose that the exponent values are universal, i.e. independent of particle or interaction details. Heterogeneous microscopic dynamics is a frequently reported feature in various glassy or jamming systems investigated experimentally or by simulation, with a lengthscale of fluctuating cooperative motion well beyond the single-particle diameter, with a characteristic timescale of such fluctuations, and with accelerated particle motion under load [33, 39–48]. Several studies report a divergence of

such properties in approach of the yield stress, with power laws in stress, rate or distance $|\Delta\phi|$ [38, 42, 49–57]. These observations have suggested that, in spite of important differences [47, 58–60], close analogies exist between glasses and jammed systems (see e.g. [11, 44]) and have given support to the idea [9, 10, 13–15] that the transition from flow to arrest in complex disordered systems under external load is a dynamic analogue of thermodynamic second-order phase transitions, with analogous mesoscopic heterogeneity and power-law scaling, and that this transition is generic to a broad variety of such complex systems. Paredes et al. [20] outlined a simple microscopic two-state scaling theory that could rationalize the observed macroscopic flow and transition in terms of a critical divergence in the microscopic heterogeneous dynamics, with two independent microscopic scaling exponents only that agreed with their experiments.

The aim of this chapter is threefold. First, we seek more systematic order in the experimental results by comparing the flow behavior of a number of systems that are all 3D and overdamped, but have different particle interactions. The focus is thereby mainly on the supercritical Herschel-Bulkley regime. Second, we elaborate in more detail the two-state microscopic model that was briefly outlined in [20]. Third, we compare the predictions of this model with our own experimental results and with a broad range of literature data, ordering the latter in comparable classes.

This chapter is organized as follows. In the next section we experimentally investigate the steady-state rheology of different systems that exhibit a jamming transition. First, the difference between emulsions with mobile and rigid droplet surfaces is considered; second, the flow curves of two other complex liquids, a foam and a Carbopol gel, are examined. Scaling of the data onto master curves is investigated and the scaling exponents of the four systems are compared. In the following section the master-curve scaling and the critical transition from flow to jamming are described using a Scaling Ansatz, following [33]. To rationalize this Scaling Ansatz from a more microscopic point of view, we develop a model of the heterogeneous dynamics. The model results in a number of relations among the scaling exponents that can be verified experimentally. A comparison with our own flow-curve data and data from the literature is made. In a final section conclusions are summarized, in particular on the microscopic origin of the observed scaling around the jamming transition and on the universality in this scaling among different systems.

7.2 Experimental rheology

In this section the steady-state rheology of four different systems that exhibit a jamming transition is studied. First two types of yield stress emulsions have been prepared, one system with mobile particle surfaces and one with rigid surfaces. In general most type of surfactant-stabilized emulsions are considered as having mobile droplet surfaces and it is usually assumed that this leads to harmonic interactions between the drops [19]. Our mobile emulsions were stabilized using Sodium Dodecyl Sulfate (SDS, from Sigma Aldrich), which is an ionic surfactant with molar formula $CH_3(CH_2)_{11}SO_4^-Na^+$. The rigid emulsions were stabilized using a protein solution composed of bovine serum albumin (BSA, from Sigma Aldrich) and a co-surfactant propylene glycerol alginate (PGA, from Dextra); this creates rigid surfaces on the droplets [61] and will thereby increase the drops' resistance to deformation and slow down the drainage of liquid channels between the droplets. As a consequence, the mechanical properties of the system change and one would expect to see a difference in the flow curves.

As a third system, SDS-stabilized foam was chosen. Data for this foam were obtained from previous research of S. Marze et al. [62], who studied the steady flow of three-dimensional aqueous foams at different volume fractions. The fourth system is a Carbopol 'gel', for which different volume fractions were prepared.

7.2.1 Mobile emulsion

The results on the mobile emulsions were already reported in [20]. Flow curves were obtained by performing a shear-rate sweep as shown in Fig. 7.1(a). From these flow curves we determined that $\phi_c \approx 0.645$; a linear extrapolation of the yield stress to zero gives $\phi_c = 0.648 \pm 0.004$, whereas a quadratic fit works better and gives $\phi_c = 0.645 \pm 0.005$. The curves above ϕ_c can each be fitted separately with the Herschel-Bulkley equation (1). However, the data for all these supercritical volume fractions can also be mapped onto one master curve by plotting $\sigma/|\Delta\phi|^{\Delta}$ versus $\dot{\gamma}/|\Delta\phi|^{\Gamma}$ and fitting $\Delta = 2.13$ and $\Gamma = 3.84$, see Fig. 7.1(b). Interestingly the flow data below ϕ_c then also collapse automatically, onto a curve that coincides with the supercritical one at high rates. The supercritical master branch accurately follows the Herschel-Bulkley equation with $\beta = \Delta/\Gamma = 0.55$ and $K = 0.87$. The branch corresponding to fractions below ϕ_c can be fitted to the Cross equation

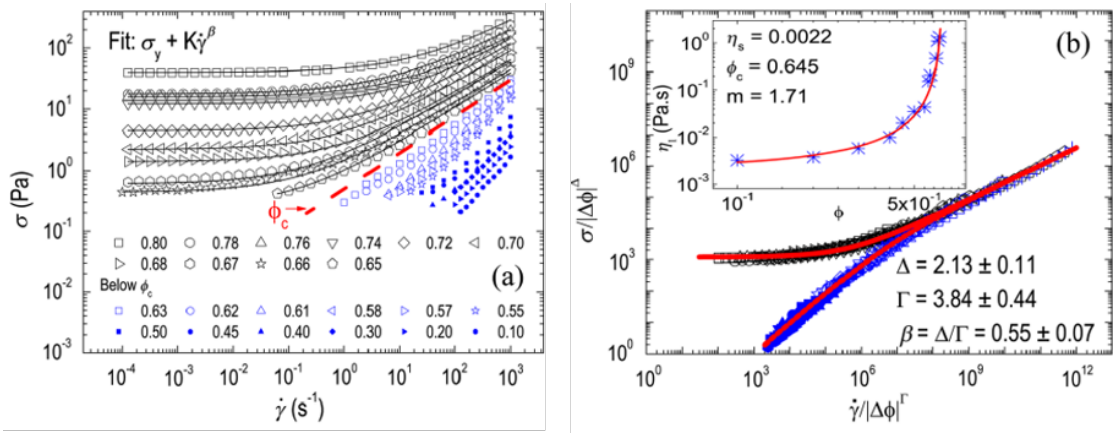

FIGURE 7.1: (a) Flow curves of mobile emulsions: Castor oil in water with 1wt% SDS, for different internal volume fractions, showing Herschel-Bulkley fittings for $\phi > \phi_c$; symbols represent different volume fractions of the internal (oil) phase. (b) Master curve showing collapse of flow curves onto two branches, one for samples with $\phi > \phi_c$ and one for $\phi < \phi_c$, when plotted as $\sigma/|\Delta\phi|^\Delta$ versus $\dot{\gamma}/|\Delta\phi|^\Gamma$; the red lines are supercritical and subcritical branches representing the Herschel-Bulkley and the Cross fits of the master curve, respectively. Black symbols correspond to samples with $\phi > \phi_c$ and blue symbols correspond to samples with $\phi < \phi_c$; fit parameters are given in Table 7.1. Inset in (b): Fit of the low-shear viscosity to the Krieger-Dougherty equation, giving $eta_{sol} = 2.2x10^{-3}Pas$ and $M = 1.71$ with $\phi_c = 0.645$ [20].

(3) with $\delta = \beta$ and $C = \eta_N/K$, with the same values of β and K as above ϕ_c. The supercritical data can independently be scaled as σ/σ_y versus $\dot{\gamma}/\sigma_y^{1/\beta}$, giving a collapse with b = 0.60. All fitted parameters, including the prefactors σ_0 and η_0 , are summarized with their uncertainties in Table 7.1. Note that in [20] the Newtonian viscosity η_n was independently measured and found to accurately satisfy the Krieger-Dougherty equation (4), with an exponent fully consistent with the above exponent values, i.e. $M = \Gamma - \Delta = 1.71$ (see the inset of Fig. 7.1(b)); the supercritical shear modulus G was found to vanish with $\Delta\phi$ with the same exponent as the yield stress. These linear-response aspects will not be further discussed here, and we will focus on the flow curves.

7.2.2 Rigid emulsion

The flow curves obtained for the rigid emulsions are shown in Fig. 7.2(a). From these curves, using again a quadratic fit of the yield stresses versus Dj it is determined that $\phi_c = 0.64 \pm 0.006$. All flow curves for supercritical volume fractions, each obeying the Herschel-Bulkley equation, can be rescaled onto one master plot in the same manner as above, using $\Delta = 2.04$ and $\Gamma = 3.80$; these collapsed data

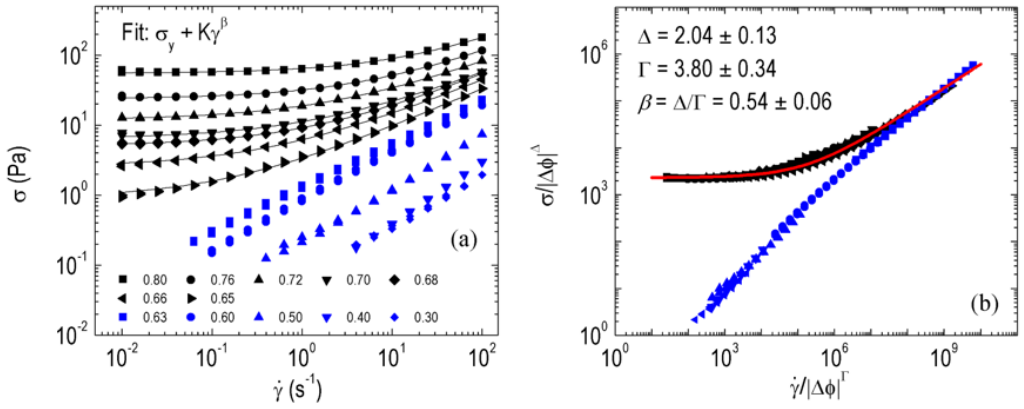

FIGURE 7.2: (a) Flow curves of rigid emulsions: Castor oil in water with 0.4wt% BSA and 0.4wt% PGA, for different internal volume fractions.(b) Master curve showing collapse of flow curves onto two branches, one for samples with $\phi > \phi_c$ and one for $\phi < \phi_c$, when plotted as $\sigma/|\Delta\phi|^{\Delta}$ versus $\dot{\gamma}/|\Delta\phi|^{\Gamma}$; the red line isthe supercritical branches representing the Herschel-Bulkley master fit. Black symbols correspond to samples with $\phi > \phi_c$ and blue symbols correspond to samples with $\phi < \phi_c$; fit parameters are given in Table 7.1.

fit to a Herschel-Bulkley equation with $\beta = \Delta/\Gamma = 0.54$ and $K = 4.25$. Once again all flow data below ϕ_c then automatically also collapse with this procedure onto a single curve, which meets the supercritical one at high rate, Fig. 7.2(b). However, as is clear from the slopes in Fig. 7.2(a), all subcritical samples are still shear-thinning even at the lowest rates. As a consequence, no reliable value for η_0 can be obtained from a master fit of the collapsed data to the Cross equation. Direct scaling of σ/σ_y versus $\dot{\gamma}/\sigma_y^{1/\beta}$ also gives $\beta = 0.54$. The final results are very similar to the rescaling found for the mobile emulsions, see Table 7.1.

7.2.3 Foam

All flow curves as measured by S. Marze et al. [62] for different volume fractions were fitted with the Herschel-Bulkley equation, Fig. 7.3(a). The critical volume fraction was determined by a quadratic fit of the yield stresses, resulting in $\phi_c = 0.68 \pm 0.03$; this value is somewhat higher than that of random close packing, which may be due to the larger size polydispersity. Once again all flow curves can be rescaled and collapsed onto one master curve when plotted as $\sigma/|\Delta\phi|^{\Delta}$ versus $\dot{\gamma}/|\Delta\phi|^{\Gamma}$, for $\Delta = 2.21$ and $\Gamma = 3.75$, Fig. 7.3(b). The Herschel-Bulkley representation of the latter gives $\beta = \Delta/\Gamma = 0.59$ and $K = 2.53$. Direct scaling of σ/σ_y versus $\dot{\gamma}/\sigma_y^{1/\beta}$ gives $\beta = 0.57$, see also Table 7.1.

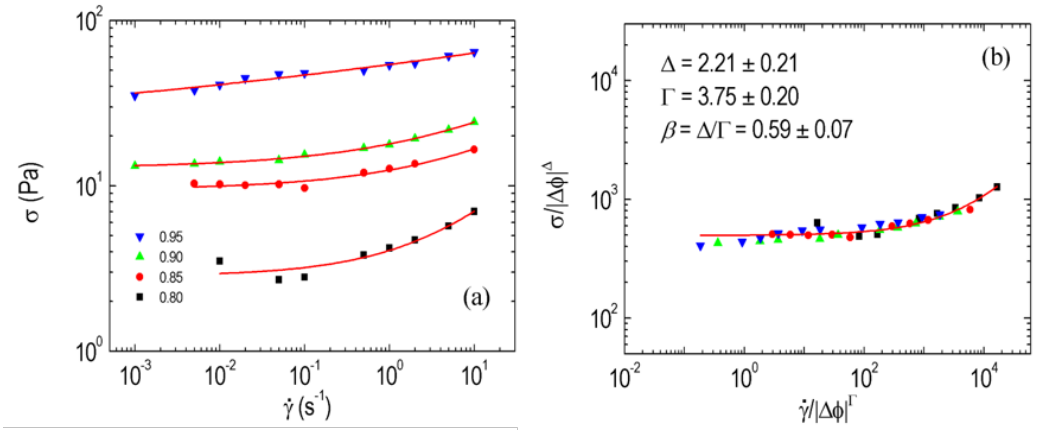

FIGURE 7.3: (a) Flow curves for SDS foams for different liquid volume fractions (experimental data from [62]). The red lines show Herschel-Bulkley fittings. (b) Master curve showing the collapse of flow curves onto one, when plotted as $\sigma/|\Delta\phi|^{\Delta}$ versus $\dot{\gamma}/|\Delta\phi|^{\Gamma}$. The different symbols represent different volume fractions; fit parameters are given in Table 7.1.

7.2.4 Carbopol

For the Carbopol gels with different volume fraction the flow curves were obtained by performing the same rheological procedure as for the yield stress emulsions, Fig. 7.4(a). The considered weight fractions are very low, but due to the strong pH-dependent swelling of the sponge-like particles a Herschel-Bulkley fit with a yield stress and shear thinning is showing up at all concentrations. It is hard to define a meaningful single critical volume fraction for these expanding gels, but the data for all volume fractions can still be collapsed onto one master curve by direct scaling with the yield stress, Fig. 7.4(b). The master curve fits the Herschel-Bulkley equation with $\beta = 0.48$ and $K = 11.85$. The relatively large error bound of about 30% in b is mainly due to the lowest concentration; if the data for this concentration are omitted a much better master fit follows, with $\beta = 0.55$ and $K = 11.77$, see also Table 7.1.

7.2.5 Summary of the experimental data

Different systems were investigated and rescaled with simple power laws in the distance to jamming, giving supercritical and (where accessible) subcritical master curves. As indicated before by Paredes et al. [20], the combined Herschel-Bulkley and Cross equations nicely describe such flow behavior for a single simple yield

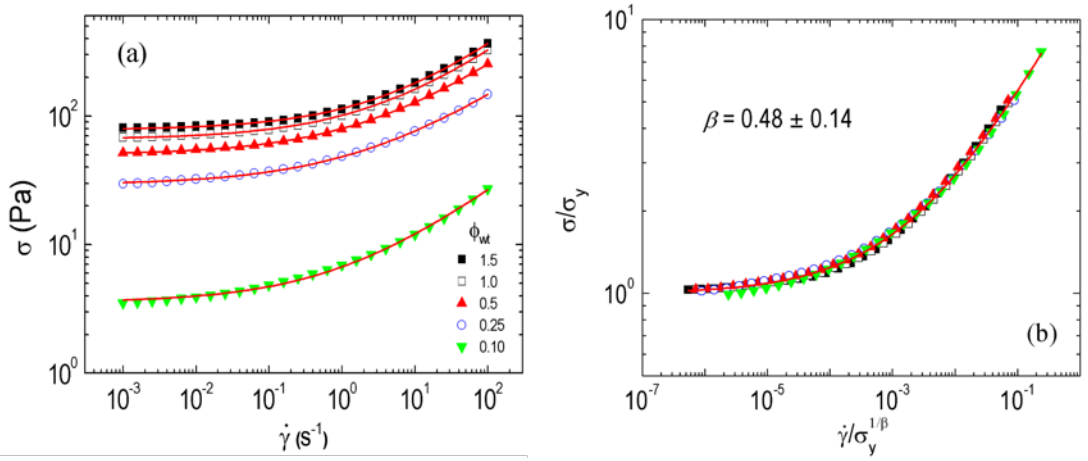

FIGURE 7.4: (a) Flow curves of Carbopol for different internal volume fractions. The red lines show the Herschel-Bulkley fittings. (b) Master curve showing collapse of all flow curves onto one, when plotted as σ/σ_y versus $\dot{\gamma}/\sigma_y^{1/\beta}$. The different symbols represent different volume fractions; fit parameters are given in Table 7.1.

stress emulsion. We have shown here that these combined equations can be used to successfully describe the flow behavior near jamming for four different systems: mobile and rigid emulsions, foam and Carbopol. All of the individual systems are rescaled onto one single master curve by plotting $\sigma/|\Delta\phi|^{\Delta}$ versus $\dot{\gamma}/|\Delta\phi|^{\Gamma}$, with fitting parameters as shown in Table 7.1. As a remarkable result, all different systems can be rescaled with exponents that within numerical uncertainty have common values: $\Delta \approx 2.1$, $\Gamma \approx 3.8$ and $\beta = \Delta/\Gamma \approx 0.55$. This strongly supports the conclusion that the flow behavior of such overdamped yield-stress materials can be described by one universal scaling form, independent of the mechanical properties of the system. A similar claim was made recently by Vågberg et al. [38], based on two simulated 2D systems.

7.3 Scaling and microscopic model

7.3.1 Scaling ansatz

The collapse of all rheological data on two master curves by the scaling of the two axes with the appropriate power laws in $|\Delta\phi|$, as demonstrated in Figs. 7.1-7.4, leads to the assumption that the rheology above and below the jamming concentration has one common origin. Such a collapse was already shown for

TABLE 7.1: Overview of all rescaling parameters for the four systems: mobile and rigid emulsions, foam, and Carbopol. The factor in the lowest row of the table is added as a numerical consistency check: the scaling approach to be discussed below shows that it should be of order unity.

Parameter	Mobile emulsions	Rigid emulsion	Foam	Carbopol
ϕ_c	0.645 ± 0.005	0.64 ± 0.006	0.68 ± 0.03	
Δ	2.13 ± 0.11	2.04 ± 0.13	2.21 ± 0.21	
Γ	3.84 ± 0.44	3.80 ± 0.34	3.75 ± 0.20	
$\beta = \Delta/\Gamma$	0.55 ± 0.07	0.54 ± 0.06	0.59 ± 0.07	
β (from σ_y scaling)	0.60 ± 0.08	0.54 ± 0.08	0.57 ± 0.09	0.48 ± 0.14 0.55 ± 0.04*
K	0.87	4.25 ± 0.39	2.53 ± 0.12	11.85 ± 0.11 11.77 ± 0.18*
σ_0 [Pa]	1100	2315 ± 59	497 ± 10	
η_0 [Pa s]	0.001			
$\sigma_0^{1-\beta}\eta_0^{\beta}/K$	0.60			

* Leaving out the lowest concentration of 0.10 wt% (see text).

other soft-colloid dispersions [32] and also seen in simulations [33–35, 63]. The assumption is mathematically expressed by a Scaling Ansatz [33] similar to the Widom scaling for equilibrium critical phase transitions:

$$\sigma = \sigma_0|\Delta\phi|^{\Delta}F_{\pm}(\eta_N\dot{\gamma}/\sigma_y) = \sigma_0|\Delta\phi|^{\Delta}F_{\pm}(\eta_0\dot{\gamma}/\sigma_0|\Delta\phi|^{\Gamma}) \tag{7.6}$$

Here $F_{\pm}(z)$ is a crossover function that modifies the supercritical linear-elastic behavior depending on the ratio of viscous to elastic stresses, both for supercritical (+) and for subcritical (-) concentrations. So for $z \ll 1$ we must have $F_+(z) = 1$ and $F_-(z) = z$; for $z \gg 1$ we get $F_{\pm}(z) = Az^{\beta}$, with $\beta = \Delta/\Gamma$ to ensure that it is independent of concentration in the critical limit $\phi = \phi_c$; A is an unspecified constant of order unity. The equation for large z corresponds to the shear-thinning regime, since it implies $\sigma = A\sigma_0(\eta_0\dot{\gamma}/\sigma_0)^{\beta}$. It expresses that here the super- and subcritical systems become indistinguishable. This is obviously the case at the critical concentration, but as the argument of the crossover function shows the critical regime widens at high rate, with crossover rates for critical shear-thinning behavior at either side of ϕ_c satisfying (apart from a constant of order unity):

$$\dot{\gamma}_{co} = (\sigma_0/\eta_0)|\Delta\phi|^{\Gamma} \tag{7.7}$$

Identifying the above results with the power laws in the empirical Herschel-Bulkley,

Cross and Krieger-Dougherty equations we have $\beta = \delta$, $K = \eta_N/C = A\sigma_0^{1-\beta}\eta_0^{\beta}$, $M = \Gamma - \Delta$. Note that apart from a constant of order unity the relaxation rates $1/\tau_{HB}$ and $1/\tau_c$ of the Herschel-Bulkley and Cross equations equal the critical crossover rate 7.7. While the Scaling Ansatz is thus able to reproduce with only two independent scaling exponents the phenomenology of the observed rheology scaling across the critical concentration, both in the linear and shear-thinning regimes, a microscopic model is still needed to explain it.

7.3.2 Microscopic model of heterogeneous dynamics

Based on the experimentally observed scalings we propose a simple model of microscopic heterogeneous dynamics to explain the macroscopic rheology around the critical concentration for jamming. As mentioned in the introduction, the observed flow mechanics is common to many experimental and simulated systems for which such heterogeneous dynamics has been reported and has led to the suggestion that the underlying cause is a generic second-order critical transition in the dynamics, between a stagnant and a fluid phase. We follow this suggestion and attempt to explain the data from a simple two-state model for such a transition. Here we repeat the main idea of the model as it has been already described by Paredes et al. [20] and we elaborate in more detail in Appendix B.

When our yield-stress materials are under stress above the yield stress the stagnant phase starts flowing. We assume that under stress a fraction s of the particles remains stagnant in neighbor cages while the fraction $(1 - s)$ becomes fluidized. This simple two-state picture represents what are in reality two sides of a very broad mobility distribution. In view of the observations we make an analogy with the linear regime and assume that the lengthscale ξ of correlated, heterogeneous dynamics diverges when s approaches a critical value s_c where macroscopic flow halts. Following the idea that the divergence is similar to that near a second-order phase transition, we can then choose the divergent lengthscale as the single dominant variable that governs macroscopic behavior, while the other variables exhibit a power law dependence on ξ:

$$\xi \sim |1 - s/s_c|^{-\nu} \tag{7.8}$$

Subsequently, we assign the local viscosity, η_f, to the fluidized phase and treat the arrested domains as a dispersed solid phase. Hence we postulate the viscosity η

with the same exponent m as in the low-shear limit below ϕ_c:

$$\eta = \eta_f(1 - s/s_c)^{-m} \tag{7.9}$$

This interpretation is a logical generalization of 7.4 if we choose the same exponent $m = M$ as in the Krieger-Dougherty equation. The associated diverging time scale, $\tau_\eta(s)$, is much shorter than the lifetime of the fluctuating heterogeneity pattern, $\tau_{het}(s)$, i.e., the time τ_A in which mobile particles get arrested again is:

$$\tau_A(s) \sim (1 - s/s_c)^{-n} \tag{7.10}$$

with $n > m$. The time evolution of the stagnant fraction $s(t)$ can then be given by a simple first-order kinetic equation:

$$ds/dt = -\frac{s}{\tau_R} + \frac{1 - s}{\tau_A} \tag{7.11}$$

with $1/\tau_R$ the relaxation rate for the arrested particles to become mobile and $1/\tau_A$ the rate with which mobile particles become arrested again. The relaxation rate $1/\tau_R$ can be determined as the sum or maximum of either the Eyring-type rate [64] for stress-induced escape out of a cage or the rate $\dot{\gamma} = \sigma/\eta$ at which the average cage vanishes. The Eyring-type rate has a deep minimum at $\sigma = 0$ and a steep increase towards a plateau value for increasing σ. The ratio $\tau_A(0)/\tau_R(0)$ is effectively zero above ϕ_c, but increases rapidly below ϕ_c.

The full flow curve follows from the steady state solution $ds/dt = 0$, which gives the correlation between s and σ and subsequently the shape of the flow curve:

$$\eta(\sigma) \sim \tau_A(s)^{m/n} \tag{7.12}$$

We can recognize two limiting cases: when s approaches s_c from below ($\tau_R \gg \tau_A(0)$), and when s approaches 0 ($\tau_R \ll \tau_A(0)$). For σ approaching 0, we find:

$$\frac{\eta}{\eta_f} = \left[\frac{\tau_R(0)}{\tau_A(0)}\right]^{m/n} \tag{7.13}$$

this implies an infinite viscosity and hence a yield stress above ϕ_c. For $\sigma > \sigma_y$ the function 7.13 equals $\dot{\gamma}^{-1}$, from which we can derive the shear-thinning regime $\sigma = K\dot{\gamma}^\beta$ of the Herschel-Bulkley expression with $K = \eta_f/[\tau_a(0)]^{m/n}$ and $\beta = 1 - m/n$. Since $m = \Gamma - \Delta$ we can make the identification $n \equiv \Gamma$. The yield stress itself

follows from $\dot{\gamma} = 1/\tau_R(\sigma)$, with the result that the crossover rate to shear thinning decreases to effectively zero for decreasing σ_y and $|\Delta\phi|$. Below ϕ_c a very similar analysis can be done but now the ratio $\tau_R(0)/\tau_A(0)$, i.e., the low-stress viscosity is finite and decreases rapidly with decreasing ϕ. In this case shear thinning starts at $\dot{\gamma} = 1/\tau_R(0)$, which increases again with $|\Delta\phi|$.

In order to understand the origin of the heterogeneity time scale and the associated exponent $n > m$ we make a variation on Mott's argument for explaining creep via dislocation motion in metals [65]. We consider a collective rearranging region of N particles that share a collective free volume v to make rearrangements possible. Over a time τ_η the N particles will, on average, have move to a neighboring position. Consequently, each particle will experience an individual free volume change δv, which will typically scale as v/N. If we assume the fluctuations to be random (δv will be of either sign), we have for the average over time $\langle \sum \delta v \rangle = 0$, while the average squared fluctuation will scale with $\langle (\sum \delta v)^2 \rangle = \langle \sum (\delta v)^2 \rangle \sim N(v/N)^2 \sim 1/N$. In the critical limit of diverging N this will also vanish and within the considered time τ_η nothing of consequence happens: the rearrangements will continue. However, the squared Gaussian fluctuations keep adding up linearly with time, so after a time $\tau_A = N\tau_\eta$ we have $\langle \Sigma(\delta v)^2 \rangle \sim v^2$. At this point the free-volume distribution has become such that there is a finite probability of the region to arrest, so τ_A is the lifetime of the mobile region. With $N \sim \xi^d$, we then find $n \equiv \Gamma = m + d\nu$ or $\Delta = d\nu$. Note that Δ is the yield stress exponent and that we derive it here from the rheology, without considering the elastic interaction.

In conclusion, the model explains the experimentally observed yield stresses (above ϕ_c) versus the Newtonian-liquid behavior (below ϕ_c) at low rates, and the continuity across ϕ_c in the power-law shear-thinning regime at high rates, with microscopic interpretations of the scaling exponents.

7.4 Comparing the model to experimental data

7.4.1 Universal steady-state rheology

To judge the merits of the model we first note that it gives a microscopic basis for the Scaling Ansatz 7.6, which is accurately satisfied by the experimental data in figures 7.1-7.4. As is clear from Table 7.1, the microscopic exponents $m =$

$\Gamma - \Delta$ and $n = \Gamma$ or $m/n = 1 - \beta$ derived from the fits show little difference for the different experimental systems, notably for the two emulsions with strongly different particle interactions. Considering the numerical errors the exponents may well be universal to such 3D shear-driven dissipative systems, with typical values $m = 1.7$ and $n = 3.8$. The two microscopic timescales τ_a and τ_b that can be derived from our data in each case differ by many orders of magnitude: τ_b can be estimated from the crossover rate to shear thinning; on the other hand the high-rate Newtonian regime IV above τ_a^{-1} is nowhere within reach, and as a consequence the asymptotic parameters τ_a and η_a cannot be determined from the data. Since the spatial heterogeneity has not been measured the third microscopic exponent ν cannot be determined either. In the literature a value around 0.7 has been suggested more than once [14, 20, 33, 52]; together with our model prediction $\Delta = d\nu$ this would result in a realistic value $d = 3.0$. Furthermore, as shown already in [20] the soft emulsion gives within experimental accuracy a single power-law exponent$\Delta = B$ for the yield stress and shear modulus, respectively, and consequently a nonvanishing yield strain near ϕ_c.

7.4.2 Literature data

In the literature many other jamming systems have already been analyzed for their mechanical, rheological or microstructural scaling laws, with a broad range of exponent values, partly at variance with the present data. For instance, in several papers [9, 10, 34–37] it is suggested that exponents should be independent of spatial dimension, but sensitively dependent on the type of interparticle interaction; also the exponent Δ for the vanishing yield stress is claimed to be larger than the exponent B for the vanishing shear modulus, with a consequent vanishing of the yield strain near ϕ_c. These suggestions are supported by simulation data; however, it is not clear that the assumptions underlying these simulations would hold for all kinds of studied systems. Apart from the spatial dimension one should a priori distinguish e.g. athermal versus Brownian systems and crossovers between the two [58–60, 66, 67], dry or wet systems with inertial effects and a subcritical Bagnold regime [34, 35], and (quasi-)static simulated systems that are fully energy-minimized [9, 10]; in particular the conclusions of interaction-dependent and dimension-independent exponents and of a vanishing yield strain are reached in the latter cases. Beyond the variety in studied systems is the problem of often limited data range and accuracy, which may lead to practical curve fits rather

than asymptotic scaling analysis, with correspondingly inaccurate exponents. In Appendix B we have collected measured or simulated exponent values for a broad range of systems (Table C-I), with similar systems grouped there together. In the present discussion we compare in Table 7.2 our experimental data and model only with those systems that are clearly overdamped and athermal. Where possible and relevant we have added in red (light grey) italics additional exponent values that would result from applying our model to the published exponent values.

The flow-curve scaling demonstrated by [32] for an athermal soft suspension gives exponents very comparable to those in figures 7.1-7.4: $\Gamma = 4.1$, $\Delta = 2.1$, so $m = 2.0$, $n = 4.1$. By contrast, the scaling around the jamming transition of overdamped simulated disks [33] gives $\Delta = 1.2$, $M = 1.65$, hence $\beta = 0.42$, and thus markedly different exponents $m = 1.65$, $n = 2.85$ in dimension 2; in a later study on the same 2D system by partly the same authors [38] a slightly lower value $\beta \approx 0.30$ is reported but still the exponents are argued to be universal for overdamped systems, so independent of details of particle interactions. The same authors also comment on the deviating results and conclusions of [36].

The simulated value $\nu = 0.73$ in [52] connects well with our equation $\Delta = d\nu$ and a yield stress exponent $\Delta = 2.1$ as obtained here, while in the 2D simulations of [33] the values of Δ and d are different but the model prediction $\Delta = d\nu$ is still satisfied. In the 2D study of [33] there is also an accurately satisfied Scaling Ansatz for ξ vs. σ, with a consequential relation $\xi \sim \sigma^{-\nu/\Delta}$ in the critical regime; with our identification $\Delta = n - m$ this relation is the same as (13). In the related study of [38] ξ has been measured near ϕ_c as a power of $\dot{\gamma}^{-1}$, with the result $\nu/\Gamma = \nu/n = 1/5.6$; within the reported numerical accuracy for ν this is consistent with the exponents of [33]. In the 3D simulation of [55] ξ has been measured close to ϕ_c as a power of $\dot{\gamma}^{-1}$, with an exponent 0.23; for our emulsions, assuming $\nu = 0.7$, equation (13) would give an exponent 0.18. The model assumption that for concentrations above ϕ_c the correlation length diverges on approach of the yield stress, i.e., that the scale of the heterogeneous dynamics becomes of the system size L in the quasistatic limit, has been confirmed in the simulations of [53, 54, 68].

The divergence of the microscopic timescales τ_η and τ_{het} has little been studied in a direct and quantitative manner. In the simulations by [52] of a 3D overdamped system a power-law divergence of the heterogeneity timescale was indeed found, with an exponent $n = 3.3$ somewhat below our value 3.8 for Γ. The simulations in [55] of the velocity autocorrelation and the spatial correlations imply a ratio

TABLE 7.2: Experimental, simulated or predicted scaling exponents for shear-driven overdamped systems. In bold italic additional exponents are given that result from applying our model to the published exponent values (*second entry: lowest concentration omitted).

Ref	System		Exponents of flow-curve scaling				Exponents of microscopic time- and lengthscales			
			Yield Stress	Cross-over rate	Shear thinning	Krieger-Dougherty	Single-particle mobility	Cooperative dynamics	Correlation length	
			Δ	Γ	β	M	m	n	ν below ϕ_c	above ϕ_c
	Model prediction	all d	$n-m$	n	$1-m/n$	m			$(n-m)/d$	$\zeta \sim L$ at $\sigma=\sigma_y$
This work	soft emulsion $\sim 3.2\mu m$ (data from [20])	$d=3$	2.13	3.84	0.55	1.71				
					0.55	***1.71***	***1.71***	***3.84***	***0.71***	
	rigid emulsion		2.04	3.80	0.54					
					0.54	***1.76***	***1.76***	***3.80***	***0.68***	
	foam (data from [62])		2.21	3.75	0.57					
					0.59	***1.54***	***1.54***	***3.75***	***0.74***	
	Carbopol gel				0.48/0.55*					
							m/n = 0.52/0.45*			
[32]	NiPa $\sim 1\mu m$	$d=3$	2.1	4.1	0.48					
					0.51	***2.0***	***2.0***	***4.1***	***0.7***	
[52]	overdamped simulations harmonic interaction							3.3	0.73	
			2.1	***3.3***	***0.64***	***1.2***	***1.2***			
[55]					0.64		$m/n=0.27, \nu/n=0.23$			
					0.69-0.73		**$m/n = 0.36$**			
[63]	overdamped simulations unspecified interaction					1.7				
[33]	overdamped simulations harmonic interaction	$d=2$	1.2			1.65			0.6	
				2.85	***0.42***		***1.65***	***2.85***	***0.6***	
[38]			1.08		0.30				$\nu = 0.18n$ at $\phi=\phi_c$	
				3.0-3.6	***0.36***	***1.9-2.5***	***1.9-2.5***	***3.0-3.6***	***0.54-0.65***	
[53]									0.9	$\xi \sim L$ at $\sigma=\sigma_y$
[54]			1.05							$\xi \sim L$ at $\sigma=\sigma_y$
[36]					0.5					
	overdamped model harmonic interaction			3/2		1/2				
				3		***3/2***	***3/2***	***3***	***1/2***	

of exponents $m/n = 0.27$, so indeed a strong separation of the two timescales, although this actual value is below our ratio of ca. 0.45. The samples of [32] that showed much similarity to ours in the scaling of flow curves, have also been investigated for their microscopic and heterogeneous dynamics [56]. Data covering the shear-thinning regime as well as the plateau regime show a single power-law relation between the mass of cooperative regions and the single-particle relaxation time, strengthening the concept of one dominant variable close to the critical transition. Using our equality $\tau_{het} = N\tau_\eta$ these results translate into a fairly low Herschel-Bulkley exponent $\beta = 1 - m/n = 0.24$, much lower also than earlier reported [32] from flow-curve scaling. The authors also report a very accurate scaling of the mass and relaxation time with the product of variables $\dot{\gamma}|\Delta\phi|^4$ cannot be explained by our model; we expect the dependence on these two variables to be different. The origin of the discrepancy remains unclear, but we note that in the measurements a significant stress and rate gradient was present over the larger cooperative domains, thus making the relation between the domain size and a single value for the order parameter s meaningless.

In sum, table 7.2 shows that there is often good agreement when comparing the present theory and emulsion data with the steady-state rheology of other over-damped and athermal literature systems, especially as regards the existence of the scaling laws. The exponent values in the table support the idea that the scaling around the jamming transition is universal for such systems, being only dependent on the spatial dimension but not on details of the interaction. The larger collection of data in Appendix B, table B.1 reveals much more variety in the exponent values, partly due to numerical inaccuracy but, more importantly, as a result of different underlying mechanisms or simulation assumptions.

In this chapter the main focus is on steady-state rheology. However, one of the key issues in the behavior of yield-stress fluids is the creep behavior, which as shown above can also be covered by the model. It was demonstrated recently [27, 28] that creep was the reason for sometimes wrongly interpreted "liquid like" behavior of yield-stress materials below σ ; in fact the creep is then so slow that a steady state is not reached within experimental timescales and so the apparent "viscosity" keeps on increasing in time, following the Andrade law (5). From the exponents m and n that characterize the steady-state rheology, our model predicts the exponent for the transient Andrade creep as $\alpha = m/(n-1)$. This prediction was tested on the soft emulsion with volume fraction $\phi = 0.66$, just above ϕ_c [20].

The steady-state data predict $\alpha = 0.60$, whereas the creep data accurately satisfy $\alpha = 0.6$, in close correspondence also with many observations in the literature.

7.5 Conclusion

We have determined and numerically analyzed the experimental steady-state flow behavior of four different yield stress systems: two emulsions, with mobile and rigid particle surfaces respectively, a 3D foam and a Carbopol gel. While the particle interactions of all four overdamped systems can be assumed rather different, their rheology near and across the critical jamming transition was found to obey universality: by appropriate scaling with the distance to jamming all systems allowed a data collapse onto supercritical Herschel-Bulkley and (where accessible) subcritical Cross master curves that meet at critical shear thinning; moreover the four sets of two independent scaling exponents proved the same within numerical error. To rationalize such critical scaling we have presented a simple microscopic two-state theory in which the steady state is a balance between stagnant and fluidized particles and where the stagnant fraction is the internal order parameter that is driven to criticality. Heterogeneous microscopic dynamics is at the heart of this theory and the two empirical scaling exponents could be related to exponents for two diverging timescales: for the single-particle fluidity and for the lifetime of the fluctuating heterogeneous domains. A third microscopic exponent describes the critical divergence of the heterogeneity length scale, not only near the jamming point but along the full yield-stress line. A heuristic argument based on fluctuations in the local free volume explains the origin of the heterogeneous dynamics and is able to give a scaling relation among the exponents. The theory also predicts power-law creep. The experimentally determined exponents and the predictions of the microscopic model have been compared with a large set of literature data, giving additional support both for the model and for the assumed universality among overdamped frictionless yield-stress systems of the same dimension.

References

[1] R. G. Larson. *The Structure and Rheology of Complex Fluids*. Oxford University Press, 1999.

[2] M. M. Denn and D. Bonn. Issues in the flow of yield-stress liquids. *Rheologica acta*, 50(4):307–315, 2011.

[3] D. Bonn, J. Paredes, M. M. Denn, L. Berthier, T. Divoux, and S. Manneville. Yield stress materials in soft condensed matter. *arXiv preprint arXiv:1502.05281*, 2015.

[4] A. J. Liu and S. R. Nagel. Nonlinear dynamics: Jamming is not just cool any more. *Nature*, 396(6706):21–22, 1998.

[5] A. Liu and S. R. Nagel. *Jamming and Rheology*. CRC Press, 2001.

[6] V. Trappe, V. Prasad, L. Cipelletti, P.N. Segre, and D.A. Weitz. Jamming phase diagram for attractive particles. *Nature*, 411(6839):772–775, 2001.

[7] F. Da Cruz, F. Chevoir, D. Bonn, and P. Coussot. Viscosity bifurcation in granular materials, foams, and emulsions. *Physical Review E*, 66(5):051305, 2002.

[8] D. Bonn, P. Coussot, H. T. Huynh, F. Bertrand, and G. Debrégeas. Rheology of soft glassy materials. *EPL (Europhysics Letters)*, 59(5):786, 2002.

[9] C. S. O'Hern, S. A. Langer, A. J. Liu, and S. R. Nagel. Random packings of frictionless particles. *Physical Review Letters*, 88(7):075507, 2002.

[10] C. S. O'hern, L. E. Silbert, A. J. Liu, and S. R. Nagel. Jamming at zero temperature and zero applied stress: The epitome of disorder. *Physical Review E*, 68(1):011306, 2003.

[11] A. J. Liu and S. R. Nagel. The jamming transition and the marginally jammed solid. *Annu. Rev. Condens. Matter Phys.*, 1(1):347–369, 2010.

[12] L. Berthier, G. Biroli, J.-P. Bouchaud, L. Cipelletti, and W. van Saarloos. *Dynamical Heterogeneities in Glasses, Colloids, and Granular Materials*. Oxford University Press, 2011.

[13] M. Miguel, A. Vespignani, M. Zaiser, and S. Zapperi. Dislocation jamming and andrade creep. *Physical review letters*, 89(16):165501, 2002.

[14] J. A. Drocco, M. B. Hastings, C. J. O. Reichhardt, and C. Reichhardt. Multiscaling at point j: Jamming is a critical phenomenon. *Physical review letters*, 95(8):088001, 2005.

[15] G. Biroli. Jamming: A new kind of phase transition? *Nature Physics*, 3(4):222–223, 2007.

[16] W. H. Herschel and R. Bulkley. Konsistenzmessungen von gummi-benzollösungen. *Colloid & Polymer Science*, 39(4):291–300, 1926.

[17] M. M. Cross. Rheology of non-newtonian fluids: a new flow equation for pseudoplastic systems. *Journal of colloid science*, 20(5):417–437, 1965.

[18] I. M. Krieger and Thomas J. Dougherty. A mechanism for non-newtonian flow in suspensions of rigid spheres. *Transactions of the Society of Rheology*, 3(1):137–152, 1959.

[19] B. P. Tighe. Relaxations and rheology near jamming. *Physical review letters*, 107(15):158303, 2011.

[20] J. Paredes, M. A. J. Michels, and D. Bonn. Rheology across the zero-temperature jamming transition. *Physical review letters*, 111(1):015701, 2013.

[21] E. N. C. Andrade. On the viscous flow in metals, and allied phenomena. *Proceedings of the Royal Society of London. Series A, Containing Papers of a Mathematical and Physical Character*, pages 1–12, 1910.

[22] M. Miguel, P. Moretti, M. Zaiser, and S. Zapperi. Statistical dynamics of dislocations in simple models of plastic deformation: Phase transitions and related phenomena. *Materials Science and Engineering: A*, 400:191–198, 2005.

[23] M. Miguel, L. Laurson, and M. J. Alava. Material yielding and irreversible deformation mediated by dislocation motion. *The European Physical Journal B-Condensed Matter and Complex Systems*, 64(3):443–450, 2008.

[24] L. Laurson, M. Miguel, and M. J. Alava. Dynamical correlations near dislocation jamming. *Physical review letters*, 105(1):015501, 2010.

[25] M. Siebenbürger, M. Ballauff, and T. Voigtmann. Creep in colloidal glasses. *Physical review letters*, 108(25):255701, 2012.

[26] G. B. McKenna. Mechanical rejuvenation in polymer glasses: Fact or fallacy? *Journal of Physics: Condensed Matter*, 15(11):S737, 2003.

[27] P. C. F. Møller, A. Fall, and D. Bonn. Origin of apparent viscosity in yield stress fluids below yielding. *EPL (Europhysics Letters)*, 87(3):38004, 2009.

[28] P. Moller, A. Fall, V. Chikkadi, D. Derks, and D. Bonn. An attempt to categorize yield stress fluid behaviour. *Philosophical Transactions of the Royal Society of London A: Mathematical, Physical and Engineering Sciences*, 367(1909):5139–5155, 2009.

[29] J. W. Dudley, M. T. Myers, R. D. Shew, M. M. Arasteh, et al. Measuring compaction and compressibilities in unconsolidated reservoir materials by time-scaling creep. *SPE Reservoir Evaluation & Engineering*, 1(05):430–437, 1998.

[30] J. Rosti, J. Koivisto, L. Laurson, and M. J. Alava. Fluctuations and scaling in creep deformation. *Physical review letters*, 105(10):100601, 2010.

[31] C. D. Agosti, K. M. Bell, D. J. Plazek, J. Larson, J. D. Kang, L. G. Gilbertson, and P. Smolinski. Analysis of power law models for the creep of nucleus pulposus tissue. *Biorheology*, 47:143, 2010.

[32] K. N. Nordstrom, E. Verneuil, P. E. Arriata, A. Basu, Z. Zhang, A. G. Yodh, J. P. Gollub, and D. J. Durian. Microfluidic rheology of soft colloids above and below jamming. *Phys. Rev. Lett.*, 115:175701, 2010.

[33] P. Olsson and S. Teitel. Critical scaling of shear viscosity at the jamming transition. *Phys. Rev. Lett.*, 99:178001, 2007.

[34] M. Otsuki and H. Hayakawa. Universal scaling for the jamming transition. *Prog. Theor. Phys.*, 121:647, 2009.

[35] M. Otsuki and H. Hayakawa. Critical behaviors of sheared frictionless granular materials near the jamming transition. *Phys. Rev. E.*, 80:011308, 2009.

[36] B. P. Tighe, E. Woldhuis, J. C. Remmers, W. van Saarloos, and M. van Hecke. Model for the scaling of stresses and fluctuations in flows near jamming. *Phys. Rev. Lett.*, 105:088303, 2010.

[37] G. Katgert, B. P. Tighe, and M. van Hecke. The jamming perspective on wet foams. *Soft Matter*, 9:9739, 2013.

[38] D. Vågberg, P. Olsson, and S. Teitel. Universality of jamming criticality in overdamped shear-driven frictionless disks. *Phys. Rev. Lett.*, 113:148002, 2014.

[39] M. D. Ediger. Spatially heterogeneous dynamics in supercooled liquids. *Annu. Rev. Phys. Chem.*, 51:99, 2000.

[40] R. Richert. Heterogeneous dynamics in liquids: fluctuations in space and time. *J. Phys. Condens. Matter*, 14:R703, 2002.

[41] E. Aharonov, E. Bouchbinder, H. G. E. Hentschel, V. Ilyin, N. Makedonska, I. Procaccia, and N. Schupper. Direct identification of the glass transition: Growing length scale and the onset of plasticity. *EPL*, 77:56002, 2007.

[42] R. A. Riggleman, H.-N. Lee, M. D. Ediger, and J. J. de Pablo. Free volume and finite-size effects in a polymer glass under stress. *Phys. Rev. Lett.*, 99:215501, 2007.

[43] R. A. Riggleman, K. S. Schweizer, and J. J. de Pablo. Nonlinear creep in a polymer glass. *Macromolecules*, 41:4969, 2008.

[44] H.-N. Lee, K. Paeng, S. F. Swallen, and M. D. Ediger. Direct measurement of molecular mobility in actively deformed polymer glasses. *Science*, 323:231, 2009.

[45] D. A. Sessoms, I. Bischofsberger, L. Cipelletti, and V. Trappe. Multiple dynamic regimes in concentrated microgel systems. *Trans. Roy. Soc. A*, 367:5013, 2009.

[46] R. A. Riggleman, H.-N. Lee, M. D. Ediger, and J. J. de Pablo. Heterogeneous dynamics during deformation of a polymer glass. *Soft Matter*, 6:287, 2010.

[47] S. Maccarone, G. Brambilla, O. Pravaz, A. Duri, M. Ciccotti, J.-M. Fromental, E. Pashkovski, A. Lips, D. Sessoms, V. Trappe, and L. Cipelletti. Ultra-long range correlations of the dynamics of jammed soft matter. *Soft Matter*, 6:5514, 2010.

[48] H.-N. Lee and M. D. Ediger. Mechanical rejuvenation in poly (methyl methacrylate) glasses? molecular mobility after deformation. *Macromolecules*, 43:5863, 2010.

[49] A. S. Keys, A. R. Abate, S. C. Glotzer, and D. J. Durian. Measurement of growing dynamical length scales and prediction of the jamming transition in a granular material. *Nat. Phys.*, 3:260, 2007.

[50] A. R. Abate and D. J. Durian. Topological persistence and dynamical heterogeneities near jamming. *Phys. Rev. E*, 76:021306, 2007.

[51] F. Lechenault, O. Dauchot, G. Biroli, and J. P. Bouchaud. Critical scaling and heterogeneous superdiffusion across the jamming/rigidity transition of a granular glass. *EPL*, 83:46003, 2008.

[52] T. Hatano. Growing length and time scales in a suspension of athermal particles. *Phys. Rev. E*, 79:050301(R), 2009.

[53] C. Heussinger, L. Berthier, and J.-L. Barrat. *EPL*, 90:20005, 2010.

[54] C. Heussinger and J.-L Chaudhuri, P. and. Barrat. Fluctuations and correlations during the shear flow of elastic particles near the jamming transition. *Soft Matter*, 6:3050, 2010.

[55] T. Hatano. Rheology and dynamical heterogeneity in frictionless beads at jamming density. *J. Phys. Conf. Ser.*, 319:012011, 2011.

[56] K. N. Nordstrom, J. P. Gollub, and D. J. Durian. Dynamical heterogeneity in soft-particle suspensions under shear. *Phys. Rev. E*, 84:021403, 2011.

[57] Y. Rahmani, K. van der Vaart, B. van Dam, Z. Hu, V. Chikkadi, and P. Schall. Dynamic heterogeneity in hard and soft sphere colloidal glasses. *Soft Matter*, 8:4264, 2012.

[58] A. Ikeda, L. Berthier, and P. Sollich. Unified study of glass and jamming rheology in soft particle systems. *Phys. Rev. Lett.*, 109:018301, 2012.

[59] A. Ikeda, L. Berthier, and P. Sollich. Disentangling glass and jamming physics in the rheology of soft materials. *Soft Matter*, 9:7669, 2013.

[60] P. Olsson and S. Teitel. Athermal jamming versus thermalized glassiness in sheared frictionless particles. *Phys. Rev. E.*, 88:010301(R), 2013.

[61] S. A. Koehler, S. Hilgenfeldt, E. R. Weeks, and H.A. Stone. Drainage of single plateau borders: Direct observation of rigid and mobile interfaces. *Phys. Rev. E*, 66:040601 (R), 2002.

[62] S. Marze, D. Langevin, and A. Saint-Jalmes. Aqueous foam slip and shear regimes determined by rheometry and multiple light scattering. *Journal of Rheology*, 52:1091–1111, 2008.

[63] T. Hatano. Scaling properties of granular rheology near the jamming transition. *Phys. Soc. Jpn.*, 77:123002, 2008.

[64] H. Eyring. Viscosity, plasticity, and diffusion as examples of absolute reaction rates. *J. Chem. Phys.*, 4:283, 1936.

[65] N. F. Mott. Lxxviii. a theory of work-hardening of metals ii: Flow without slip-lines, recovery and creep. *Philos. Mag.*, 44:742, 1953.

[66] F. Scheffold, F. Cardinaux, and T. G. Mason. Linear and nonlinear rheology of dense emulsions across the glass and the jamming regimes. *J. Phys. Condens. Matter*, 25:502101, 2013.

[67] A. Basu, Y. Xu, T. Still, P. E. Arriata, Z. Zhang, K. N. Nordstrom, J. M. Rieser, J. P. Gollub, D. J. Durian, and A. G. Yodh. Rheology of soft colloids across the onset of rigidity: scaling behavior, thermal, and non-thermal responses. *Soft Matter*, 10:3027, 2014.

[68] K. Martens, L. Bocquet, and J.-L. Barrat. Connecting diffusion and dynamical heterogeneities in actively deformed amorphous systems. *Phys. Rev. Lett.*, 106:156001, 2011.

Chapter 8

Rheology scaling of thermal glasses and jammed systems: cross-over and universality

8.1 Introduction

The transition between solid-like and liquid-like behavior in yield-stress fluids is a well-known phenomenon [1, 2], which remains difficult to understand quantitatively [3, 4]. Interestingly, thermal (e.g. glassy colloidal suspension) and athermal systems (e.g. foams and most emulsions) share important similarities at the rheological level. Both have a critical volume fraction ϕ_c at which solidity emerges, i.e., above this concentration the amorphous solid behaves elastically for small deformation but flows when a stress larger than the yield stress is applied. Below ϕ_c the material is a fluid whose viscosity increases rapidly with ϕ. Thermal systems have a glass transition $\phi_c = \phi_G \sim 0.58$, while purely athermal ones have a jamming transition $\phi_c = \phi_J \sim 0.64$. Flow properties of both types of systems are often well described by the Herschel-Bulkley equation $\sigma = \sigma_y + K\dot{\gamma}^\beta$ (above ϕ_c) and the Cross equation $\sigma = \eta_N\dot{\gamma}/(1 + C\dot{\gamma}^{1-\delta})$ (below ϕ_c)[1]. In case of athermal jamming, the yield stress and the crossover rate to shear thinning are regularly reported to have a power-law dependence on the distance to ϕ_c, with power-law exponents in the same range: $\sigma_y = \sigma_0|\Delta\phi|^\Delta$ and $\dot{\gamma}_{co} = \dot{\gamma}_0|\Delta\phi|^\Gamma$, with $|\Delta\phi| = |\phi - \phi_c|$. Olsson and Teitel [5] were the first to suggest, based on numerics, that for a single system this can lead to a collapse of all concentration-dependent flow curves onto one supercritical and one subcritical branch, which merge in the shear-thinning region.

In theory the scaling exponents for athermal systems depend on the details of the interactions between particles [6–9], whereas experiments in the previous chapter suggest that it is rather universal. In the previous chapter we have shown experimentally that athermal jamming data collapse onto single super- and subcritical master-curve branches, with universal scaling exponents across a range of systems. An interesting follow-up question is: Can we define a universal rescaling of flow curves for thermal and athermal systems? This question is supported by several interesting findings from previous studies. Bonn et al. [10] show that the flow curves of thermal and athermal particles are very similar. Van der Vaart et al. [11] compare soft and hard-sphere thermal systems and also suggest that they behave similarly, only with different stress scales. Ikeda et al. [12, 13] simulate the cross-over between thermal en athermal systems and suggest that the effect of different stress scales is simply additive.

[1] Here σ is the shear stress, σ_y is the yield stress, $\dot{\gamma}$ the shear rate, η_N the newtonian viscosity, and K, β, C and δ are adjustable parameters.

In the case of athermal jamming the characteristic stress and time scales originate from the interaction energy (ϵ) of the particles. We consider compressed, elastic emulsions that have an repulsive interaction energy which is due to the deformation of the droplets. The energy scale is therefore set by the surface tension and the stress scale is given by the Laplace pressure:

$$\sigma_0 = \frac{\epsilon(R)}{R^3} = \frac{\Sigma}{R} \tag{8.1}$$

with Σ the surface tension and R the particle radius. The corresponding time scale is:

$$\tau_0 = \frac{\eta_0}{\sigma_0} \tag{8.2}$$

with η_0 the solvent-viscosity. Likewise, we can define the stress and time scales for Brownian motion with the thermal energy k_BT:

$$\sigma_T = \frac{k_BT}{R^3} \tag{8.3}$$

$$\tau_T = \eta_0 \frac{R^3}{k_BT} \tag{8.4}$$

From the above expressions it becomes clear that the thermal and mechanical stress are comparable when $k_BT \approx \epsilon$, while they become increasingly separated in the athermal limit when $k_BT \ll \epsilon$ [13].

In the previous chapter we showed experimental jamming data that collapse onto a single master curve, with universal scaling exponents across a range of systems, and present a model to describe the microscopic dynamics underlying the critical transition and these scaling laws. In this chapter we extend those studies and investigate the cross-over between thermal and athermal yield-stress regimes, by comparing the experimental flow curves of a variety of thermal and athermal systems. First we show that the flow curves of three different athermal emulsions, with different inter-particle interactions, can be collapsed with respect to the jamming transition, by using the Laplace pressure as the stress scale and with a common set of exponent values. Secondly, we show that the flow curves of thermal systems can be scaled in a similar way as the athermal systems and with very similar common exponent values. However now the scaling is achieved with respect to the glass transition and with the osmotic pressure as the stress scale. Finally we demonstrate that all yield stress flow curves of both thermal and athermal systems, over

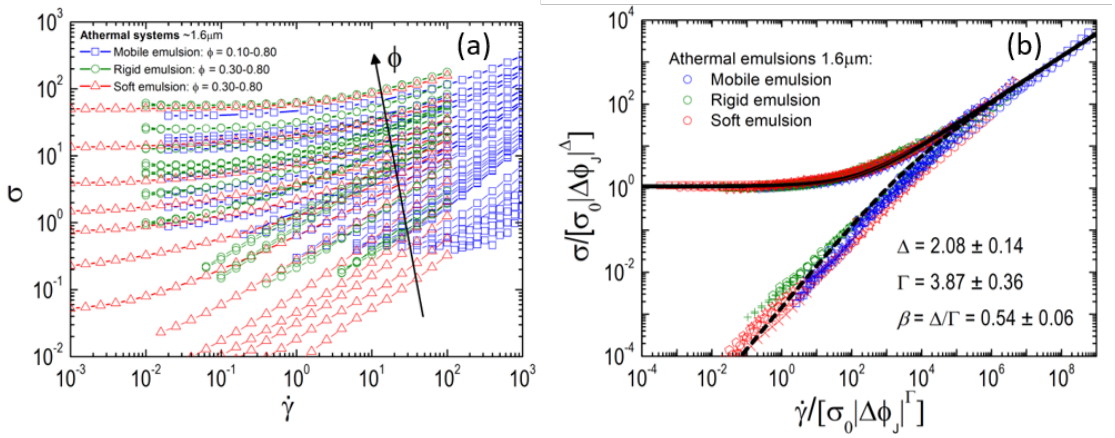

FIGURE 8.1: (a) Flow curves of athermal emulsions with different interactions (mobile and rigid particle surfaces and soft electrostatic repulsion). All are castor oil-in-water emulsions with different volume fractions ϕ (from bottom to top with increasing ϕ). (b) Rescaled flow curves for athermal emulsions. The stress and rate are scaled with the Laplace pressure ($\sigma_0 = \Sigma/R$) times a power law of the distance to jamming ($|\Delta\phi_J| = |\phi - \phi_J|$ where $\phi_J = 0.64$). The black line and black dotted line are fits to the Herschel-Bulkley and Cross equation, respectively.

a full concentration range of the glass and jamming regimes, can be collapsed onto a single master curve.

8.2 Athermal systems

First we consider athermal systems, and study the steady-state rheology of three different athermal emulsions. The emulsions are castor oil-in-water emulsions and have a radius of $R \sim 1.6\mu m$ (with a polydispersity of 20%). The continuous phase consists of demineralized water (mili-Q®) and different surfactants, creating different interactions between the droplet surfaces: $1wt\%$ SDS in water (creating mobile surfaces), $0.4wt\%$ BSA and $0.4wt\%$ PGA (creating rigid surfaces) [14], and $1wt\%$ SDS in $0.05M$ NaCl (creating softer electrostatic interaction). More details about the interaction and preparation are described in chapter 2. Emulsions with different volume fractions were prepared and the corresponding flow curves are

TABLE 8.1: Parameters for the different systems at $T = 25^oC$.

	PMMA	Emulsion 250nm	Emulsion 530nm	Emulsion 740nm	Emulsion mobile	Emulsion rigid	Emulsion soft
$R[m]$	$1.83 \cdot 10^{-7}$	$2.50 \cdot 10^{-7}$	$530 \cdot 10^{-7}$	$7.40 \cdot 10^{-7}$	$1.6 \cdot 10^{-6}$	$1.6 \cdot 10^{-6}$	$1.6 \cdot 10^{-6}$
$\Sigma[Nm/s]$	-	$9.80 \cdot 10^{-3}$	$9.80 \cdot 10^{-3}$	$9.80 \cdot 10^{-3}$	$1.50 \cdot 10^{-3}$	$3.60 \cdot 10^{-3}$	$1.40 \cdot 10^{-3}$
σ_0	-	$3.92 \cdot 10^{4}$	$1.85 \cdot 10^{4}$	$1.32 \cdot 10^{4}$	$9.38 \cdot 10^{2}$	$2.25 \cdot 10^{3}$	$8.75 \cdot 10^{2}$
σ_T	$2.90 \cdot 10^{3}$	$9.10 \cdot 10^{3}$	$9.55 \cdot 10^{2}$	$3.51 \cdot 10^{2}$	$3.47 \cdot 10^{1}$	$3.47 \cdot 10^{1}$	$3.47 \cdot 10^{1}$

plotted in figure 8.1(a). In chapter 7 we have shown that the flow curves of the individual systems can be collapsed onto two separate master curves; one for the super-critical data and one for the sub-critical data. The critical volume fraction chosen as $\phi_J = 0.64$, which is at random close packing (RCP) [15]. Here we focus on how all these individual systems can be collapsed onto the same master curve. The flow properties of compressed emulsions depend on the packing and deformation of droplets and their intrinsic elasticity [16]. The elasticity of the droplets and their deformation under compression are controlled by the Laplace pressure, $\sigma_0 = \Sigma/R$ (the parameters for the different systems are given in Table 8.1). By plotting $\sigma/\sigma_0|\Delta\phi_J|^\Delta$ versus $\dot{\gamma}/\sigma_0|\Delta\phi_J|^\Gamma$ all the flow curves of the compressed emulsions can be collapsed onto one curve[2] (figure 8.1(b)). For each system and volume fraction the exponents Δ and Γ are adjusted to achieve the collapse, but their values remain in a narrow range; the mean values with standard deviation are $\Delta = 2.08 \pm 0.14$ and $\Gamma = 3.87 \pm 0.36$. Using the same exponents the sub-critical flow curves (corresponding to fractions below ϕ_J) collapse automatically also. The super-critical master curve can be fit with the Herschel-Bulkley equation with $\beta = 0.54$ and $K = 0.065$ and the sub-critical branch can be fitted to the Cross equation with $\delta = \beta$ and $C = \eta_N/K = 0.023$ (both K and C in SI units).

8.3 Thermal systems

Remarkably similar flow curves are observed for thermal mono-disperse emulsions [16] and a PMMA hard-sphere colloidal glass [17], however the main difference is that thermal fluctuations are important and a glass transition can be observed to occur around $\phi_G \approx 0.58$. Here we find that thermal emulsions and colloidal hard-spheres show very similar behavior, indicating that this transition appears independently of the interactions or hardness of the particles. The flow curves of all thermal systems are shown in figure 8.2(a). First only the flow curves that are purely thermal are considered ($\phi_G < \phi < \phi_J$); all these flow curves can be collapsed using a similar scaling as for the athermal systems, but now with respect to the glass transition and with the stress scale given by thermal fluctuations k_BT/R^3. Figure 8.2(b) shows this rescaling of flow curves, with strikingly similar values for

[2]Note that for a correct dimension of the rate-scaling the solvent-viscosity η_0 should be included, however for now this can be neglected ($\eta_0 \sim 1mPa \cdot s$ for all studied systems here).

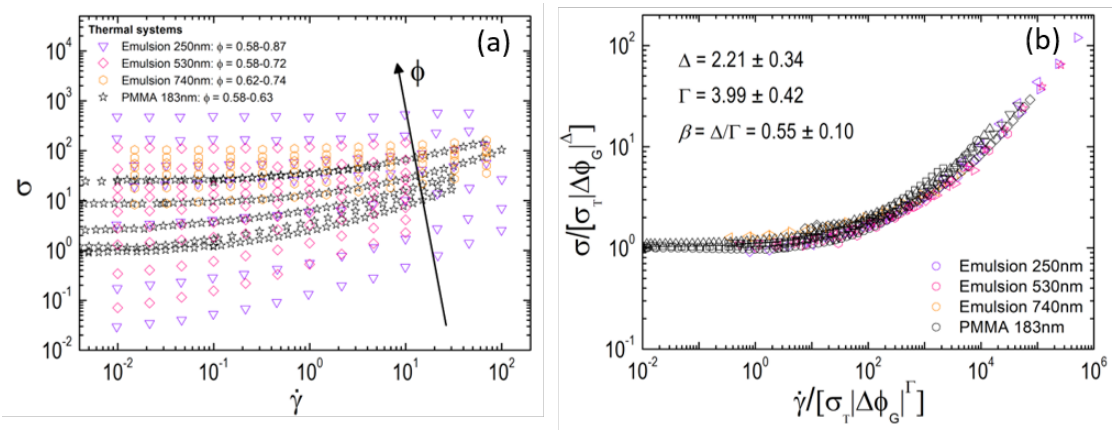

FIGURE 8.2: (a) Flow curves of thermal systems: different droplets sizes of silicone oil-in-water emulsions and PMMA particles (from bottom to top with increasing ϕ). (b) Data collapse of thermal systems with $\phi_G < \phi < \phi_J$, plotted with the same parameters as for the athermal systems, but with respect to the glass transition ($|\Delta\phi_G| = |\phi - \phi_G|$ where $\phi_G = 0.58$) and the osmotic pressure due to thermal fluctuations ($\sigma_T = \alpha k_B T/R^3$, with $\alpha = 35000$).

Δ and Γ as for the athermal flow curves. The stress scale to achieve the rescaling and normalize the stress plateau is given by $\sigma_T = \alpha k_B T/R^3$ with $\alpha = 35000$. The physical meaning and value of α is not entirely clear, but a large prefactor for thermal yield stress glasses is also reported in the literature [11, 18].

8.4 Universal scaling and cross-over

The yield stress that is observed for the thermal systems for $\phi_G < \phi < \phi_J$, has an entropic nature and is dominated by the osmotic pressure [12]. However, for $\phi > \phi_J$ the nature of the yield stress changes from being entropic to being controlled by the elastic deformation of the particles. Both the glassy yield point and the jamming yield point can be understood in terms of particle cage escape across a microscopic stress barrier, as pictured in our microscopic model for the critical transition (chapter 7). In a combined treatment of both transitions it is then natural to add the entropic and enthalpic parts of the characteristic barrier stress, and in view of the relation between characteristic stresses and timescales, to add up also the characteristic cage-escape rates (this is further explained in 8.4.1).

We find that an additive combination of the characteristic glass and jamming stresses and rates enables to collapse all thermal flow curves, see figure 8.3, by

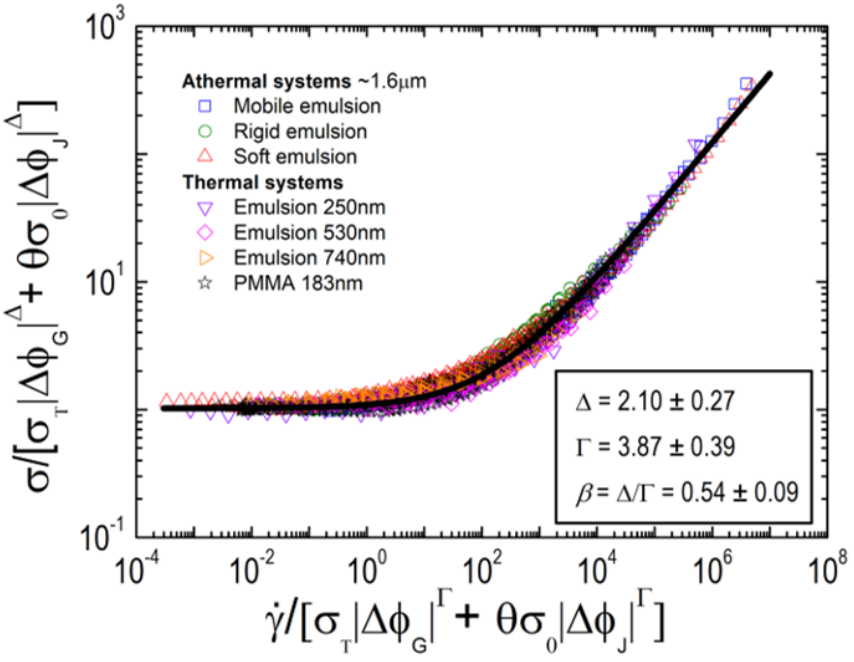

FIGURE 8.3: Collapse of all thermal and athermal flow curves for $\phi > \phi_G$. By plotting $\sigma/[\alpha\frac{k_BT}{R^3}|\Delta\phi_G|^\Delta + \theta\frac{\Sigma}{R}|\Delta\phi_J|^\Delta]$ versus $\dot{\gamma}/[\alpha\frac{k_BT}{R^3}|\Delta\phi_G|^\Gamma + \theta\frac{\Sigma}{R}|\Delta\phi_J|^\Gamma]$, with $\Delta = 2.07$ and $\Gamma = 3.85$. The black line shows a Herschel-Bulkley fit $\sigma = 1.0 + 0.07\dot{\gamma}^{0.54}$.

plotting $\sigma/[\sigma_T|\Delta\phi_G|^\Delta + \theta\sigma_0|\Delta\phi_J|^\Delta]$ versus $\dot{\gamma}/[\sigma_T|\Delta\phi_G|^\Gamma + \theta\sigma_0|\Delta\phi_J|^\Gamma]$, with θ being a step function with $\theta = 0$ if $\phi < \phi_J$ and $\theta = 1$ if $\phi > \phi_J$. Accordingly, the flow curves of all thermal systems for $\phi > \phi_G$ collapse. Automatically this scaling works for the athermal emulsions, since in the limit of large R the scaling reduces to the athermal scaling in figure 8.1 because $\sigma_0 \gg \sigma_T$. The striking conclusion is that in this way all the flow curves, both thermal and athermal, collapse onto a single master curve with universal values for the scaling exponents Δ and Γ within the experimental accuracy. Even tough there is some variation in the exponents of the individual systems, it is remarkable that they all follow the same slope given by β (see figure 8.4). Also remarkable is that this allows us to predict the yield stress and flow behavior using only the volume fraction, particle size and surface tension in a universal fashion.

8.4.1 Extension of the microscopic model to thermal glassy behavior

The microscopic model of heterogeneous dynamics that we describe in chapter 7, assumes the existence of two characteristic microscopic timescales of the fluid:

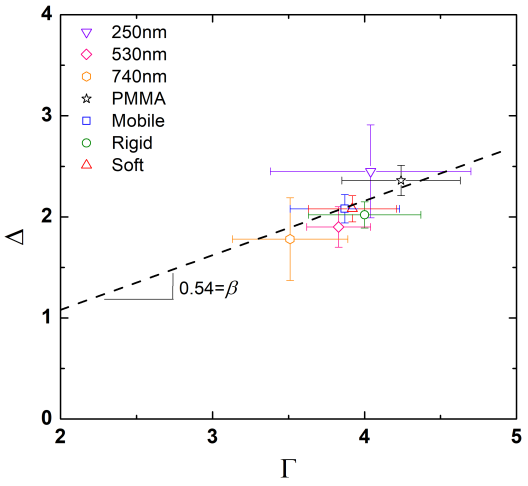

FIGURE 8.4: Δ versus Γ for the different thermal and athermal systems with corresponding standard deviation.

τ_η proportional to the viscosity η for the single-particle mobility, and τ_{het} for the lifetime of the fluctuating pattern of stagnant and mobile regions. Both time scales increase and become widely separated when the stagnant fraction increases, with $\tau_{het} \gg \tau_\eta$. Like in second-order critical transitions the characteristic length scale ξ of the heterogeneous domains diverges as a power-law in approach of the yield-stress line and becomes the dominant variable. All the other variables then have again a power-law dependence on ξ:

$$\frac{\xi(s)}{\xi(0)} = \left[\frac{\tau_\eta(s)}{\tau_\eta(0)}\right]^{\nu/m} = \left[\frac{\tau_{het}(s)}{\tau_{het}(0)}\right]^{\nu/n} = \left[1 - \frac{s}{s_c}\right]^{-\nu} \tag{8.5}$$

with $n > m$. Here s is the fraction of particles arrested in cages, and s_c the critical fraction where macroscopic flow halts. The viscosity $\eta = \sigma/\dot{\gamma}$ is proportional to τ_η and hence the macroscopic rheology follows similarly:

$$\eta(s) = \eta(0)[1 - s/s_c]^{-m}. \tag{8.6}$$

The stress-dependent steady-state value of s follows from a balance between stress-induced cage escape and arrest through free-volume fluctuations. The average cage-escape rate can then be equated to the decay rate of the heterogeneity patterns; the escape rate contains two terms and is dominated by whichever is the fastest:

$$s\left[\frac{1}{\tau_b} f(\sigma/\sigma_y) + \dot{\gamma}\right] = \frac{1}{\tau_{het}(s)}. \tag{8.7}$$

The two terms between square brackets cover two extreme cases, the static and collective-flow limits, respectively. The first term represents the stress-induced escape of a stagnant particle from the static cage of particles surrounding it, the second term represents the case where the cage itself is flowing with the particle. The first term $1/\tau_b = \sigma_y/\eta_N = (\sigma_0/\eta_0)|\Delta\phi|^{\Delta+M}$ is a characteristic rate for barrier crossing, with $\sigma_y = \sigma_0|\Delta\phi|^{\Delta}$ the yield stress and $\eta_N = \eta_0|\Delta\phi|^{-M}$ the Newtonian viscosity. Below σ_y no cage escape is possible, so $1/\tau_b$ has to be multiplied by a function $f(\sigma/\sigma_y)$ that is zero if its argument is below unity. Above σ_y the probability of barrier crossing rapidly increases, so above unity $f(\sigma/\sigma_y)$ will be a steeply increasing function of its argument. Crossover to collective shear-thinning flow of all particles takes over when the typical rate for barrier crossing, $1/\tau_b$, becomes of the order of the average rate, i.e. equal to the second term between square brackets; so the crossover rate $\dot{\gamma}_{co}$ equals $1/\tau_b = (\sigma_0/\eta_0)|\Delta\phi|^{\Gamma}$, with $\Delta + M = \Gamma$. At this crossover point the excess (viscous) stress $\sigma - \sigma_y$ becomes of the order of the elastic stress, i.e. of order σ_y, so $f(2)$ can be chosen of order unity. For still higher stresses $f(\sigma/\sigma_y)$ saturates around that level and the first term between square brackets becomes irrelevant. So typically $f(x) = 0$ when $x < 1$ and $f(x) = 2(x-1)^p/[1+(x-1)^p]$ when $x \geq 1$.

In chapter 7 we show how the solution of the above balance equation for s at given stress or rate leads to the correct asymptotic high- and low-rate forms of the Herschel-Bulkley and Cross equations, and their merging at high rates. The macroscopic exponents are found to follow from the microscopic ones through the identification $m \equiv M = \Gamma - \Delta$ and $n \equiv \Gamma$. Moreover we derive from a scaling of free-volume fluctuations that $\Delta \equiv n - m = d\nu$, with d the (possibly fractal) dimension of the heterogeneous domains; in the literature a correlation-length exponent $\nu \cong 0.7$ is regularly reported, this would lead to $\Delta \cong 2.1$ in case $d = 3$ (see chapter 7 and references therein).

If we postulate that the above microscopic mechanisms of heterogeneous dynamics and critical behavior applies both to the glass and the jamming transition, with the same critical exponents, we only need to choose in each case the appropriate characteristic stress (σ_0 or σ_T), characteristic timescale (σ_0/η_0 or σ_T/η_T), and relevant critical volume fraction (ϕ_J or ϕ_G). When considering the two transitions simultaneously it is logical to take the barrier stress for cage escape σ_y as the sum of both the random entropic thermal stress and the enthalpic deformational stress. Accordingly, when rescaling the experimental stress data one should then use the

additive yield stresses as the scale factor:

$$\sigma_{co} = \sigma_T |\Delta\phi_G|^{\Delta} + \theta\sigma_0 |\Delta\phi_J|^{\Delta} \tag{8.8}$$

with $\theta = 0$ below ϕ_J and $\theta = 1$ above ϕ_J.

Equation (8.7) shows that to rescale the experimental flow rates one should then use the added yield stresses as the scale factor for the glass and jamming cases:

$$\dot{\gamma}_c o = (\sigma_T/\eta_0) |\Delta\phi_G|^{\Gamma} + \theta(\sigma_0/\eta_0) |\Delta\phi_J|^{\Gamma} \tag{8.9}$$

So we conclude that this microscopic two-state picture of a balance between caged and flowing particles can be applied both to the jamming and the glass transition.

8.5 Conclusion

We have investigated the flow behavior of yield-stress fluids and colloidal glasses for a range of different volume fractions, particle size and interactions. First we show that the flow curves of three athermal emulsions, having different inter-particle interactions, can be scaled onto a universal curve with respect to the jamming transition and with the Laplace pressure as stress scale. Secondly, we investigated the cross-over between thermal and athermal yield-stress regimes. Thereby we show that the flow curves of thermal systems can be collapsed in a similar way as the athermal systems, with respect to the glass transition instead of the jamming transition. All yield stress flow curves can be collapsed using the Laplace pressure as stress scale for the athermal systems and the osmotic pressure for the thermal systems. An additive combination of glass and jamming stresses, respectively rates, is sufficient to achieve this.

The extension from jamming to the glass transition can be very logically based on our microscopic model. The reason being that the model in first instance does not discuss the volume-fraction dependence but the dependence on the fraction s of stagnant caged particles, which itself satisfies a balance equation and thereby becomes a function of the distance to the yield-stress line. The macroscopic flow-rate dependence of the stress then follows from the microscopic rate of stress-induced cage escape and its relation to a length scale of cooperative motion. This heterogeneity length scale diverges as a power-law in $|s - s_c|$ when approaching the

critical yield stress, implying that we consider a second-order dynamical critical transition.

In conclusion, we propose a scaling that applies for both thermal and athermal systems, finding universal exponents for the jamming and glass effects. Amazingly we can predict, rather then fit, characteristic stress and rate prefactors from material properties.

References

[1] R. G. Larson. *The structure and rheology of complex fluids*. Oxford university press New York, 1999.

[2] P. Coussot. *Rheometry of pastes, suspensions, and granular materials: applications in industry and environment*. John Wiley & Sons, 2005.

[3] L. Berthier and G. Biroli. Theoretical perspective on the glass transition and amorphous materials. *Reviews of Modern Physics*, 83(2):587, 2011.

[4] A. J. Liu and S. R. Nagel. The jamming transition and the marginally jammed solid. *Annu. Rev. Condens. Matter Phys.*, 1(1):347–369, 2010.

[5] P. Olsson and S. Teitel. Critical scaling of shear viscosity at the jamming transition. *Phys. Rev. Lett.*, 99:178001, 2007.

[6] C. S. O'Hern, S. A. Langer, A. J. Liu, and S. R. Nagel. Random packings of frictionless particles. *Physical Review Letters*, 88(7):075507, 2002.

[7] C. S. O'Hern, L. E. Silbert, A. J. Liu, and S. R. Nagel. Jamming at zero temperature and zero applied stress: The epitome of disorder. *Physical Review E*, 68(1):011306, 2003.

[8] B. P. Tighe, E. Woldhuis, J. C. Remmers, W. van Saarloos, and M. van Hecke. Model for the scaling of stresses and fluctuations in flows near jamming. *Phys. Rev. Lett.*, 105:088303, 2010.

[9] G. Katgert, B. P. Tighe, and M. van Hecke. The jamming perspective on wet foams. *Soft Matter*, 9:9739, 2013.

[10] D. Bonn, M. M. Denn, L. Berthier, T. Divoux, and S. Manneville. Yield stress materials in soft condensed matter. *Rev. Mod. Phys.*, 89:035005, Aug 2017.

[11] K. van der Vaart, Y. Rahmani, R. Zargar, Z. Hu, D. Bonn, and P. Schall. Rheology of concentrated soft and hard-sphere suspensions. *Journal of Rheology*, 57(4):1195–1209, 2013.

[12] A. Ikeda, L. Berthier, and P. Sollich. Unified study of glass and jamming rheology in soft particle systems. *Phys. Rev. Lett.*, 109:018301, 2012.

[13] A. Ikeda, L. Berthier, and P. Sollich. Disentangling glass and jamming physics in the rheology of soft materials. *Soft Matter*, 9:7669, 2013.

[14] S. A. Koehler, S. Hilgenfeldt, E. R. Weeks, and H. A. Stone. Drainage of single plateau borders: Direct observation of rigid and mobile interfaces. *Phys. Rev. E*, 66:040601 (R), 2002.

[15] J. L. Finney. Random packings and the structure of simple liquids. i. the geometry of random close packing. In *Proceedings of the Royal Society of London A: Mathematical, Physical and Engineering Sciences*, volume 319, pages 479–493. The Royal Society, 1970.

[16] T. G. Mason, J. Bibette, and D. A. Weitz. Yielding and flow of monodisperse emulsions. *Journal of Colloid and Interface Science*, 179(2):439–448, 1996.

[17] G. Petekidis, D. Vlassopoulos, and P. N. Pusey. Yielding and flow of sheared colloidal glasses. *Journal of Physics: Condensed Matter*, 16(38):S3955, 2004.

[18] A. Ikeda and L. Berthier. Yield stress in amorphous solids: A mode-coupling-theory analysis. *Physical Review E*, 88(5):052305, 2013.

Appendix A

Thermally induced shear banding

In continuation of Chapter 6 we here show some additional rheological tests and mathematics. The model and the mathematics that is described here and in chapter 6 is in collaboration with Thijs Michels[1].

A.1 Additional rheological tests

Detailed rheological tests are done to investigate the appearance of the hysteresis loop or shear band in the Carbopol. To determine whether a steady state is reached in the hysteretic carbopol viscosity bifurcation measurements are done, figure A.1 shows the viscosity in time for constant imposed stresses. Generally, in these experiments there is a deviation between liquid-like and mechanically solid-like behavior; the viscosity reaches a constant value at imposed stresses above the yield stress, and the viscosity increases to infinitely high values for stresses below the yield stress. For the simple yield stress Carbopol there is a sharp deviation between the two regimes (figure. A.1a), however for the hysteretic Carbopol this is less clear (figure A.1b). These results represent thixotropic behavior as shown in previous work on thixotropic materials [1].

The buildup of the viscosity in time at constant imposed shear rates reveals a first significant insight (figure A.2). We see the elastic response of the yielded material, that at some point reaches a constant viscosity plateau (figure A.2a).

[1]From Eindhoven University of Technology, Theory of Polymers and Soft Matter, Department of Applied Physics.

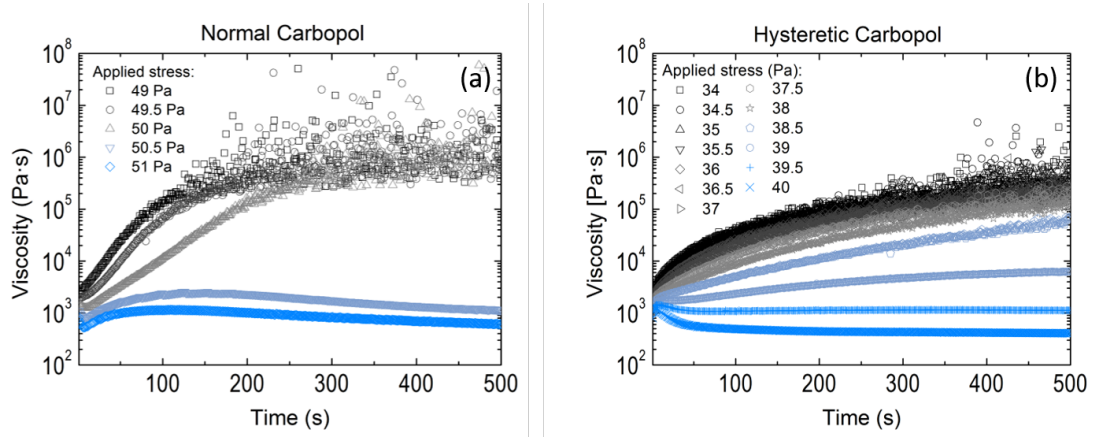

FIGURE A.1: Viscosity bifurcation measurements: viscosity as a function of time for constant imposed stresses for (a) a simple yield stress carbopol sample and (b) a hysteretic carbopol sample (both 0,6wt% Ultrez U10 in water).

In the case of the hysteretic sample a stress overshoot is observed (figure A.2b). This directly relates to the observed hysteresis loop from the flow curves. A more instructive way to present this data is in a stress versus strain plot (figure A.3), where there is an overlap up to a strain of 20% showing the linear response of the yielded material from a startup flow. For the hysteretic carbopol the stress overshoot appears and has a maximum at 50%, after which a constant plateau is reached. The corresponding flow curves are shown in figure A.4. The underlying mechanism causing this overshoot is revealed by confocal microscopy. A time video of the both carbopol samples shows that there are thermal parts present in the carbopol. There is an increase in thermal composites in the hysteretic carbopol (after heavy stirring), that causes shear banding.

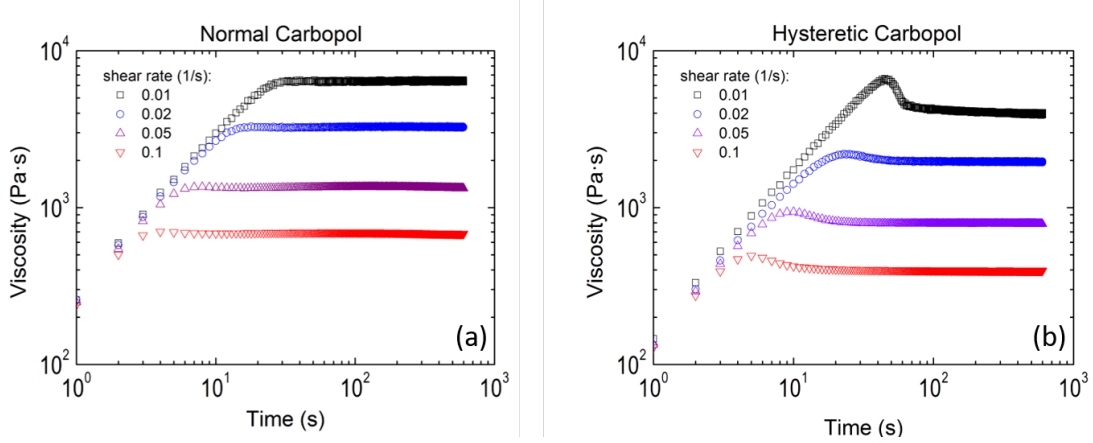

FIGURE A.2: Viscosity as a function of time for constant imposed shear rates for (a) a simple yield stress carbopol and (b) hysteretic carbopol (both 0,6wt% Ultrez U10 in water).

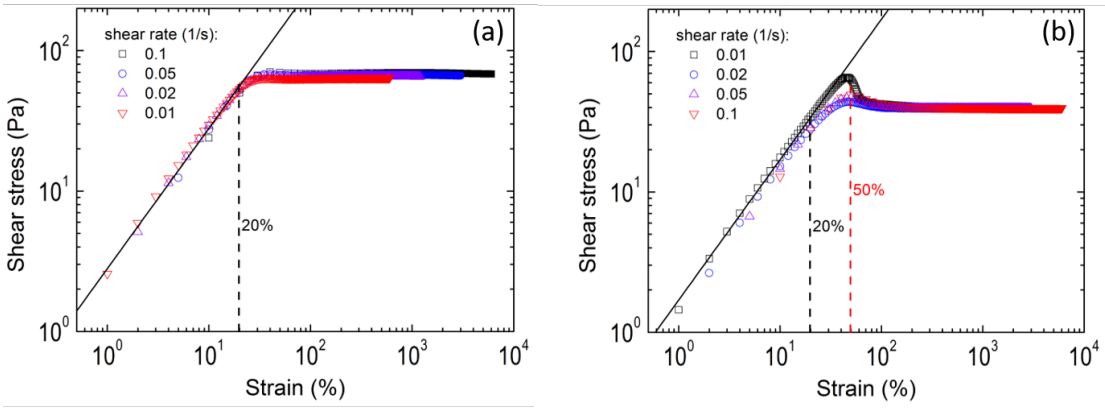

FIGURE A.3: Startup of stress as a function of strain for constant imposed shear rates for (a) a simple yield stress Carbopol sample and (b) Carbopol after intensive stirring.

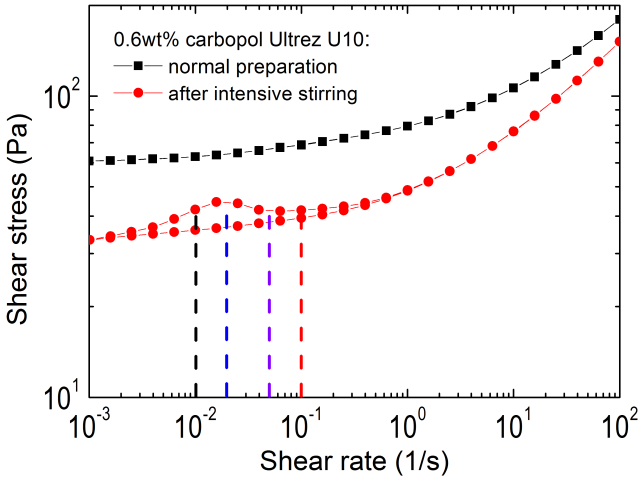

FIGURE A.4: Flow curve of different Carbopol samples, corresponding to figure A.3.

A.2 Theoretical approach

To do the mathematics of the quantitative model we simplify the notation by introducing the dimensionless rate $x = (\tau_{ag}\dot{\gamma})^n$ and considering the $R \equiv \tau(0)/\tau(\infty)$. A large value of R corresponds with a strong drop in intrinsic relaxation time. Thus we get:

$$x^2 - [n(R-1) - (R+1)]x + R = 0 \tag{A.1}$$

with the roots

$$x_{\pm} = \frac{[n(R-1) - (R+1)]}{2}\left(1 \pm \sqrt{1 - \frac{4R}{[n(R-1) - (R+1)]^2}}\right) \tag{A.2}$$

These roots will be real, allowing a Van der Waals loop, if

$$[n(R-1)-(R+1)]^2 \geq 4R \tag{A.3}$$

or

$$R \geq R_c(n) \equiv \left(\frac{n+1}{n-1}\right)^2 \tag{A.4}$$

Here we divided out a factor (R–1), using $R > 1$. So a Van der Waals loop can indeed be realized above the critical ratio of relaxation times $R_c(n)$. For positive roots $x_\pm$ we have to choose $n > 1$. In the limit $R \gg 4/(n-1)^2$ the positions of the maximum and minimum of the Van der Waals loop are approximated by:

$$x_- \equiv x_{max} \approx \frac{1}{n-1}, x_+ \equiv x_{min} \approx (n-1)R \tag{A.5}$$

with *max* and *min* referring to the maximum and minimum of the stress, so $x_{max} < x_{min}$. Note that the factor $(n-1)^{n/1}$ remains bounded and of order unity for $n > 2$, while it vanishes for $n \downarrow 1$.

References

[1] P. C. F. Møller, J. Mewis, and D. Bonn. Yield stress and thixotropy: on the difficulty of measuring yield stresses in practice. *Soft matter*, 2(4):274–283, 2006.

Appendix B

Universal rescaling: microscopic model

Here we discuss in more detail the microscopic model that is described in chapter 7, and give a broad range of literature data. The model is developed in collaboration with Thijs Michels[1].

B.1 Microscopic model

B.1.1 Two-state heterogeneous dynamics

The power-law divergence of the Newtonian viscosity and the power-law vanishing of the shear modulus or yield stress are commonly understood from the existence of a diverging lengthscale ξ that characterizes correlated motion, i.e., the typical length over which particle displacements cannot be considered independent. In experiments [1–6] and simulations [7–14] such a divergent lengthscale has been observed both in the linear regime around ϕ_c and when approaching the yield stress line of quasi-static flow at higher concentrations ϕ.

Since under stresses above the yield stress the stagnant phase starts flowing, we assume that under stress a fraction s of the particles remains stagnant in neighbor cages while the fraction $(1 - s)$ becomes fluidized. This simple two-state picture

[1]From Eindhoven University of Technology, Theory of Polymers and Soft Matter, Department of Applied Physics.

represents what are in reality two sides of a very broad mobility distribution. In view of the observations we make an analogy with the linear regime and assume that the lengthscale ξ of correlated, heterogeneous dynamics diverges when s approaches a critical value s_c where macroscopic flow halts. Following the idea that the divergence is similar to that near a second-order phase transition, we can subsequently choose the divergent lengthscale as the single dominant variable that governs macroscopic behavior. Mathematically this single relevant variable implies that ξ can only diverge power-law in the distance $\Delta s = |s - s_c|$ from critical jamming and that other variables in their dependence on s near s_c derive from ξ again as power laws, with similar critical behavior. In particular this applies to the lifetime τ_{het} of the fluctuating heterogeneity pattern and to the average time τ_η for the single-particle mobility, i.e. the time for the average particle to move over a distance of its own diameter. The latter timescale τ_η is directly proportional to the average viscosity η of the system. So in fact $\xi(s)$, $\tau_{het}(s)$, $\tau_\eta(s)$, $\eta(s)$ are all interrelated by power laws in Δs. Normalizing them to their values at $s = 0$ and introducing critical exponents ν , m and n we can then write:

$$\xi(s)/\xi_a = [\tau_{het}(s)/\tau_a]^{\nu/n} = [\tau_\eta(s)/\tau_a]^{\nu/m} = [\eta(s)/\eta_a]^{\nu/m} = |1 - s/s_c|^{-\nu} \qquad \text{(B.1)}$$

The lengthscale ξ_a is of the order of the single-particle diameter. The limiting times $\tau_\eta(0)$ and $\tau_{het}(0)$ will have a similar scale and have for simplicity been taken equal to a single time τ_a; however, for an increasing fraction s of stagnant particles the heterogeneity lifetime τ_{het} will become much larger than the fluidity time τ_η, so its associated exponent will be larger: $n > m$. Since the ratio τ_{het}/τ_η of the two microscopic timescales diverges near s_c we can interpret $\eta_a = \eta(s = 0)$ as the asymptotic viscosity of a fully fluidized phase and treat the arrested domains as a dispersed solid phase. Note that in this interpretation the last equality in (B.1) is a logical generalization of (4) if we choose the same exponent $m = M$ as in the Krieger-Dougherty equation. This supposes a deep relation between the linear and the nonlinear rheology, with the same physics in (4) and (B.1); indeed a deep connection is already implied by the empirical collapse of data over the full dynamic range in Figs. 7.1-7.4, with a direct relation between the empirical exponents M, Γ and Δ, viz. $M = \Gamma - \Delta$. We will return to this point later. Both τ_a and η_a will be continuous functions ofϕ near ϕ_c and in comparison with the functions that depend power-law on $|\Delta\phi|$ they may be treated as constants sufficiently close to ϕ_c; together they define a characteristic asymptotic high stress $\sigma_a = \eta_a/\tau_a$.

The internal parameter of our model, the stagnant fraction s, is determined by a competition between stress-induced escape of arrested particles from their cages, and fluctuation-induced arrest of mobile particles; the latter arrest mechanism will be dependent on this internal variable s and will be detailed later. The time evolution of the stagnant fraction $s(t)$ can then be given by a simple first-order kinetic equation:

$$ds/dt = -s/\tau_R + (1-s)/\tau_A \tag{B.2}$$

with $1/\tau_R$ the relaxation rate for the arrested particles to become mobile and $1/\tau_A$ the rate with which mobile particles become arrested again.

The relaxation rate $1/\tau_R$ can be considered as resulting from either of two typical mechanisms. For low stress we may consider that particles are caged by a large energy barrier ϵ and that the applied stress, thermal energy, or a combination of both, facilitates barrier crossing of single particles; this process is characterized by a typical barrier stress σ_b. Subsequently, with increasing stress and hence increasing number of such crossings a collective flow process develops in which the cage itself vanishes; the latter process takes over when the average rate $\dot{\gamma}$ becomes of the order of the single-particle escape rate or larger. So in a simple approximation we can write:

$$1/\tau_R = (1/\tau_b) f(\sigma/\sigma_b) + \dot{\gamma} \tag{B.3}$$

with τ_b the typical time for barrier crossing at stresses near σ_b; around the solid-fluid transition that we are interested in this timescale will be orders of magnitude larger than τ_a. In fact, the ratio τ_b/τ_a , still a function of ϕ , will be the dominant large parameter in the model and will be much larger than any dimensionless experimental timescale $(\tau_a \dot{\gamma}_{exp})^{-1}$ in the limit $\phi \uparrow \phi_c$ and beyond.

For athermal jamming systems repulsive energies dominate over thermal energies, and the limit of zero temperature has to be assumed before applying shear [15–17]. The barrier stress σ_b is then a sharply defined yield stress $\sigma_y(\phi)$ below which the deformation is elastic and no flow is possible; it scales as ϵv_{act} , with v_{act} some local activation volume needed for a single relaxation event, and vanishes below the critical volume fraction ϕ_c. So above ϕ_c we can assume the simple form $f_+(x) = (x-1)^p$ for $x > 1$ and $f_+(x) = 0$ for $x < 1$, with some positive exponent p to be discussed later. Below ϕ_c we can take $f_-(x) = 1$ since at low stress the

rheology should be Newtonian. Note that there is continuity in $f(x)$ across the jamming point ϕ_c along the line $x = 2$, i.e., $\Delta\sigma = \sigma_y$.

For high but finite ratios ϵ/k_bT thermal processes may at very large timescales still relax the elastic stress in the solid within experimental timescales. This intermediate case between glassy dynamics and jamming may be described by adding up the probabilities for stress-induced and thermally induced cage escape, i.e., adding to (B.3) the rate for thermal barrier crossing. That process is an Eyring-type cage escape [[18]], for which the characteristic time constant τ_b is the equilibrium α-relaxation time and the typical barrier stress σ_b is k_bT/v_{act} . The stress dependence above ϕ_c is in the Eyring model given by $f_+(x) = x^{-1}sinhx$; it crosses over from parabolic at low stress to exponential at high stress. This thermal scenario applies to glasses, i.e., when shear is applied before considering the limit of low temperatures [15–17, 19, 20]. Heterogeneous dynamics, accelerated dynamics in approach of the yield point and subsequent flow of monomers has also been studied in polymer glasses, and the analogy with jamming has been noted [21–24]. An Eyring-type near-Gaussian decrease of the single-particle relaxation time with stress, as discussed around equation (B.3) is revealed in simulations [[25]]. In view of the nature of the systems that we studied experimentally we henceforth consider the athermal limit of frictionless repulsive particles only. Effects of particle friction and attraction will change the local dynamics and bulk rheology and have been studied e.g. in [26, 27]. With the expression (B.3) a deep connection is again assumed between the dynamics near equilibrium and far in the nonlinear regime. It is worthwhile noting that a similar expression was introduced to explain strain-rate/frequency superposition in the rheology of soft materials [28].

B.1.2 The steady-state

The steady-state stagnant fraction s, and hence the viscosity (B.1), follows as a function of σ or $\dot{\gamma}$ by putting the left-hand side of (B.2) equal to zero, which gives the rate balance $s/\tau_R = (1 - s)/\tau_A$; either of these terms may now be taken as the rate $1/\tau_{het}$ with which the heterogeneity pattern fluctuates. So we get as the steady-state condition for s and η:

$$s[(\tau_a/\tau_b)f(\sigma/\sigma_y) + \tau_a\dot{\gamma}] = (1 - s/s_c)^n = (\eta_a/\eta)^{n/m} \tag{B.4}$$

Solving this set of equations we can derive the flow curve of σ versus $\dot{\gamma}$, or equivalently the viscosity η versus σ, and simultaneously have insight in the underlying microscopic heterogeneity through the instantaneous stagnant fraction $s = s(\sigma)$. The mathematics is worked out in [29]. In the solution four different regimes of flow are recognized: (I) Newtonian flow at low rate in absence of a yield stress, so for subcritical concentrations; (II) a stress plateau ending in the yield stress at vanishing rate, so for supercritical concentrations; (III) power-law shear-thinning flow that makes the distinction between the two low-rate regimes (I) and (II) vanish at rates above $1/\tau_b$; and (IV) a second Newtonian regime above the very high relaxation rate $1/\tau_a$, for both concentration domains. The regimes I-III are easily identified as those seen in the experimental data of Figs. 7.1-7.4. The regime IV may well be inaccessible experimentally for many systems, but is predicted by our model; it will not be discussed here further. For the regimes I-III the model predictions coincide with the empirical Herschel-Bulkley and Cross equations (1) and (3) when we make the identifications $\eta_N = \eta_a(\tau_b/\tau_a)^{m/n}$, $K = \eta_N/C = \eta_a/\tau_a^{m/n}$, $\beta = \delta = 1 - m/n = 1/p$.

B.1.3 Recovering the scaling ansatz

The model describes the different regimes around the solid-fluid transition in a unified manner. It focuses on the dependence on flow rate $\dot{\gamma}$ and, via the stress- or rate-dependent order parameter s, on the relation with the heterogeneity in the microscopic kinetics; in particular the power laws involving the exponents m and n relate to diverging microscopic timescales. So far, the mathematical solution makes no connection with the dependence on the concentration ϕ or with the empirical exponents Γ, Δ, $M = \Gamma - \Delta$. This connection is now easily made by employing the assumed relation between the microscopic physics of the quasistatic and nonlinear regimes; the equations (4) and (B.1) for η , valid in these two regimes respectively, both express the dependence of a fluid viscosity on solids content, so the exponents may be identified: $M = m$. From the result $\Delta/\Gamma = \beta = 1 - m/n$ we then immediately get $\Gamma = n$, $\Delta = n - m$. Having thus found the macroscopic exponents in terms of the microscopic ones we can also incorporate the ϕ-dependence by equating the macroscopic crossover rate (7.7) to $1/\tau_b$, which gives $\tau_b = (\eta_0/\sigma_0)|\Delta\phi|^{-n}$. Inserting this into the expression just found for η_N we recover the Krieger-Dougherty result (4), with the asymptotic high-rate viscosity η_a now also related to the yield stress prefactor σ_0 and to the

solvent viscosity $\eta_{sol} = \eta_0/\phi_c^M$, i.e. to the parameters of the linear response: $\eta_a = \eta_0(\tau_a\sigma_0/\eta_0)^{m/n}$. The equation (2) for the dependence of the yield stress on ϕ is now automatically implied, since it was used to derive (B.2) and hence τ_b; the prefactor σ_0 in this equation relates to the elastic deformation, which is discussed in chapter 8 for emulsions. In summary, with all these identifications we have recovered the full Scaling Ansatz (7.6) from the microscopic model.

B.1.4 Heterogeneous dynamics around the critical transition

The development of the heterogeneous dynamics as a function of stress and concentration σ and ϕ is recovered from the model by using the relation (B.4) of the microscopic order parameter s with the viscosity $\eta = \eta(\sigma, \phi)$. In particular it gives in the low-rate Newtonian regime, and hence also at the crossover (co), a linear scaling of $|\Delta s|$ with $|\Delta\phi|$:

$$|\Delta s/s_c| = |\Delta s_{co}/s_c| = (\eta_0/\sigma_0\tau_a)^{-1/n}|\Delta\phi| \tag{B.5}$$

This shows that our two-state model predicts even in the low-rate Newtonian regime a finite and increasing heterogeneity on approach of ϕ_c . In reality this discrete heterogeneity should be interpreted as a strong broadening of the continuous mobility distribution. Similarly the heterogeneity lengthscale ξ and timescale τ_{het} follow from the solution of $\eta(\sigma, \phi)$ by using (B.1). In particular at the critical concentration, and by extension also in the regime of critical shear thinning, they are found to diverge in a power-law fashion for vanishing stress or rate:

$$\xi/\xi_a = [\tau_{het}/\tau_a]^{\nu/n} = [\eta_a/\tau_a\sigma]^{\nu/(n-m)} = (\tau_a\dot{\gamma})^{-\nu/n} \qquad (\phi = \phi_c) \tag{B.6}$$

We will come back to this result later. A more extensive discussion of near-critical heterogeneous dynamics and the nature of the critical transition is given in [29].

B.1.5 Origin of the heterogeneous dynamics

Based on evidence from experiments and simulations we have so far assumed that there are two diverging microscopic timescales, τ_η, for the single-particle mobility and $\tau_{het} \gg \tau_\eta$ for the lifetime of the heterogeneous mobility pattern, the latter

associated with a diverging correlation length ξ. Their dependence on the distance $|\Delta s|$ from criticality is given in our model by the power laws in B.1, with critical exponents m, $n > m$ and ν, respectively. However, the origin of the growing heterogeneity in the dynamics upon approach of the critical point $s = s_c$ has not yet been discussed here. Fundamental aspects of this heterogeneous dynamics are still a subject of active research in the literature (see e.g. [30–33], [34, 35]), both for glasses and jammed systems, and a detailed explanation is far beyond the scope of the present paper. For glasses at rest extensive simulations have been made from which both timescales could be recovered by analyzing the four-point dynamic correlation [36–39]. These simulations not only show the growing length- and timescales, but also their power-law interdependence.

Here we limit ourselves to a rather heuristic reasoning to understand the origin of the heterogeneity timescale and the associated exponent $n > m$. As is classically done for glasses [40] we consider a collectively rearranging region (CRR) of N particles and assume that they share one collective free volume v, of the order of a single-particle volume, to make rearrangements possible. We define a time τ such that all N particles will on average each have moved to a neighbor position. Associated with this, each particle will have experienced an individual free-volume change δv. For the statistics of this free-volume redistribution we now invoke a simple argument that is a variation on Mott's argument to explain creep by dislocation motion in metals [41] (see also ref.s [42]; Mott actually considers stress redistribution rather than free-volume redistribution). The fluctuations δv will scale as v/N and will be of either sign. If we assume them to be Gaussian, the average over a time $t = \tau$ the CRR-summed fluctuation will vanish,$\langle \Sigma \delta v \rangle$, while the average squared fluctuation will scale as $\langle (\Sigma \delta v)^2 \rangle = \langle \Sigma (\delta v)^2 \rangle \sim N(v/N)^2 \sim 1/N$. In the critical limit of diverging N this will also vanish and within the considered time τ nothing dramatic happens: the rearrangements will continue. However, the squared Gaussian fluctuations keep adding up linearly with time, so after a time $\tau' = N\tau$ we have $\langle \Sigma (\delta v)^2 \rangle \sim v^2$. At this point the free-volume distribution has become such that there is a finite probability of arrest, so τ' is the lifetime τ_A of the mobile region. The rates $1/\tau$ and $1/\tau'$ refer to particles that are a priori taken as mobile, so $1/\tau_\eta = (1-s)/\tau'$ and $1/\tau_{het} = (1-s)/\tau'$. Accordingly we have $\tau_{het} = N\tau_\eta$. This argument shows that the large-scale fluctuating heterogeneity is a natural consequence of local fluctuations in the free volume and that in the critical limit in particular the ratio τ_{het}/τ_ηdiverges, whence $n > m$. If we characterize the CRR by its typical size ξ and (possibly fractal) dimension d we get with B.1:

$$N = (\xi/\xi_a)^d = |1 - s/s_c|^{-\nu d} = |1 - s/s_c|^{m-n} \tag{B.7}$$

This gives us the relation $n = m + d\nu$ between the critical exponents. If we use this in (13) we see that the dependence of the size ξ of heterogeneous domains on the applied stress takes a very simple form at the critical concentration $\phi = \phi_c$, and by extension then also in the full critical shear-thinning region [29]: $\sigma\xi^d = \sigma_a\xi_a^d$ constant. It expresses that the domain mass varies inversely proportional to the applied stress, the total energy supplied to a domain thus remaining constant. With the above exponent relation also the empirical yield stress exponent $\Delta = \Gamma - M = n - m$ takes the very simple form $\Delta = d\nu$. We have derived this yield stress exponent without considering the elastic phase explicitly, but only considering that the crossover should take place when $\sigma_{visc} \approx \sigma_{el} \approx \sigma_y$. It is intriguing to note that in [43] an exponent Δ of the same form is proposed for the elastic modulus near the critical gelation point of gels with entropic elasticity.

B.1.6 Power-law creep

So far, we only discussed the steady-state solution of equation B.2. However, as discussed in the introduction, transient creeping flow under non-steady conditions is a generic feature of simple yield-stress fluids and many other materials. In fact, when the fluid is first exposed to a steady high stress and subsequently the stress is lowered to below the yield stress, a stress-independent viscosity develops that keeps increasing power-law in time [44, 45]. In terms of our model this means that a system with $\phi > \phi_c$ is initially brought to a value $s(t)$ for the stagnant fraction that is well below s_c . In the rate equation B.2 the dominant last term for particle arrest then rapidly brings s up near s_c again when the stress is lowered below σ_y , whereupon further arrest slows down. A time-dependent creep regime thus develops below σ_y in which $(1 - s/s_c)$ is already small but the arrest rate $1/\tau_A$ still dominates over the relaxation rate $1/\tau_R$. In this regime the timescales τ_A and τ_R have strongly increased and are well-separated while the heterogeneity lengthscale ξ has correspondingly grown large. Just as in the steady state this heterogeneity scale will govern the dynamics and the same power laws apply, with the time entering via the nonconserved order parameter $s(t)$. So we get from B.2:

$$ds/dt \approx (1 - s)/\tau_A \approx (1 - s_c)(1 - s/s_c)^n/\tau_a, \qquad (|\Delta s \ll s_c|) \tag{B.8}$$

This is trivially integrated, with the result that for $\tau \gg \tau_a$ the distance from criticality $1 - s/s_c$ scales as an inverse power of time. Hence all power laws in this distance, or equivalently in ξ, also become power laws in time. In particular we get for the viscosity of the creeping flow in the limit $\tau \gg \tau_a$ the functional form (5) proposed by Andrade [46] and verified for many different systems [44, 45, 47–55]: $\eta(t) \sim (t/\tau_a)^{m/(n-1)}$. So the Andrade creep exponent α can be expressed in terms of our exponents m and n as $\alpha = m/(n-1)$. Note that the creeping-flow viscosity is indeed independent of the subcritical stress, due to the fact that far from steady state the stress-dependent relaxation term in the rate equation B.2 could be ignored. Accordingly the exponent α differs from the linear-response exponent $1 - \beta = m/n$ that would follow from the steady-state shear-thinning viscosity $\eta \sim \dot{\gamma}^{\beta-1}$.

B.2 Table of literature data

In Table B.1 we have collected experimental or simulated exponent values for a broad range of systems, with similar systems grouped together to ease comparison. In spite of the variety in all these values some observations can still be made in addition to those already discussed in the main text for athermal overdamped systems. The table includes additional overdamped experimental systems [1, 6, 20, 56] which are supposed to be influenced, at least in part, by thermal effects.

The exponent values from flow-curve scaling for inertial systems with Bagnold scaling below ϕ_c , both obtained theoretically and by simulation [57, 58] are clearly different from those of the overdamped systems, and turn out to be interaction-dependent and dimension-independent. In [59] the flow-curve scaling for a simulated inertial system gave exponents somewhat different from [57, 58] but still clearly interaction-dependent and different from ours. Note that athermal systems with weak viscous damping may also crossover to an inertia-dominated shear-thickening Bagnold regime very close to ϕ_c [60]. Such systems should be modeled by particle exchange between three rather than two microscopic states. However, extension from the present model is not straightforward since the inertial dynamics introduces important new mechanisms beyond what is covered in the rate equation (9) with (8) and (10).

As is clear also from Table B.1 there are broad indications for heterogeneous dynamics as also assumed in our model, with a diverging associated lengthscale ξ when ϕ_c is approached from below [1, 3, 4, 6, 8, 61, 62]. Note that the definition of ξ may vary here; in particular both two-point and four-point correlations have been considered. Often there is evidence for a power-law divergence in $|\Delta\phi|$, with the associated exponent ν generally below unity. Interestingly a correlation-length exponent around 0.7 is obtained both in overdamped and inertial 2D and 3D systems.

Heterogeneous dynamics is also frequently observed in liquids approaching the thermal glass transition, with a growing correlation length and a separation of two timescales; power laws are often assumed. However, as pointed out [15–17, 20] both the microscopic dynamics, the critical concentration and the rheology scaling are different then. Combined fits can even be made of the glass and jamming singularities [15, 16, 19], although this may influence an accurate determination of the separate rheological exponents. For glasses at rest (not included in the table) power-law relations between a heterogeneity lengthscale and well-separated microscopic timescales have been accurately established by simulations, with implied exponent ratios $n/m = 1.5$ and $n/\nu = 5.4$ for soft spheres [36, 37, 39] and $n/m = 1.75$ for 2D colloids [38].

TABLE B.1: Experimental, simulated or predicted scaling exponents from a broad range of rheological and microscopic data. In the third column aspects are indicated in which systems essentially differ from the yield-stress fluids studied in this thesis.

Ref	System		Exponents of flow-curve scaling			Linear-response		Exponents of microscopic time- and lengthscales			
			Yield Stress	Cross-over rate	Shear thinning	Viscosity	Shear Modulus	Single-particle mobility	Cooperative dynamics	Correlation length	
			Δ	Γ	β	M	B	m	n	ν below ϕ_c	above ϕ_c
	Model prediction	all d	$n-m$	n	$1-m/n$	m				$(n-m)/d$	$\zeta \sim L$ at $\sigma = \sigma_y$
This work	soft emulsion $\sim 3.2\mu m$ (data from [63])	$d=3$	2.13	3.84	0.55	1.71	2.1				
	rigid emulsion		2.04	3.80	0.54						
	foam (data from [64])		2.21	3.75	0.57						
	Carbopol gel				0.48/0.55*						
[65]	NiPa $\sim 1\mu m$	$d=3$	2.1	4.1	0.48						
[62]	overdamped simulations								3.3	0.73	
[66]	harmonic interaction				0.64				$m/n = 0.27, \nu/n = 0.23$		
[59]	overdamped simulations unspecified interaction					1.7					
[56]	NiPa $\sim 0.6 - 1.0\mu m$	$d=3$							$N_{CRR} \sim \tau_\eta^{0.31}$		
[6]	NiPa $\sim 0.6 - 0.8\mu m$									0.5	
[20]	NiPa $\sim 0.6\mu m$		2.6	5.0-5.6	0.52-0.46		1.0				
[1]	NiPa $\sim 0.1\mu m$					2.25					$\zeta \sim L$ at $\sigma = 0, \phi = \phi_c$
[16]	range of literature data	$d=3$	1.0-2.0		0.4-0.6	2.0					
[19]	emulsion $\sim 0.5 - 1.1\mu m$		1.2				0.82				
[15]	overdamped simulations harmonic interactions		1.2		0.4	2.0					

Ref	System		Exponents of flow-curve scaling			Linear-response		Exponents of microscopic time- and lengthscales			
			Yield Stress	Cross-over rate	Shear thinning	Viscosity	Shear Modulus	Single-particle mobility	Cooperative dynamics	Correlation length	
			$\boldsymbol{\Delta}$	$\boldsymbol{\Gamma}$	$\boldsymbol{\beta}$	$\boldsymbol{M}$	$\boldsymbol{B}$	$\boldsymbol{m}$	$\boldsymbol{n}$	$\boldsymbol{\nu}$ below $\boldsymbol{\phi_c}$	above $\boldsymbol{\phi_c}$
[7]			1.2			1.65				0.6	
[67]			1.08		0.30					$\nu = 0.18n$ at $\phi = \phi_c$	
[8]	overdamped simulations harmonic interaction	$d = \mathbf{2}$	1.05							0.9	$\xi \sim L$ at $\sigma = \sigma_y$
[9]											$\xi \sim L$ at $\sigma = \sigma_y$
[68]	overdamped model harmonic interaction			3/2	0.5	1/2		1/2			
[57] [58]	inertial model harmonic interactions	all d	1	5/2	Δ/Γ	$2\Gamma - \Delta$					
	inertial model hertzian interactions		3/2	11/4							
	inertial simulations harmonic interactions	$d = \mathbf{2-4}$	1.0	2.5	0.4	4.0					
[59]	inertial simulations harmonic interactions	$d = \mathbf{3}$	1.2	1.9							
	inertial simulations hertzian interactions		1.8	2.4							
[5]	air-driven beads	$d = \mathbf{2}$								1.7	
[4]	air-fluidized beads								1.03	0.72	
[61]	quasistatic simulations harmonic interactions	$d = \mathbf{2, 3}$					0.5				0.71 at $\sigma = 0$
	quasistatic simulations hertzian interactions						1.0				0.71 at $\sigma = 0$

References

[1] D. A. Sessoms, I. Bischofsberger, L. Cipelletti, and V. Trappe. Multiple dynamic regimes in concentrated microgel systems. *Trans. Roy. Soc. A*, 367:5013, 2009.

[2] S. Maccarone, G. Brambilla, O. Pravaz, A. Duri, M. Ciccotti, J.-M. Fromental, E. Pashkovski, A. Lips, D. Sessoms, V. Trappe, and L. Cipelletti. Ultra-long range correlations of the dynamics of jammed soft matter. *Soft Matter*, 6:5514, 2010.

[3] A. S. Keys, A. R. Abate, S. C. Glotzer, and D. J. Durian. Measurement of growing dynamical length scales and prediction of the jamming transition in a granular material. *Nat. Phys.*, 3:260, 2007.

[4] A. R. Abate and D. J. Durian. Topological persistence and dynamical heterogeneities near jamming. *Phys. Rev. E*, 76:021306, 2007.

[5] F. Lechenault, O. Dauchot, G. Biroli, and J. P. Bouchaud. Critical scaling and heterogeneous superdiffusion across the jamming/rigidity transition of a granular glass. *EPL*, 83:46003, 2008.

[6] Y. Rahmani, K. van der Vaart, B. van Dam, Z. Hu, V. Chikkadi, and P. Schall. Dynamic heterogeneity in hard and soft sphere colloidal glasses. *Soft Matter*, 8:4264, 2012.

[7] P. Olsson and S. Teitel. Critical scaling of shear viscosity at the jamming transition. *Phys. Rev. Lett.*, 99:178001, 2007.

[8] C. Heussinger, L. Berthier, and J.-L. Barrat. *EPL*, 90:20005, 2010.

[9] C. Heussinger and J.-L Chaudhuri, P. and. Barrat. Fluctuations and correlations during the shear flow of elastic particles near the jamming transition. *Soft Matter*, 6:3050, 2010.

[10] M. Wyart, S. R. Nagel, and T. A. Witten. Geometric origin of excess low-frequency vibrational modes in weakly connected amorphous solids. *Europhys. Lett.*, 72:486, 2005.

[11] W. G. Ellenbroek, E. Somfai, M. van Hecke, and W. van Saarloos. Critical scaling in linear response of frictionless granular packings near jamming. *Phys. Rev. Lett.*, 97:258001, 2006.

[12] C. Heussinger and J.-L. Barrat. Jamming transition as probed by quasistatic shear flow. *Phys. Rev. Lett.*, 102:218303, 2009.

[13] K. Martens, L. Bocquet, and J.-L. Barrat. Connecting diffusion and dynamical heterogeneities in actively deformed amorphous systems. *Phys. Rev. Lett.*, 106:156001, 2011.

[14] C. P. Goodrich, W. G. Ellenbroek, and A. J. Liu. Stability of jammed packings i: the rigidity length scale. *Soft Matter*, 9:10993, 2013.

[15] A. Ikeda, L. Berthier, and P. Sollich. Unified study of glass and jamming rheology in soft particle systems. *Phys. Rev. Lett.*, 109:018301, 2012.

[16] A. Ikeda, L. Berthier, and P. Sollich. Disentangling glass and jamming physics in the rheology of soft materials. *Soft Matter*, 9:7669, 2013.

[17] P. Olsson and S. Teitel. Athermal jamming versus thermalized glassiness in sheared frictionless particles. *Phys. Rev. E.*, 88:010301(R), 2013.

[18] H. Eyring. Viscosity, plasticity, and diffusion as examples of absolute reaction rates. *J. Chem. Phys.*, 4:283, 1936.

[19] F. Scheffold, F. Cardinaux, and T. G. Mason. Linear and nonlinear rheology of dense emulsions across the glass and the jamming regimes. *J. Phys. Condens. Matter*, 25:502101, 2013.

[20] A. Basu, Y. Xu, T. Still, P. E. Arriata, Z. Zhang, K. N. Nordstrom, J. M. Rieser, J. P. Gollub, D. J. Durian, and A. G. Yodh. Rheology of soft colloids across the onset of rigidity: scaling behavior, thermal, and non-thermal responses. *Soft Matter*, 10:3027, 2014.

[21] R. A. Riggleman, H.-N. Lee, M. D. Ediger, and J. J. de Pablo. Free volume and finite-size effects in a polymer glass under stress. *Phys. Rev. Lett.*, 99:215501, 2007.

[22] H.-N. Lee, K. Paeng, S. F. Swallen, and M. D. Ediger. Direct measurement of molecular mobility in actively deformed polymer glasses. *Science*, 323:231, 2009.

[23] R. A. Riggleman, H.-N. Lee, M. D. Ediger, and J. J. de Pablo. Heterogeneous dynamics during deformation of a polymer glass. *Soft Matter*, 6:287, 2010.

[24] H.-N. Lee and M. D. Ediger. Mechanical rejuvenation in poly (methyl methacrylate) glasses? molecular mobility after deformation. *Macromolecules*, 43:5863, 2010.

[25] R. A. Riggleman, K. S. Schweizer, and J. J. de Pablo. Nonlinear creep in a polymer glass. *Macromolecules*, 41:4969, 2008.

[26] M. Grob, C. Heussinger, and A. Zippelius. Jamming of frictional particles: A nonequilibrium first-order phase transition. *Phys. Rev. E*, 89:050201, 2014.

[27] E. Irani, P. Chaudhuri, and C. Heussinger. Impact of attractive interactions on the rheology of dense athermal particles. *Phys. Rev. Lett.*, 112:188303, 2008.

[28] H. M. Wyss, K. Miyazaki, J. Mattsson, Z. Hu, D. R. Reichman, and D. A. Weitz. Strain-rate frequency superposition: A rheological probe of structural relaxation in soft materials. *Phys. Rev. Lett.*, 98:238303, 2007.

[29] M. Dinkgreve, J. Paredes, M. A. J. Michels, and D. Bonn. Universal rescaling of flow curves for yield-stress fluids close to jamming. *Physical Review E*, 92(1):012305, 2015.

[30] L. Berthier, G. Biroli, J.-P. Bouchaud, L. Cipelletti, and W. van Saarloos. *Dynamical Heterogeneities in Glasses, Colloids, and Granular Materials*. Oxford University Press, 2011.

[31] G. Biroli, J.-P. Bouchaud, K. Miyazaki, and D. R. Reichman. Inhomogeneous mode-coupling theory and growing dynamic length in supercooled liquids. *Phys. Rev. Lett.*, 97:195701, 2006.

[32] D. Hajnal and M. Fuchs. Flow curves of colloidal dispersions close to the glass transition. *Eur. Phys. J. E*, 28:125, 2009.

[33] E. Flenner and G. Szamel. Dynamic heterogeneity in a glass forming fluid: Susceptibility, structure factor, and correlation length. *Phys. Rev. Lett.*, 105:217801, 2010.

[34] C. Fusco, T. Albaret, and A. Tanguy. *Eur. Phys. J. E*, 37:43, 2014.

[35] J. Lin, E. Lerner, A. Rosso, and M. Wyart. Scaling description of the yielding transition in soft amorphous solids at zero temperature. *Proc. Natl. Acad. Sci. U.S.A.*, 111:14382, 2014.

[36] K. Kim and S. Saito. Multiple time scales hidden in heterogeneous dynamics of glass-forming liquids. *Phys. Rev. E*, 79:060501(R), 2009.

[37] K. Kim and S. Saito. Multi-time density correlation functions in glass-forming liquids: Probing dynamical heterogeneity and its lifetime. *J. Chem. Phys.*, 133:044511, 2010.

[38] H. Tanaka, T. Kawasaki, H. Shintani, and K. Watanabe. Critical-like behaviour of glass-forming liquids. *Nat. Mater.*, 9:324, 2010.

[39] K. Kim and S. Saito. Multiple length and time scales of dynamic heterogeneities in model glass-forming liquids: A systematic analysis of multi-point and multi-time correlations. *J. Chem. Phys.*, 138:12A506, 2013.

[40] G. Adam and J. H. Gibbs. On the temperature dependence of cooperative relaxation properties in glass-forming liquids. *J. Chem. Phys.*, 43:139, 1965.

[41] N. F. Mott. Lxxviii. a theory of work-hardening of metals ii: Flow without slip-lines, recovery and creep. *Philos. Mag.*, 44:742, 1953.

[42] F. Louchet and P. Duval. Andrade creep revisited. *Int. J. Mater. Res.*, 100:1433, 2009.

[43] X. Xing and P. M. Mukhopadhyay, S. andGoldbart. Scaling of entropic shear rigidity. *Phys. Rev. Lett.*, 93:225701, 2004.

[44] P. C. F. Møller, A. Fall, and D. Bonn. Origin of apparent viscosity in yield stress fluids below yielding. *EPL (Europhysics Letters)*, 87(3):38004, 2009.

[45] P. Moller, A. Fall, V. Chikkadi, D. Derks, and D. Bonn. An attempt to categorize yield stress fluid behaviour. *Philosophical Transactions of the Royal Society of London A: Mathematical, Physical and Engineering Sciences*, 367(1909):5139–5155, 2009.

[46] E. N. C. Andrade. On the viscous flow in metals, and allied phenomena. *Proceedings of the Royal Society of London. Series A, Containing Papers of a Mathematical and Physical Character*, pages 1–12, 1910.

[47] M. Miguel, A. Vespignani, M. Zaiser, and S. Zapperi. Dislocation jamming and andrade creep. *Physical review letters*, 89(16):165501, 2002.

[48] M. Miguel, P. Moretti, M. Zaiser, and S. Zapperi. Statistical dynamics of dislocations in simple models of plastic deformation: Phase transitions and related phenomena. *Materials Science and Engineering: A*, 400:191–198, 2005.

[49] M. Miguel, L. Laurson, and M. J. Alava. Material yielding and irreversible deformation mediated by dislocation motion. *The European Physical Journal B-Condensed Matter and Complex Systems*, 64(3):443–450, 2008.

[50] L. Laurson, M. Miguel, and M. J. Alava. Dynamical correlations near dislocation jamming. *Physical review letters*, 105(1):015501, 2010.

[51] M. Siebenbürger, M. Ballauff, and T. Voigtmann. Creep in colloidal glasses. *Physical review letters*, 108(25):255701, 2012.

[52] G. B. McKenna. Mechanical rejuvenation in polymer glasses: Fact or fallacy? *Journal of Physics: Condensed Matter*, 15(11):S737, 2003.

[53] J. W. Dudley, M. T. Myers, R. D. Shew, M. M. Arasteh, et al. Measuring compaction and compressibilities in unconsolidated reservoir materials by time-scaling creep. *SPE Reservoir Evaluation & Engineering*, 1(05):430–437, 1998.

[54] J. Rosti, J. Koivisto, L. Laurson, and M. J. Alava. Fluctuations and scaling in creep deformation. *Physical review letters*, 105(10):100601, 2010.

[55] C. D. Agosti, K. M. Bell, D. J. Plazek, J. Larson, J. D. Kang, L. G. Gilbertson, and P. Smolinski. Analysis of power law models for the creep of nucleus pulposus tissue. *Biorheology*, 47:143, 2010.

[56] K. N. Nordstrom, J. P. Gollub, and D. J. Durian. Dynamical heterogeneity in soft-particle suspensions under shear. *Phys. Rev. E*, 84:021403, 2011.

[57] M. Otsuki and H. Hayakawa. Universal scaling for the jamming transition. *Prog. Theor. Phys.*, 121:647, 2009.

[58] M. Otsuki and H. Hayakawa. Critical behaviors of sheared frictionless granular materials near the jamming transition. *Phys. Rev. E.*, 80:011308, 2009.

[59] T. Hatano. Scaling properties of granular rheology near the jamming transition. *Phys. Soc. Jpn.*, 77:123002, 2008.

[60] A. Fall, A. Lemaître, F. Bertrand, D. Bonn, and G. Ovarlez. Shear thickening and migration in granular suspensions. *Phys. Rev. Lett.*, 105:268303, Dec 2010.

[61] C. S. O'hern, L. E. Silbert, A. J. Liu, and S. R. Nagel. Jamming at zero temperature and zero applied stress: The epitome of disorder. *Physical Review E*, 68(1):011306, 2003.

[62] T. Hatano. Growing length and time scales in a suspension of athermal particles. *Phys. Rev. E*, 79:050301(R), 2009.

[63] J. Paredes, M. A. J. Michels, and D. Bonn. Rheology across the zero-temperature jamming transition. *Physical review letters*, 111(1):015701, 2013.

[64] S. Marze, D. Langevin, and A. Saint-Jalmes. Aqueous foam slip and shear regimes determined by rheometry and multiple light scattering. *Journal of Rheology*, 52:1091–1111, 2008.

[65] K. N. Nordstrom, E. Verneuil, P. E. Arriata, A. Basu, Z. Zhang, A. G. Yodh, J. P. Gollub, and D. J. Durian. Microfluidic rheology of soft colloids above and below jamming. *Phys. Rev. Lett.*, 115:175701, 2010.

[66] T. Hatano. Rheology and dynamical heterogeneity in frictionless beads at jamming density. *J. Phys. Conf. Ser.*, 319:012011, 2011.

[67] D. Vågberg, P. Olsson, and S. Teitel. Universality of jamming criticality in overdamped shear-driven frictionless disks. *Phys. Rev. Lett.*, 113:148002, 2014.

[68] B. P. Tighe, E. Woldhuis, J. C. Remmers, W. van Saarloos, and M. van Hecke. Model for the scaling of stresses and fluctuations in flows near jamming. *Phys. Rev. Lett.*, 105:088303, 2010.

Summary

Traffic jams are a common phenomenon on highways; when there are too many cars on the road the traffic gets stuck. A similar jamming phenomenon also occurs in yield-stress fluids that consist of a dispersion of a material in a liquid, such as suspensions of particles or polymers, foams or emulsions. At high concentrations, these materials behave like solids (like in traffic jams there is no flow), and they only start to flow when enough stress is applied. For example, toothpaste behaves like a solid at rest but it starts to flow when you squeeze it out of the tube. This threshold stress that is needed to initiate flow is called the yield stress, hence the name yield-stress material. It is important to understand these kinds of properties and the flow behavior (rheology) of these materials since they are widely applied in the cosmetic, oil and food industry. We seek to understand the transition from mechanically solid-like to fluid-like behavior on a fundamental level. The associated jamming transition between solid and liquid "states" has similarities to classical phase transitions like those between solid, liquid, gas and plasma phases. However it is not completely clear how general the jamming description is, and to what extent the mechanical behavior of jammed materials can be fully described by considering the jamming transition to be analogous to a classical phase transition. In this thesis we study the flow behavior (the rheology) of a variety of yield-stress materials in the aim of describing, understanding and predicting the rheology of jamming.

Chapter 1 gives the motivation for this research and a general introduction to the main topics related to this thesis are explained: the jamming phase diagram, rheology and yield-stress materials. In **chapter 2** the experimental techniques and the different materials that were used are discussed. Rheology was the main method used to understand the flow properties of the different materials and a variety of rheological tests is described in detail.

Since the notion of a yield-stress fluid was introduced by Bingham in 1922, these fluids have become more and more popular. However, in the nineties Barnes and Walters published a provocative paper entitled "the yield stress myth?" from which a huge discussion arose whether the yield stress really existed or that it was just an experimental artifact. In **chapter 3** we review the definition of the yield stress and demonstrate the significance of the pre-yielding behavior through a number of elementary measurements, showing that the yield stress is real. Secondly, in **chapter 4**, we compare different methods of measuring the yield stress with conventional rheometers that have been used in the literature on a variety of materials. Subsequently, an overview is given of the different values that are found for the yield stress and yield strain.

In **chapter 5** we investigate the stability of Laponite-stabilized Pickering emulsions under shear. Often, colloidal particles are used to make Pickering emulsions that have been reported to be very stable. Commonly the stabilization is a combined effect of particles adsorbing at the fluid interface and a particle network in the continuous phase, however the contribution of each to the overall stability is difficult to assess. To clarify the structure of the emulsion and the role of the clay particles, we fluorescently label the clay particles by adsorbing the dye onto the particle surfaces. This allows us to show directly by using confocal microscopy, that the clay particles are not only located at the interface but also aggregate and form a gel in the continuous aqueous phase. This reveals that the formation of the emulsions with clay particles only, without surfactant, is mostly due to gel formation of the clay particles in the continuous phase, rather than that the clay is an emulsifier.

In **chapter 6** we demonstrate experimentally that a simple yield-stress fluid, can undergo a transition to thermally induced shear banding. The experiments suggest that both types of behavior may be found in the same type of material, however the presence of thermal parts in addition to athermal jamming leads to a depletion interaction that causes an apparent shear band to appear. A set of rheological test are done to study this transition in a Carbopol gel. Flow visualization experiments, with fluorescently labelled Carbopol, elucidate the difference between simple and shear banding behavior and reveal the presence of thermal particles in the system. We therefore show that a simple yield-stress fluid can be transformed to a shear banding yield-stress fluid by different preparation protocols.

In **chapter 7** we aim to describe, understand and predict the flow behavior (stress vs. shear rate) of simple yield-stress fluids. The experimental flow curves of four different athermal yield-stress fluids are studied near the jamming point. By scaling with the distance to the jamming volume fraction all rheology data can be collapsed onto master curves below and above jamming. A two-state microscopic theory of heterogeneous dynamics is presented to rationalize the observed transition. Finally the experimental data and the microscopic theory are compared with much of the literature data for yield-stress systems. We conclude that all our athermal yield-stress materials can be described by one universal scaling form, independent of the mechanical properties of the system, but a discrepancy between theory and simulations remains.

In this last chapter (**chapter 8**) we investigate the cross-over between thermal and athermal yield-stress regimes, by looking at the effect of volume fraction, particles size and the inter-particle interactions on the flow behavior. Interestingly, the flow curves of thermal systems can be scaled onto a universal curve in a similar way as the athermal systems, with respect to the glass transition instead of the jamming transition. In addition, we find that all yield stress flow curves of both thermal and athermal systems can be collapsed, using the Laplace pressure as stress scale for athermal systems and osmotic pressure as the stress scale for the thermal systems. In conclusion, we can predict, rather then fit, characteristic stress and rate scales from material properties.

Samenvatting

Files zijn een algemeen fenomeen op snelwegen; als er teveel auto's op de weg zijn loopt het verkeer vast. Een soortgelijk file-effect komt ook voor in yield-stress vloeistoffen, dit zijn vloeistoffen die bestaan uit een dispersie van een materiaal in een vloeistof, zoals suspensies van deeltjes of polymeren, emulsies of schuim. Bij hoge concentraties gedragen deze materialen zich als een "vaste stof" (zoals in een file zit het materiaal vast), en ze beginnen alleen te stromen als er een druk op uitgeoefend wordt. Bijvoorbeeld, tandpasta gedraagt zich in rust als een vaste stof, maar begint te stromen als je in de tube knijpt. De druk of afschuifspanning (in het Engels 'stress') die nodig is om stroming te initiëren wordt de yield stress genoemd, vandaar de naam yield-stress materiaal. Het is belangrijk om dit soort eigenschappen en het stromings gedrag (de rheologie) van deze materialen te begrijpen omdat yield-stress materialen een brede toepassing hebben in zowel de cosmetische-, olie- en voedselindustrie. We proberen de overgang van mechanisch vloeistof achtig naar vaste stof-achtig gedrag op een fundamenteel niveau te begrijpen. De geassocieerde jamming overgang tussen vaste stof en vloeistof toestanden heeft vergelijkingen met klassieke faseovergangen zoals tussen vaste stof, vloeistof, gas en plasma. Echter is het nog niet geheel duidelijk hoe algemeen de jamming overgang is, en of deze volledig beschreven kan worden aan de hand van klassieke faseovergangen. In dit proefschrift onderzoeken wij het stromingsgedrag (d.m.v. rheologie metingen) van een aantal verschillende yield-stress materialen, met als doel om de rheologie van jamming te kunnen beschrijven, begrijpen en uiteindelijk te kunnen voorspellen.

Hoofdstuk 1 geeft de motivatie voor dit onderzoek en een algemene introductie van de hoofdonderwerpen die hieraan gerelateerd zijn: de jamming fasediagram, rheologie en yield-stress vloeistoffen. In **hoofdstuk 2** worden de experimentele technieken en gebruikte materialen besproken. Rheologie is de belangrijkste metho-de om het stromingseigenschappen van de verschillende materialen te onderzoeken en de verschillende rheologische testen worden nauwkeurig beschreven.

Sinds het begrip van een yield-stress vloeistof voor het eerst was geïntroduceerd door Bingham in 1922, zijn deze vloeistoffen steeds populairder geworden. Echter, in de jaren negentig verscheen er een provocerend artikel van Barnes en Walters genaamd "de yield stress mythe" waarna er een discussie ontstond of de yield stress echt bestaat of slechts een experimenteel artefact is. In **hoofdstuk 3** bespreken we de definitie van de yield stress en demonstreren het belang van het pre-yielding gedrag aan de hand van een aantal elementaire metingen, die laten zien dat de yield stress echt is. In **hoofdstuk 4** vergelijken we verschillende methodes en metingen om de yield stress te meten en geven een overzicht van de verschillende waardes van de yield stress die worden gevonden.

In **hoofdstuk 5** onderzoeken we de rol van Laponiet kleideeltjes bij het stabiliseren van geconcentreerde Pickering-emulsies. Vaak worden kleine colloïdale deeltjes gebruikt om emulsies te stabiliseren en deze blijken zeer stabiel te zijn. Over het algemeen is de stabilisatie een gecombineerd effect van geabsorbeerde deeltjes aan het druppeloppervlak en de netwerkvorming van deeltjes in de continue vloeistoffase, echter de bijdrage van elk effect is moeilijk vast te stellen. Om de structuur van de emulsies en de rol van de kleideeltjes daarin te verduidelijken, markeren we de kleideeltjes met fluorescerende moleculen die aan de kleideeltjes hechten. Door middel van confocale microscopie laten we zien dat de kleideeltjes niet alleen op het oppervlak van de druppels zit maar ook aggregeren en een gel vormen in de continue waterfase. Dit toont aan dat de formatie van emulsies gestabiliseerd met enkel kleideeltjes, voornamelijk het gevolg is van de gel-vorming van de kleideeltjes in plaats van dat de deeltjes als een emulgator optreden.

In **hoofdstuk 6** demonstreren we met experimentele data dat een vermoedelijk simpele yield-stress vloeistof, een transitie kan ondergaan tot thermisch geïnduceerde shear banding. De experimenten laten zien dat beide soorten gedrag gevonden kunnen worden in hetzelfde materiaal, echter de aanwezigheid van thermische deeltjes in aanvulling op de athermische jamming leidt tot een depletie interactie die een

schijnbare shear banding laat zien. We hebben een serie aan rheologiemetingen gedaan om deze transitie in een Carbopol-gel te onderzoeken. Stromingsvisualisatie metingen met gelabelde Carbopol onthullen de aanwezigheid van thermische deeltjes in het systeem. We laten daarmee zien dat het stromingsgedrag van een Carbopol gel floeistof afhangt van het voorbereidingsprotocol.

In **hoofdstuk 7** streven we er naar om het stromingsgedrag van simpele yield-stress vloeistoffen te beschrijven, te begrijpen en te voorspellen. We onderzoeken de stromingscurves (afschuifspanning vs. afschijfsnelheid) van vier verschillende athermische yield-stress vloeistoffen. Door de rheologiedata te schalen met de afstand tot de jammingconcentratie vallen alle stromingscurves over elkaar op twee master curves; onder en boven de jamming concentratie. We presenteren een twee-toestanden microscopische theorie voor heterogene dynamica om de geobserveerde transitie te rationaliseren. Tot slot vergelijken we het theoretische model met de experimentele data en een groot deel van de literatuur over yield-stress vloeistoffen. We concluderen dat onze athermische yield-stress materialen beschreven kunnen worden door een universele schalingsform, die onafhankelijk is van de mechanische interacties van de systemen.

In het laatste hoofdstuk (**hoofdstuk 8**), onderzoeken we de crossover van thermische en athermische regimes door te kijken naar het effect van de volumefractie, deeltjes grootte en de interacties tussen deeltjes op het stromingsgedrag. Interessant genoeg, kunnen de stromingscurves van thermische systemen op eenzelfde manier geschaald worden als de athermische systemen, met betrekking tot de glasovergang in plaats van de jammingovergang. Alle yield stress stromingscurves kunnen voor zowel thermisch als athermisch worden geschaald, met de Laplace druk als stress schaal voor de athermische systemen en de osmotische druk als stress schaal voor de thermische. Ten slotte, zijn we in staat om te voorspellen aan de hand van de materiaaleigenschappen wat de karakteristieke afschuifspanning en afschuifsnelheid schalen zijn.

Scientific Résumé

Publications related to this thesis

Chapter 3

- M. Dinkgreve, J. Paredes, M. M. Denn and D. Bonn
  "On different ways of measuring the yield stress"
  Journal of Non-Newtonian Fluid Mechanics, 238, 233-241 (2016)

Chapter 4

- M. Dinkgreve, M. M. Denn and D. Bonn
  "'Everything flows?': elastic effects on startup flows of yield stress fluids"
  Rheological Acta, 56, 189-194 (2017)

Chapter 5

- M. Dinkgreve, K. P. Velikov and D. Bonn
  "Stability of Laponite-stabilized high internal phase Pickering emulsions under shear"
  Physical Chemistry Chemical Physics, 18, 22973-22977 (2016)

Chapter 6

- M. Dinkgreve, M. Fazilati, M. M. Denn and D. Bonn
  "Carbopol: from a simple to a thixotropic yield stress fluid"
  Manuscript submitted.

Chapter 7

- M. Dinkgreve, J. Paredes, M. A. J. Michels and D. Bonn
  "Universal rescaling of flow curves for yield-stress fluids close to jamming"
  Physical Review E., 92, 012305 (2015).

Chapter 8

- M. Dinkgreve, M. A. J. Michels and D. Bonn
  "Rheology scaling of thermal glasses and jammed systems: cross-over and universality"
  Manuscript in preparation.

Other publications

- M. Habibi, M. Dinkgreve, J. Paredes, M. M. Denn and D. Bonn *"Normal stress measurements in foams and emulsions in the presence of slip"*
  Journal of Non-Newtonian Fluid Mechanics, 238, 33-43 (2016)
- M. Mermet-Guyennet, M. Dinkgreve, M. Habibi, N. Martzel, R. Sprik, M. M. Denn and D. Bonn *"Normal stress measurements in foams and emulsions in the presence of slip"*
  Rheological Acta, 56, 583-589 (2017)

Acknowledgments

Finally my PhD thesis is finished and thereby this journey has come to an end... I would not have managed to do this without the collaboration and support of my colleagues, friends and family.

First of all, I want to express my gratitude to my supervisor and promotor Daniel Bonn. Three years ago you convinced me to start this PhD journey, but I had one odd condition: I wanted to do this within 3 years instead of 4. As surprised as you were (normally people ask for more time instead of less), you supported me in this and I could not have done this without you. Thank you for your support and wisdom, and your patience with my endless desire to plan and organize almost everything. I have learned a lot from you, therefore I am very grateful.

Additionally, I would like to thank my co-promotor Noushine. Thank you for your collaboration and support, your door was always open for me.

During my research I have had the honor of having two other valuable collaborations with two very special people: Prof. Morton Denn and Prof. Thijs Michels, your extensive knowledge about the physical subjects related to my research is impressive and I am grateful for our interesting discussions and your valuable support during my PhD.

A big part of my gratitude goes to the Soft Matter group. I immediately felt part of the group and I made a lot of new friends. Jose you guided me through my master and inspired me for my PhD. It was always fun working with you. I also want to thank the girls from my office Laura, Julie and Karla for all the precious memories. And Chris who could always cheer me up with a homemade cappuccino. Of course I also want to thank all my other colleagues from the group: Peter, Rudolf, Marius, Dominik, Janaina, Anh, Triet, Rojman, Dimitri, Odile, Mehdi, Tahn, Georgios, Corentin, Carlos, Bruce, Bart, Henri, Ines, Bijoy,

Mohsin, Simon, Emunuele, Thijs, Rinse, Antoine, Etienne, Luci, Joep, Tom, Sanne and Riande. I will never forget the wonderful Soft Matter Christmas dinner: with Thijs who was showing us his hilarious dance moves and Mohsin's amazing curry. I will miss those moments.

I would also like to thank all the other people from the IoP for the great collaborations and social times: the monthly PhD and PostDoc drinks, the IoP bbq, the people from the workshop fixing the (very old) computers in the lab and modifying or making new geometeries for my setup, the incredible ladies from the secretariaat, especially Rita, Natalie and Anne-Marieke, and Joost, the best manager the IoP could ever wish for. I could always talk to you for advise and I liked to discuss about the things going on at the IoP. Also thanks to my colleagues of the PhD and PostDoc council: Laurens, Antonio, Carla, Niki, Jaco, Damian and Thijs.

Special thanks goes to my paranymphs, Robbie and Bijoy, you both supported me during my PhD and I feel very save having you by my side during my defense.

I want to thank my friends from physics (de schaduw hark): Koen, Etienne, Joris, Adri, Tim, Sidoeri, Sarah, Niki, Robbie and Reinier. And all my friend from hockey, especially Sanne and Mariska. My friends from climbing: Alex, Soraya, Parisa, Oleg and Franzi. And of course my best and oldest friends: Natasha, Daan and Robbie. You are always there for me!

Thanks to the people from the OFL and the Recess College, participating to the OFL course was a very valuable experience for me and helped me a lot in my work and general life.

Nick, I don't even know where to begin to express my gratitude to you. You are so important to me, as my boyfriend, but also because you know exactly how it is to do a PhD. You know how to calm me down when I am stressed and how to cheer me up when I am sad. But most important you make me happy, and sharing all the good moments in my life with you makes it even better. I love you.

Last but not least, I want to thank my family. Thanks to my uncles and aunts, nephews and nieces for supporting me. I specially want to thank my parents, Marc and Astrid, for raising me and making me the person who I am today: thank you papa and mama for your endless love and support. Finally, my sister Patricia, thank you little Chicken for being my sister and my very good friend.

Thank you!